



Cemdata18: A chemical thermodynamic database for hydrated Portland cements and alkali-activated materials



Barbara Lothenbach^{a,*}, Dmitrii A. Kulik^b, Thomas Matschei^c, Magdalena Balonis^d,
Luis Baquerizo^e, Belay Dilnes^f, George D. Miron^b, Rupert J. Myers^{g,1}

^a Empa, Laboratory for Concrete & Construction Chemistry, CH-8600 Dübendorf, Switzerland

^b Paul Scherrer Institut, Laboratory for Waste Management, 5232 Villigen PSI, Switzerland

^c HTW Dresden University of Applied Sciences, Department of Civil Engineering, 01069 Dresden, Germany

^d Department of Materials Science and Engineering, University of California Los Angeles, Los Angeles, CA, USA

^e Lafarge Centre de Recherche, 38291 Saint-Quentin Fallavier, France

^f BASF Schweiz AG, 5082 Kaisten, Switzerland

^g University of Sheffield, Department of Materials Science and Engineering, Sheffield S1 3JD, UK

ARTICLE INFO

Keywords:

Thermodynamic modelling
Cement
Database
Solubility
C-S-H

ABSTRACT

Thermodynamic modelling can reliably predict hydrated cement phase assemblages and chemical compositions, including their interactions with prevailing service environments, provided an accurate and complete thermodynamic database is used. Here, we summarise the Cemdata18 database, which has been developed specifically for hydrated Portland, calcium aluminate, calcium sulfoaluminate and blended cements, as well as for alkali-activated materials. It is available in GEMS and PHREEQC computer program formats, and includes thermodynamic properties determined from various experimental data published in recent years. Cemdata18 contains thermodynamic data for common cement hydrates such as C-S-H, AFm and Aft phases, hydrogarnet, hydrogarnet, zeolites, and M-S-H that are valid over temperatures ranging from 0 to at least 100 °C. Solid solution models for AFm, Aft, C-S-H, and M-S-H are also included in the Cemdata18 database.

1. Introduction

Numerous studies have shown that chemical thermodynamic modelling, coupled with accurate and complete thermodynamic databases, can reliably predict hydrated cement phase assemblages and chemical compositions. One of the most interesting aspects of applying thermodynamics to hydrated cements has been the discovery that the chemical compositions of $\text{Al}_2\text{O}_3\text{-Fe}_2\text{O}_3$ mono (AFm) and $\text{Al}_2\text{O}_3\text{-Fe}_2\text{O}_3$ tri (Aft) phases are very sensitive to the presence of carbonate [1–3] and temperature [4–6], thus demonstrating that these factors may significantly modify hydrated cement phase assemblages. Experiments have shown that compositions of hydrate cement phase assemblages can alter rapidly, often within weeks or months, reflecting changing system compositions and temperatures. Thus, thermodynamic calculations and experiments support each other: on the one hand, calculations enable more complete interpretations of limited experimental datasets and help to identify key experiments to perform; and on the other hand, experiments provide the data that are needed to validate calculation results and model parameters.

The quality of thermodynamic modelling results depends directly on the accuracy and completeness of the input thermodynamic properties of substances and phases, which are usually supplied from a thermodynamic database. Relevant thermodynamic data for solid cementitious substances, such as the solubility products of ettringite or hydrogarnet, have been compiled in several specific “cement databases” such as (1) the Cemdata07 and Cemdata14 databases [1,7–12] (<http://www.empa.ch/cemdata>), which are available for GEMS [13,14], (2) the Thermoddem (<http://thermoddem.brgm.fr/>) database [15,16] available for the Geochemists Workbench® [17] (<https://www.gwb.com/>) and PHREEQC [18] or (3) HATCHES database [19] available for PHREEQC [18]. Data in the first two databases are generally comparable, although some differences exist, as discussed in more detail in Damidot et al. [20]. Our experience applying Cemdata in thermodynamic modelling applications underlines the importance of a careful data selection and evaluation process, and of including sensitivity analyses into the analysis and discussion of results.

Additional experimental data, and thermodynamic properties derived from these data, have become available since the first compilation

* Corresponding author.

E-mail address: barbara.lothenbach@empa.ch (B. Lothenbach).

¹ Current address: University of Edinburgh, School of Engineering, Edinburgh, EH9 3FB, UK.

of Cemdata07 in 2007/2008 and subsequent compilation of Cemdata14 in 2013/2014 [1,7,21]. Cemdata18 provides a significant update to both Cemdata07 and Cemdata14. Cemdata18 is written into a format supporting the GEM-Selektor code [13,14] and is fully compatible with the freely available GEMS-Selektor version of the PSI-Nagra 12/07 TDB [22,23] (<http://gems.web.psi.ch/>). PSI/Nagra 12/07 TDB [22] contains the same entries for aqueous species/complexes relevant to cement systems as the PSI/Nagra 01/01 [24], with only slight changes: the thermodynamic properties of $\text{Si}_4\text{O}_8(\text{OH})_4^{4-}$ and $\text{AlSiO}_3(\text{OH})_4^{3-}$ were added, while the complex $\text{AlSiO}(\text{OH})_6^-$ was removed. The GEMS version of the PSI/Nagra 12/07 TDB includes further changes to the thermodynamic properties of Al bearing species/complexes and the addition of Helgeson-Kirkham-Flowers equation of state parameters to account for changes in temperature and pressure [25,26]. Cemdata18 includes a comprehensive selection of cement hydrates commonly encountered in Portland cement (PC) systems in the temperature range of 0 to 100 °C, including calcium silicate hydrate (C-S-H), magnesium silicate hydrate (M-S-H), hydrogarnet, hydrotalcite-like phases, some zeolites, AFm and Aft phases, and various solid solutions used to describe the solubility of these phases. Solubility constants have generally been calculated based on critical reviews of all available experimental data and from additional experiments made either to obtain missing data or to verify existing data. Additional solubility data were measured and compiled using temperatures ranging from 0 to 100 °C in many instances, as documented in [9,12,27,28]. Numerous solid solutions among AFm and Aft phases, siliceous hydrogarnets, hydrotalcite-like phases, C-S-H, and M-S-H have been observed and are included in Cemdata18.

Several C-S-H solid solution models, as well as two models for hydroxide-hydrotalcite are available in Cemdata18. The CSHQ model from [11] and the OH-hydrotalcite end member with $\text{Mg}/\text{Al} = 2$ are well adapted for PC. Although the CSHQ model is able to describe the entire range of Ca/Si ratios encountered, it is best used for high Ca/Si C-S-H, as it still lacks the ability to predict aluminium uptake, which is of less importance for Portland cements than for blended cements. For alkali activated binders, the calcium (alkali) aluminosilicate hydrate (C-(N)-A-S-H) gel model, with lower calcium but higher aluminium and alkali content than in the C-S-H type phase which exists in hydrated PC, and a Mg-Al layered double hydroxide with variable Mg/Al ratio, are available.

This paper summarises Cemdata18, which includes the most important additions to the Cemdata07 and Cemdata14 databases in recent years. It also discusses the relevance and implications of these additions, and compares Cemdata07 and Cemdata18, accounting for their main differences. Summaries of the thermodynamic data compiled in the Cemdata18 database are available in formats supported (readable) by the computer programs GEM-Selektor [13,14] and PHREEQC [18]. Both of these Cemdata18 variants can be freely downloaded from <http://www.empa.ch/cemdata>.

2. Thermodynamic data for cements

Recent experimental data has enabled the Cemdata07 and Cemdata14 databases to be extended and refined [1,7,21]. We report this more comprehensive and refined dataset here as Cemdata18, compiled in several tables. Cemdata18 has been developed to predict changes in chemistry that occur during the hydration of Portland, blended and alkali activated cements, and also their interactions with service environments during use.

Table 1 reports the thermodynamic properties of minerals important for cementitious systems, while Table 2 reports their solubility products referring to the dominate species present at the high pH values of

cementitious systems. The data for hydrotalcite-like phases and detailed discussions of the different models for C-S-H are given in Sections 2.6 and 2.7. Standard thermodynamic data for minerals such as calcite, brucite and aqueous and gaseous species already documented in the PSI-Nagra chemical thermodynamic database [22] are not repeated in these tables, but given only in summary tables in Appendices B and D. To enable users to model cementitious systems using the Cemdata18 dataset with the law of mass action (LMA) geochemical modelling package PHREEQC [18], a variant of the Cemdata18 dataset has been generated as documented in Appendix B.

2.1. Solubility of $\text{Al}(\text{OH})_3$ and its effect on calcium aluminate and calcium sulfoaluminate cements

The solubility of precipitated $\text{Al}(\text{OH})_3$ decreases with time. Initially “amorphous” or poorly ordered $\text{Al}(\text{OH})_3$ precipitates with a solubility product of approximately 0 ± 0.2 . With time, the degree of ordering increases, and microcrystalline $\text{Al}(\text{OH})_3$ forms, while the solubility product decreases to -0.7 after 2 years. The solubility of hydrothermally prepared gibbsite is with -1.1 lower as illustrated in Fig. 1, however its formation is not expected within the timeframe of months to years generally considered for hydrating cements. At 60 °C and above, it is expected that microcrystalline $\text{Al}(\text{OH})_3$ does not persist, but that gibbsite forms relatively fast (Fig. 1). The solubility of $\text{Al}(\text{OH})_3$ determines whether CAH_{10} (as in the presence of $\text{Al}(\text{OH})_3$ with $\log K_{S0} \geq -0.6$ at 25 °C) is formed initially in calcium aluminate cements or whether it converts to C_3AH_6 and microcrystalline $\text{Al}(\text{OH})_3$ [12]. The decrease of the solubility of $\text{Al}(\text{OH})_3$ with time is also responsible for the initial occurrence of CAH_{10} and ettringite instead of monosulfate plus microcrystalline $\text{Al}(\text{OH})_3$ in some calcium sulfoaluminate cements, as discussed in more detail in [53].

Which $\text{Al}(\text{OH})_3$ modification (see Table 1) should be taken into account depends mainly on the timeframe and the temperature considered. While gibbsite should be allowed to form at temperatures above 60 °C, its precipitation should be suppressed for calculations at ambient temperatures, where microcrystalline $\text{Al}(\text{OH})_3$ will form instead. Within very short timeframes (minutes to hour), possibly only amorphous $\text{Al}(\text{OH})_3$ should be allowed to precipitate. Similarly, also the formation of some other stable phases such as goethite (FeOOH), hematite (Fe_2O_3) and quartz (SiO_2) should be suppressed in calculations of hydrated cements in favour of their more disperse counterparts: microcrystalline FeOOH (or microcrystalline or amorphous $\text{Fe}(\text{OH})_3$, depending on the timeframe considered), and amorphous SiO_2 .

2.2. Thaumasia

Damidot et al. [54] obtained solubility data to derive a solubility constant for thaumasite at 25 °C, at which temperature thaumasite was considered to be stable. Invariant points were calculated for phase assemblages including thaumasite in the system $\text{CaO}-\text{Al}_2\text{O}_3-\text{SiO}_2-\text{CaSO}_4-\text{CaCO}_3-\text{H}_2\text{O}$. Schmidt et al. [55] used the solubility data of Macphee and Barnett [56] to derive thermodynamic data for thaumasite over the temperature range 1 to 30 °C to confirm experimental data showing formation of thaumasite in mortars at 8 and 20 °C as shown in Fig. 2. Another set of solubility data at 8 °C for natural thaumasite was reported by Bellmann [57] who also highlighted the potential pathways of formation of thaumasite at this temperature. Macphee and Barnett [56] obtained the solubility data of ettringite-thaumasite solid solutions in the temperature range between 5 °C and 30 °C; no apparent decomposition of thaumasite and related solid solutions occurred after 6 months storage at 30 °C, which suggests the persistence of thaumasite at temperatures at least up to ~ 30 °C. A

Table 1

Cemdata18 database: Standard thermodynamic properties at 25 °C and 1 bar. Update of Cemdata07 [1,7,29]. The data are compatible with the GEMS version of the PSI/Nagra 12/07 TDB [22,23]. Standard properties of master species and properties of reactions of forming product species out of master species, commonly used in LMA programs such as PHREEQC, are compiled in the Appendix B.

	$\Delta_f G^\circ$ [kJ/mol]	$\Delta_f H^\circ$ [kJ/mol]	S° [J/K/mol]	a_0 [J/K/mol]	a_1 [J/mol/K ²]	a_2 [J K/mol]	a_3 [J/K ^{0.5} /mol]	V° [cm ³ /mol]	Ref
Aft-phases									
(Al-)ettringite ^{a,b,c}	−15,205.94	−17,535	1900	1939	0.789	−	−	707	[1,7]
C ₆ As ₃ H ₃₀ ^c	−14,728.1	−16,950.2	1792.4	1452	2.156	−	−	708	[30]
C ₆ As ₃ H ₁₃	−10,540.6	−11,530.3	1960.4	970.7	1.483	−	−	411	[30]
C ₆ As ₃ H ₉	−9540.4	−10,643.7	646.6	764.3	1.638	−	−	361	[30]
Tricarboaluminate ^a	−14,565.64	−16,792	1858	2042	0.559	−7.78·10 ⁶	−	650	[1,7]
Fe-ettringite ^b	−14,282.36	−16,600	1937	1922	0.855	2.02·10 ⁶	−	717	[1,21]
Thaumasite	−7564.52	−8700	897.1	1031	0.263	−3.40·10 ⁶	−	330	[28]
Hydrogarnet									
C ₃ AH ₆ ^d	−5008.2	−5537.3	422	290	0.644	−3.25·10 ⁶	−	150	[9,12]
C ₃ AS _{0.47} H _{5.18} ^{e,d}	−5192.9	−5699	399	310	0.566	−4.37·10 ⁶	−	146	[9]
C ₃ AS _{0.84} H _{4.32} ^{e,e}	−5365.2	−5847	375	331	0.484	−5.55·10 ⁶	−	142	[9]
C ₃ FH ₆ ^{e,f}	−4122.8	−4518	870	330	1.237	−4.74·10 ⁶	−	155	[9]
Al-Fe siliceous hydrogarnet (solid solution)									
C ₃ FS _{0.84} H _{4.32} ^{e,f}	−4479.9	−4823	840	371	0.478	−7.03·10 ⁶	−	149	[9]
C ₃ AS _{0.5} FS _{0.5} S _{0.84} H _{4.32} ^e	−4926.0	−5335	619	367	0.471	−8.10·10 ⁶	−	146	[9]
C ₃ FS _{1.34} H _{3.32}	−4681.1	−4994	820	395	0.383	−8.39·10 ⁶	−	145	[9]
Afm-phases									
C ₄ AH ₁₉	−8749.9	−10,017.9	1120	1163	1.047	−	−1600	369	[12,31]
C ₄ AH ₁₃ ^g	−7325.7	−8262.4	831.5	208.3	3.13	−	−	274	[31]
C ₄ AH ₁₁	−6841.4	−7656.6	772.7	0.0119	3.56	1.34·10 ^{−7}	−	257	[31]
C ₂ AH _{7.5}	−4695.5	−5277.5	450	323	0.728	−	−	180	[12]
CAH ₁₀	−4623.0	−5288.2	610	151	1.113	−	3200	193	[12]
C ₄ Ac _{0.5} H ₁₂	−7335.97	−8270	713	664	1.014	−1.30·10 ⁶	−800	285	[1,7]
C ₄ Ac _{0.5} H _{10.5}	−6970.3	−7813.3	668.3	0.0095	2.836	1.07·10 ^{−7}	−	261	[31]
C ₄ Ac _{0.5} H ₉	−6597.4	−7349.7	622.5	0.0088	2.635	9.94·10 ^{−8}	−	249	[31]
C ₄ AcH ₁₁	−7337.46	−8250	657	618	0.982	−2.59·10 ⁶	−	262	[1,7]
C ₄ AcH ₉	−6840.3	−7618.6	640.6	192.4	2.042	−	−	234	[31]
C ₄ AsH ₁₆	−8726.8	−9930.5	975.0	636	1.606	−	−	351	[31,32]
C ₄ AsH ₁₄	−8252.9	−9321.8	960.9	1028.5	−	−	−	332	[31,32]
C ₄ AsH ₁₁ ^{g,h}	−7778.4	−8758.6	791.6	175	2.594	−	−	310	[31,32]
C ₄ AsH _{10.5}	−7414.9	−8311.9	721	172	2.402	−	−	282	[31,32]
C ₄ AsH ₉	−7047.6	−7845.5	703.6	169	2.211	−	−	275	[31,32]
C ₂ ASH ₆ ⁱ	−5705.15	−6360	546	438	0.749	−1.13·10 ⁶	−800	216	[1,7]
C ₂ ASH ₇ ⁱ	−5464.0	−6066.8	487.6	0.0063	1.887	7.12·10 ^{−8}	−	215	[31]
C ₂ ASH _{5.5}	−5095.2	−5603.4	454.8	0.0057	1.685	6.36·10 ^{−8}	−	213	[31]
C ₄ As _{0.5} ClH ₁₂	−7533.4	−8472 ^j	820	557	1.141	−1.02·10 ⁶	751	289	[27,33]
C ₄ AlCl ₂ H ₁₀ ^k	−6810.9	−7604	731	498	0.895	−2.04·10 ⁶	1503	272	[33,34]
C ₄ A(NO ₃) ₂ H ₁₀	−6778.1	−7719.3	821	580	1.02	−2.77·10 ⁶	872	296	[34,35]
C ₄ A(NO ₂) ₂ H ₁₀	−6606.8	−7493.1	799	565	0.99	−2.24·10 ⁶	703	275	[34–36]
C ₄ FH ₁₃ ^o	−6438.6	−7435	630	694	1.113	2.02·10 ⁶	1600	286	[9]
C ₄ Fc _{0.5} H ₁₀	−5952.9	−6581	1270	308	1.201	−9.08·10 ⁵	3200	273	[8]
C ₄ FcH ₁₂	−6674.0	−7485	1230	612	1.157	−5.73·10 ⁵	−	292	[8]
C ₄ FsH ₁₂ ^h	−6873.2	−7663	1430	577	1.234	2.02·10 ⁶	−	321	[10]
C ₂ FSH ₈				Not stable					[37]
C ₄ FCl ₂ H ₁₀ ^k	−5900.1	−6528 ^l	1286	481	0.961	−1.61·10 ⁴	1503	278 ^l	[37]
Sulfates									
Cs (anhydrite)	−1322.12	−1434.60	106.7	70.2	−0.099	−	−	46	[22,23]
CsH ₂ (gypsum)	−1797.76	−2023.36	193.8	91.4	−0.318	−	−	75	[22,23]
CsH _{0.5} (hemihydrate)	−1436.34 ^m	−1575.3 ^m	134.3	124.1	−	−	−	62	[38]
Syngenite	−2884.91	−3172	326	201	0.308	−1.78·10 ⁶	−	128 ⁿ	[29]
(Hydr)oxides									
Al(OH) ₃ (am)	−1143.2	−		Not defined				32	[1]
Al(OH) ₃ (mic)	−1148.4	−1265.3 ^o	140 ^o	36	0.191	−	−	32	[12]
Al(OH) ₃ (gibbsite) ^a	−1151.0	−1288.7	70.1	36.2	0.191	−	−	32	[22,23]
Fe(OH) ₃ (am)	−700.1			Not defined					[22,23]
Fe(OH) ₃ (mic)	−711.6			Not defined					[22,23]
FeOOH(mic)	−480.14	−551.1	60	1.25	−0.233	−3.14·10 ⁵	−	21	[9,22]
FeOOH(goethite) ^a	−497.26	−568.2	60	1.25	−0.233	−3.14·10 ⁵	−	21	[22,23]
CH (portlandite)	−897.01	−985	83	187	−0.022	−	−1600	33	[22,23]
SiO ₂ (am)	−848.90	−903	41	47	0.034	−1.13·10 ⁶	−	29	[1,7]
SiO ₂ (quartz) ^a	−854.79	−909	41	47	0.034	−1.13·10 ⁶	−	29	[22,23]
Hydroxalite-pyroxaurite (solid solution)									
½M ₆ AcH ₁₃ ^p	−4339.85	−4875.9	411	512.6	−	−	−	115	[39]
½M ₆ FcH ₁₃ ^p	−3882.60	−4415.1	423	521.7	−	−	−	119	[39]

(continued on next page)

Table 1 (continued)

	$\Delta_f G^\circ$ [kJ/mol]	$\Delta_f H^\circ$ [kJ/mol]	S° [J/K/mol]	a_0 [J/K/mol]	a_1 [J/mol/K ²]	a_2 [J/K/mol]	a_3 [J/K ^{0.5} /mol]	V° [cm ³ /mol]	Ref
M-S-H (solid solution)									
M _{1.5} S ₂ H _{2.5} , Mg/Si = 0.75 ^a	−3218.43	−3507.52	270 ^f	318 ^f	−	−	−	95	[40]
M _{1.5} SH _{2.5} , Mg/Si = 1.5 ^h	−2355.66	−2594.22	216 ^f	250 ^f	−	−	−	74	[40]
Zeolites									
Zeolite P(Ca) [*]	−5057.8	−5423	779	753	−	−	−	153 ^s	[41]
Natrolite [*]	−5325.7	−5728	360	359	−	−	−	169 ^r	[41]
Chabazite	−7111.8	−7774	581	617	−	−	−	251 ^s	[41]
Zeolite X(Na)	−5847.5	−6447	566	586	−	−	−	214 ^s	[41]
Zeolite Y(Na)	−7552.5	−8327	734	739	−	−	−	283 ^u	[41]
Clinkers									
C ₃ S	−2784.33	−2931	169	209	0.036	−4.25·10 ⁶	−	73	[1,7,42]
C ₂ S	−2193.21	−2308	128	152	0.037	−3.03·10 ⁶	−	52	[1,7,42]
C ₃ A	−3382.35	−3561	205	261	0.019	−5.06·10 ⁶	−	89	[1,7,42]
C ₁₂ A ₇	−18,451.44	−19,414	1045	1263	0.274	−2.31·10 ⁷	−	518 ^v	[42]
CA	−2207.90	−2327	114	151	0.042	−3.33·10 ⁶	−	54 ^w	[42]
CA ₂	−3795.31	−4004	178	277	0.023	−7.45·10 ⁶	−	89 ^x	[42]
C ₄ AF	−4786.50	−5080	326	374	0.073	−	−	130	[1,7,42]
C (lime)	−604.03	−635	39.7	48.8	0.0045	−6.53·10 ⁵	−	17	[43]
Ks (K ₂ SO ₄ arcanite)	−1319.60	−1438	176	120	0.100	−1.78·10 ⁶	−	66	[44]
K (K ₂ O)	−322.40	−363	94	77	0.036	−3.68·10 ⁵	−	40	[43]
Ns (Na ₂ SO ₄ thenardite)	−1269.80	−1387	150	58	0.023	−	−	53	[44]
N (Na ₂ O)	−376.07	−415	75	76	0.020	−1.21·10 ⁶	−	25	[43]

a_0 , a_1 , a_2 , a_3 are the empirical coefficients of the heat capacity function: $C_p^\circ = a_0 + a_1T + a_2T^{-2} + a_3T^{-0.5}$; heat capacity functions for cement hydrates are typically valid up to 100 °C only; "−" = 0. Cement shorthand notation is used: A = Al₂O₃; C = CaO; F = Fe₂O₃; H = H₂O; M = MgO; S = SiO₂; c = CO₂; s = SO₃;
^{*} Precipitates very slowly at 20 °C, generally not included in calculations.

^{**} Tentative value.

^a Non-ideal solid solutions; miscibility gap: $X_{\text{CO}_3, \text{solid}} = 0.45\text{--}0.90$ reproduced with the dimensionless Guggenheim interaction parameters $\alpha_0 = 1.67$ and $\alpha_1 = 0.946$; downscaled in this paper to 1CO₂: 1SO₃ replacement, instead of the 3CO₂: 3SO₃ used in [4,7].

^b Non-ideal solid solution; miscibility gap: $X_{\text{Al}, \text{solid}} = 0.25\text{--}0.65$ reproduced with the dimensionless Guggenheim interaction parameters $\alpha_0 = 2.1$ and $\alpha_1 = -0.169$ [45].

^c Ideal solid solutions c.f. [9,11,30,39].

^d Ideal solid solutions c.f. [9,11,30,39].

^e Ideal solid solutions c.f. [9,11,30,39].

^f Ideal solid solutions c.f. [9,11,30,39].

^g Non-ideal solid solutions; miscibility gap: $X_{\text{OH}, \text{solid}} = 0.50\text{--}0.97$ reproduced with the dimensionless Guggenheim interaction parameters $\alpha_0 = 0.188$ and $\alpha_1 = 2.49$ [7].

^h Non-ideal solid solutions; miscibility gap: $X_{\text{Al}, \text{solid}} = 0.45\text{--}0.95$ reproduced with the dimensionless Guggenheim interaction parameters $\alpha_0 = 1.26$ and $\alpha_1 = 1.57$ [10].

ⁱ Ideal solid solutions c.f. [9,11,30,39].

^j Typing error in [27], recalculated from G_f° and S from [27].

^k Ideal solid solutions c.f. [9,11,30,39].

^l Typing error in [37], recalculated from G_f° and S from [37]. Volume calculated from XRD data [37].

^m Recalculated from ΔG_f° of −20,500 J/mol [38].

ⁿ Calculated from density data from [33,46].

^o Valid up to 60 °C only, estimated to describe solubility of microcrystalline Al(OH)₃ aged for 19 months between 5 and 60 °C [12].

^p Ideal solid solutions c.f. [9,11,30,39].

^q Ideal solid solutions c.f. [9,11,30,39].

^r Estimated from C_p and S of talc, chrysotile and H₂O using data from [43].

^s Volume from [47].

^t Calculated from XRD data: pdf 00-038-0237 [48].

^u Calculated from XRD data; pdf 00-039-1380 [49].

^v [50].

^w [51].

^x [52].

complete solubility dataset representative for the stability range of thaumasite was missing, as [56] reported the solubility data for thaumasite-ettringite solid-solutions but not for pure thaumasite. Hence, due to a lack of experimental data, no thermodynamic data for thaumasite were included in the Cemdata07 database, but were added in a first update using the data derived in Schmidt et al. [55] based on the solubility data given by Macphee and Barnett [49]. In 2015, Matschei and Glasser [28] published a new dataset obtained on apparently pure-

phase synthetic thaumasite. It was shown that pure thaumasite was thermally stable up to 68 ± 5 °C. The obtained new data agreed well, within limits of error, with those obtained by Macphee and Barnett [56], but differs significantly from the data for natural thaumasite reported by Bellmann [57] at 8 °C. Experiments done by [28,56] excluded atmospheric carbon dioxide, whereas the solubility determinations reported in [57] were made in the presence of air containing carbon dioxide. The contact with the air may lead to the decomposition of

Table 2

Equilibrium solubility products of solids and formation constants for calcium-silica complexes at 1 bar, 25 °C in Cemdata18 (as given in Table 1).

Mineral	log K_{SO}	Dissolution reactions used to calculate solubility products.
Solids		
(Al-)ettringite	−44.9	$\text{Ca}_6\text{Al}_2(\text{SO}_4)_3(\text{OH})_{12} \cdot 26\text{H}_2\text{O} \rightarrow 6\text{Ca}^{2+} + 2\text{Al}(\text{OH})_4^- + 3\text{SO}_4^{2-} + 4\text{OH}^- + 26\text{H}_2\text{O}$
tricarboaluminate	−46.5	$\text{Ca}_6\text{Al}_2(\text{CO}_3)_3(\text{OH})_{12} \cdot 26\text{H}_2\text{O} \rightarrow 6\text{Ca}^{2+} + 2\text{Al}(\text{OH})_4^- + 3\text{CO}_3^{2-} + 4\text{OH}^- + 26\text{H}_2\text{O}$
Fe-ettringite	−44.0	$\text{Ca}_6\text{Fe}_2(\text{SO}_4)_3(\text{OH})_{12} \cdot 26\text{H}_2\text{O} \rightarrow 6\text{Ca}^{2+} + 2\text{Fe}(\text{OH})_4^- + 3\text{SO}_4^{2-} + 4\text{OH}^- + 26\text{H}_2\text{O}$
thaumasite	−24.75	$\text{Ca}_3(\text{SiO}_3)(\text{SO}_4)(\text{CO}_3) \cdot 15\text{H}_2\text{O} \rightarrow 3\text{Ca}^{2+} + \text{H}_3\text{SiO}_4^- + \text{SO}_4^{2-} + \text{CO}_3^{2-} + \text{OH}^- + 13\text{H}_2\text{O}$
C_3AH_6	−20.50	$\text{Ca}_3\text{Al}_2(\text{OH})_{12} \rightarrow 3\text{Ca}^{2+} + 2\text{Al}(\text{OH})_4^- + 4\text{OH}^-$
$\text{C}_3\text{AS}_{0.41}\text{H}_{5.18}^*$	−25.35	$\text{Ca}_3\text{Al}_2(\text{SiO}_4)_{0.41}(\text{OH})_{10.36} \rightarrow 3\text{Ca}^{2+} + 2\text{Al}(\text{OH})_4^- + 0.41 \text{ SiO}(\text{OH})_3^- + 3.59\text{OH}^- - 1.23\text{H}_2\text{O}$
$\text{C}_3\text{AS}_{0.84}\text{H}_{4.32}^*$	−26.70	$\text{Ca}_3\text{Al}_2(\text{SiO}_4)_{0.84}(\text{OH})_{8.64} \rightarrow 3\text{Ca}^{2+} + 2\text{Al}(\text{OH})_4^- + 0.84 \text{ SiO}(\text{OH})_3^- + 3.16\text{OH}^- - 2.52\text{H}_2\text{O}$
C_3FH_6	−26.30 ⁺	$\text{Ca}_3\text{Fe}_2(\text{OH})_{12} \rightarrow 3\text{Ca}^{2+} + 2\text{Fe}(\text{OH})_4^- + 4\text{OH}^-$
$\text{C}_3\text{FS}_{0.84}\text{H}_{4.32}$	−32.50	$\text{Ca}_3\text{Fe}_2(\text{SiO}_4)_{0.84}(\text{OH})_{8.64} \rightarrow 3\text{Ca}^{2+} + 2\text{Fe}(\text{OH})_4^- + 0.84 \text{ SiO}(\text{OH})_3^- + 3.16\text{OH}^- - 2.52\text{H}_2\text{O}$
$\text{C}_3(\text{F,A})\text{S}_{0.84}\text{H}_{4.32}$	−30.20	$\text{Ca}_3\text{FeAl}(\text{SiO}_4)_{0.84}(\text{OH})_{8.64} \rightarrow 3\text{Ca}^{2+} + \text{Al}(\text{OH})_4^- + \text{Fe}(\text{OH})_4^- + 0.84 \text{ SiO}(\text{OH})_3^- + 3.16\text{OH}^- - 2.52\text{H}_2\text{O}$
$\text{C}_3\text{FS}_{1.34}\text{H}_{3.32}$	−34.20	$\text{Ca}_3\text{Fe}_2(\text{SiO}_4)_{1.34}(\text{OH})_{6.64} \rightarrow 3\text{Ca}^{2+} + 2\text{Fe}(\text{OH})_4^- + 1.34 \text{ SiO}(\text{OH})_3^- + 2.66\text{OH}^- - 4.02\text{H}_2\text{O}$
C_4AH_{19}	−25.45	$\text{Ca}_4\text{Al}_2(\text{OH})_{14} \cdot 12\text{H}_2\text{O} \rightarrow 4\text{Ca}^{2+} + 2\text{Al}(\text{OH})_4^- + 6\text{OH}^- + 12\text{H}_2\text{O}$
C_4AH_{13}	−25.25 ^{***}	$\text{Ca}_4\text{Al}_2(\text{OH})_{14} \cdot 6\text{H}_2\text{O} \rightarrow 4\text{Ca}^{2+} + 2\text{Al}(\text{OH})_4^- + 6\text{OH}^- + 6\text{H}_2\text{O}$
$\text{C}_2\text{AH}_{7.5}$	−13.80	$\text{Ca}_2\text{Al}_2(\text{OH})_{10} \cdot 2.5\text{H}_2\text{O} \rightarrow 2\text{Ca}^{2+} + 2\text{Al}(\text{OH})_4^- + 2\text{OH}^- + 2.5\text{H}_2\text{O}$
CAH_{10}	−7.60	$\text{CaAl}_2(\text{OH})_8 \cdot 6\text{H}_2\text{O} \rightarrow \text{Ca}^{2+} + 2\text{Al}(\text{OH})_4^- + 6\text{H}_2\text{O}$
$\text{C}_4\text{Ac}_{0.5}\text{H}_{12}$	−29.13	$\text{Ca}_4\text{Al}_2(\text{CO}_3)_{0.5}(\text{OH})_{13} \cdot 7\text{H}_2\text{O} \rightarrow 4\text{Ca}^{2+} + 2\text{Al}(\text{OH})_4^- + 0.5\text{CO}_3^{2-} + 5\text{OH}^- + 7\text{H}_2\text{O}$
$\text{C}_4\text{AcH}_{11}$	−31.47	$\text{Ca}_4\text{Al}_2(\text{CO}_3)(\text{OH})_{12} \cdot 5\text{H}_2\text{O} \rightarrow 4\text{Ca}^{2+} + 2\text{Al}(\text{OH})_4^- + \text{CO}_3^{2-} + 4\text{OH}^- + 5\text{H}_2\text{O}$
$\text{C}_4\text{AsH}_{14}$	−29.26	$\text{Ca}_4\text{Al}_2(\text{SO}_4)(\text{OH})_{12} \cdot 6\text{H}_2\text{O} \rightarrow 4\text{Ca}^{2+} + 2\text{Al}(\text{OH})_4^- + \text{SO}_4^{2-} + 4\text{OH}^- + 6\text{H}_2\text{O}$
$\text{C}_4\text{AsH}_{12}$	−29.23 ^{***}	$\text{Ca}_4\text{Al}_2(\text{SO}_4)(\text{OH})_{12} \cdot 6\text{H}_2\text{O} \rightarrow 4\text{Ca}^{2+} + 2\text{Al}(\text{OH})_4^- + \text{SO}_4^{2-} + 4\text{OH}^- + 6\text{H}_2\text{O}$
C_2ASH_8	−19.70	$\text{Ca}_2\text{Al}_2\text{SiO}_2(\text{OH})_{10} \cdot 3\text{H}_2\text{O} \rightarrow 2\text{Ca}^{2+} + 2\text{Al}(\text{OH})_4^- + \text{SiO}(\text{OH})_3^- + \text{OH}^- + 2\text{H}_2\text{O}$
Friedel's salt	−27.27	$\text{Ca}_4\text{Al}_2\text{Cl}_2(\text{OH})_{12} \cdot 4\text{H}_2\text{O} \rightarrow 4\text{Ca}^{2+} + 2\text{Al}(\text{OH})_4^- + 2\text{Cl}^- + 4\text{OH}^- + 4\text{H}_2\text{O}$
Kuzel's salt	−28.53	$\text{Ca}_4\text{Al}_2\text{Cl}(\text{SO}_4)_{0.5}(\text{OH})_{12} \cdot 6\text{H}_2\text{O} \rightarrow 4\text{Ca}^{2+} + 2\text{Al}(\text{OH})_4^- + \text{Cl}^- + 0.5\text{SO}_4^{2-} + 4\text{OH}^- + 6\text{H}_2\text{O}$
Nitrate-AFm	−28.67	$\text{Ca}_4\text{Al}_2(\text{OH})_{12}(\text{NO}_3)_2 \cdot 4\text{H}_2\text{O} \rightarrow 4\text{Ca}^{2+} + 2\text{Al}(\text{OH})_4^- + 2\text{NO}_3^- + 4\text{OH}^- + 4\text{H}_2\text{O}$
Nitrite-AFm	−26.24	$\text{Ca}_4\text{Al}_2(\text{OH})_{12}(\text{NO}_2)_2 \cdot 4\text{H}_2\text{O} \rightarrow 4\text{Ca}^{2+} + 2\text{Al}(\text{OH})_4^- + 2\text{NO}_2^- + 4\text{OH}^- + 4\text{H}_2\text{O}$
C_4FH_{13}	−30.75 ⁺	$\text{Ca}_4\text{Fe}_2(\text{OH})_{14} \cdot 6\text{H}_2\text{O} \rightarrow 4\text{Ca}^{2+} + 2\text{Fe}(\text{OH})_4^- + 6\text{OH}^- + 6\text{H}_2\text{O}$
Fe-hemicarbonate	−30.83	$\text{Ca}_4\text{Fe}_2(\text{CO}_3)_{0.5}(\text{OH})_{13} \cdot 3.5\text{H}_2\text{O} \rightarrow 4\text{Ca}^{2+} + 2\text{Fe}(\text{OH})_4^- + 0.5\text{CO}_3^{2-} + 5\text{OH}^- + 3.5\text{H}_2\text{O}$
Fe-monocarbonate	−34.59	$\text{Ca}_4\text{Fe}_2(\text{CO}_3)(\text{OH})_{12} \cdot 6\text{H}_2\text{O} \rightarrow 4\text{Ca}^{2+} + 2\text{Fe}(\text{OH})_4^- + \text{CO}_3^{2-} + 4\text{OH}^- + 6\text{H}_2\text{O}$
Fe-monosulfate	−31.57	$\text{Ca}_4\text{Fe}_2(\text{SO}_4)(\text{OH})_{12} \cdot 6\text{H}_2\text{O} \rightarrow 4\text{Ca}^{2+} + 2\text{Fe}(\text{OH})_4^- + \text{SO}_4^{2-} + 4\text{OH}^- + 6\text{H}_2\text{O}$
Fe-Friedel's salt	−28.62	$\text{Ca}_4\text{Fe}_2\text{Cl}_2(\text{OH})_{12} \cdot 4\text{H}_2\text{O} \rightarrow 4\text{Ca}^{2+} + 2\text{Fe}(\text{OH})_4^- + 2\text{Cl}^- + 4\text{OH}^- + 4\text{H}_2\text{O}$
Cs (anhydrite)	−4.357	$\text{CaSO}_4 \rightarrow \text{Ca}^{2+} + \text{SO}_4^{2-}$
CsH ₂ (gypsum)	−4.581	$\text{CaSO}_4 \cdot 2\text{H}_2\text{O} \rightarrow \text{Ca}^{2+} + \text{SO}_4^{2-} + 2\text{H}_2\text{O}$
CsH _{0.5} (hemihydrate)	−3.59	$\text{CaSO}_4 \cdot 0.5\text{H}_2\text{O} \rightarrow \text{Ca}^{2+} + \text{SO}_4^{2-} + 0.5\text{H}_2\text{O}$
synnenite	−7.20	$\text{K}_2\text{Ca}(\text{SO}_4)_2 \cdot \text{H}_2\text{O} \rightarrow 2\text{K}^+ + \text{Ca}^{2+} + 2\text{SO}_4^{2-} + \text{H}_2\text{O}$
$\text{Al}(\text{OH})_3(\text{am})$	0.24	$\text{Al}(\text{OH})_3(\text{am}) \rightarrow \text{Al}(\text{OH})_4^- - \text{OH}^-$
$\text{Al}(\text{OH})_3(\text{mic})$	−0.67	$\text{Al}(\text{OH})_3(\text{mic}) \rightarrow \text{Al}(\text{OH})_4^- - \text{OH}^-$
$\text{Al}(\text{OH})_3(\text{gibbsite})^*$	−1.12	$\text{Al}(\text{OH})_3(\text{gibbsite}) \rightarrow \text{Al}(\text{OH})_4^- - \text{OH}^-$
$\text{Fe}(\text{OH})_3(\text{am})$	−2.6	$\text{Fe}(\text{OH})_3(\text{am}) \rightarrow \text{Fe}(\text{OH})_4^- - \text{OH}^-$
$\text{Fe}(\text{OH})_3(\text{mic})$	−4.6	$\text{Fe}(\text{OH})_3(\text{mic}) \rightarrow \text{Fe}(\text{OH})_4^- - \text{OH}^-$
$\text{FeOOH}(\text{mic})$	−5.6	$\text{FeOOH}(\text{mic}) \rightarrow \text{Fe}(\text{OH})_4^- - \text{OH}^- - \text{H}_2\text{O}$
$\text{FeOOH}(\text{goethite})^*$	−8.6	$\text{FeOOH}(\text{goethite}) \rightarrow \text{Fe}(\text{OH})_4^- - \text{OH}^- - \text{H}_2\text{O}$
CH	−5.2	$\text{Ca}(\text{OH})_2 \rightarrow \text{Ca}^{2+} + 2\text{OH}^-$
$\text{SiO}_2(\text{am})$	−2.714	$\text{SiO}_2(\text{am}) \rightarrow \text{SiO}_2^0$
$\text{SiO}_2(\text{quartz})^*$	−3.746	$\text{SiO}_2(\text{quartz}) \rightarrow \text{SiO}_2^0$
$1/2\text{M}_6\text{AcH}_{13}$	−33.29 ^{***}	$\text{Mg}_3\text{Al}(\text{OH})_8(\text{CO}_3)_{0.5} \cdot 2.5\text{H}_2\text{O} \rightarrow 3\text{Mg}^{2+} + \text{Al}(\text{OH})_4^- + 0.5\text{CO}_3^{2-} + 4\text{OH}^- + 2.5\text{H}_2\text{O}$
$1/2\text{M}_6\text{FeH}_{13}$	−33.64 ^{***}	$\text{Mg}_3\text{Fe}(\text{OH})_8(\text{CO}_3)_{0.5} \cdot 2.5\text{H}_2\text{O} \rightarrow 3\text{Mg}^{2+} + \text{Fe}(\text{OH})_4^- + 0.5\text{CO}_3^{2-} + 4\text{OH}^- + 2.5\text{H}_2\text{O}$
$\text{M}_{1.5}\text{S}_2\text{H}_{2.5}$	−28.80	$(\text{MgO})_{1.5}(\text{SiO}_2)_2(\text{H}_2\text{O})_{2.5} \rightarrow 1.5\text{Mg}^{2+} + 2\text{SiO}_2^0 + 3\text{OH}^- + \text{H}_2\text{O}$
$\text{M}_{1.5}\text{SH}_{2.5}$	−23.57	$(\text{MgO})_{1.5}\text{SiO}_2(\text{H}_2\text{O})_{2.5} \rightarrow 1.5\text{Mg}^{2+} + \text{SiO}_2^0 + 3\text{OH}^- + \text{H}_2\text{O}$
<i>Zeolite P</i> (Ca) [*]	−20.3	$\text{CaAl}_2\text{Si}_2\text{O}_8 \cdot 4.5\text{H}_2\text{O} \rightarrow \text{Ca}^{2+} + 2\text{Al}(\text{OH})_4^- + 2\text{SiO}_2^0 + 0.5\text{H}_2\text{O}$
<i>Natrolite</i> [*]	−30.2	$\text{Na}_2\text{Al}_2\text{Si}_3\text{O}_{10} \cdot 2\text{H}_2\text{O} \rightarrow 2\text{Na}^+ + 2\text{Al}(\text{OH})_4^- + 3\text{SiO}_2^0 - 2\text{H}_2\text{O}$
Chabazite	−25.8	$\text{CaAl}_2\text{Si}_4\text{O}_{12} \cdot 6\text{H}_2\text{O} \rightarrow \text{Ca}^{2+} + 2\text{Al}(\text{OH})_4^- + 4\text{SiO}_2^0 + 2\text{H}_2\text{O}$
Zeolite X(Na)	−20.1	$\text{Na}_2\text{Al}_2\text{Si}_2\text{O}_9 \cdot 6.2\text{H}_2\text{O} \rightarrow 2\text{Na}^+ + 2\text{Al}(\text{OH})_4^- + 2.5\text{SiO}_2^0 + 2.2\text{H}_2\text{O}$
Zeolite Y(Na)	−25.0	$\text{Na}_2\text{Al}_2\text{Si}_4\text{O}_{12} \cdot 8\text{H}_2\text{O} \rightarrow 2\text{Na}^+ + 2\text{Al}(\text{OH})_4^- + 4\text{SiO}_2^0 + 4\text{H}_2\text{O}$
Calcium silicate complexes		
CaHSiO_3^+	1.2 ^{sv}	$\text{Ca}^{2+} + \text{HSiO}_3^{2-} \rightarrow \text{CaHSiO}_3^+$
CaSiO_3^0	4.6 ^{sv}	$\text{Ca}^{2+} + \text{SiO}_3^{2-} \rightarrow \text{CaSiO}_3^0$

* Precipitates very slowly at 20 °C, generally not included in calculations.

** Tentative value.

*** Recalculated in this paper from ΔG_f° values.*^v The formation of less strong calcium silicate complexes have been recently suggested ($\log K(\text{CaHSiO}_3^+) = 0.5$ and $\log K(\text{CaSiO}_3^0) = 2.9$. Within Cemdata18, however, the listed values for calcium silicate complexes have to be used to maintain compatibility with the C-S-H models.

thaumasite, which would make the interpretation of the solubility data invalid.

The heat capacities were estimated using a reference reaction with a solid having a known heat capacity and similar structure, as discussed in more detail in [28,55]. As shown by Helgeson et al. [43], this principle can be successfully applied to estimate the heat capacity of silicate minerals by formulating a reaction involving a structurally-related mineral of known heat capacity.

Finally, it is possible to do an internal consistency check and

recalculate solubilities under the chosen experimental conditions with the thermodynamic data of the Cemdata18 dataset. As illustrated in Fig. 3, the calculated solubility data for thaumasite show generally good agreement with the experimentally-derived dataset. Despite an underestimation of the calculated silicon concentrations at 1 °C and 5 °C, both datasets, experimental and calculated, generally agree, proving the internal consistency of the data. Especially in the temperature range from 1 to ~40 °C, where the solid phase assemblage consists mainly of thaumasite and traces of calcite, differences between

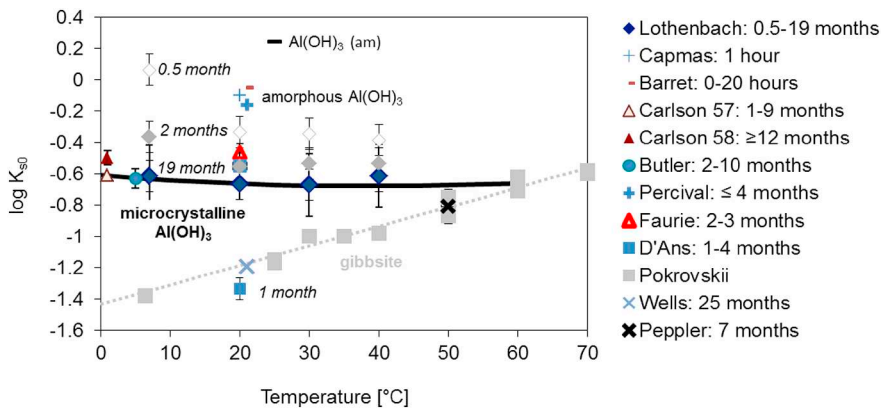


Fig. 1. Logarithm of the solubility product of Al(OH)_3 (referring to Al(OH)_4^- and OH^-) as a function of time and temperature calculated from the literature, adapted from [12]. Gibbsite solubility (dotted line) was calculated using data from the GEMS version of the PSI/Nagra 12/07 TDB [22,23], whereas the solubility of microcrystalline Al(OH)_3 (black line) and amorphous Al(OH)_3 (black hyphen) was calculated based on the data given in Table 1.

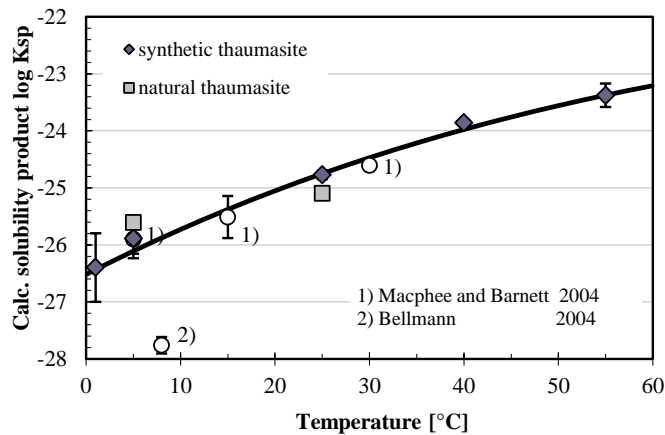


Fig. 2. Calculated solubility products referring to Ca^{2+} , SiO(OH)_3^- , SO_4^{2-} , CO_3^{2-} , OH^- and H_2O of synthetic and natural thaumasite samples from solubility experiments. The curve shows the calculated best fit using a three-term temperature extrapolation. Reproduced from [28].

experimental calcium and sulfate concentrations are within analytical errors. In the temperature range 1°C to $\sim 40^\circ\text{C}$, concentrations of calcium, sulfate and silicon increase with rising temperature, whereas calculated carbonate concentrations show a continuous decrease. At temperatures $> \sim 40^\circ\text{C}$, calcium and sulfate concentrations increase significantly, whereas silicon concentrations decrease due to the formation of C-S-H. Thaumasite is absent at temperatures above 70°C .

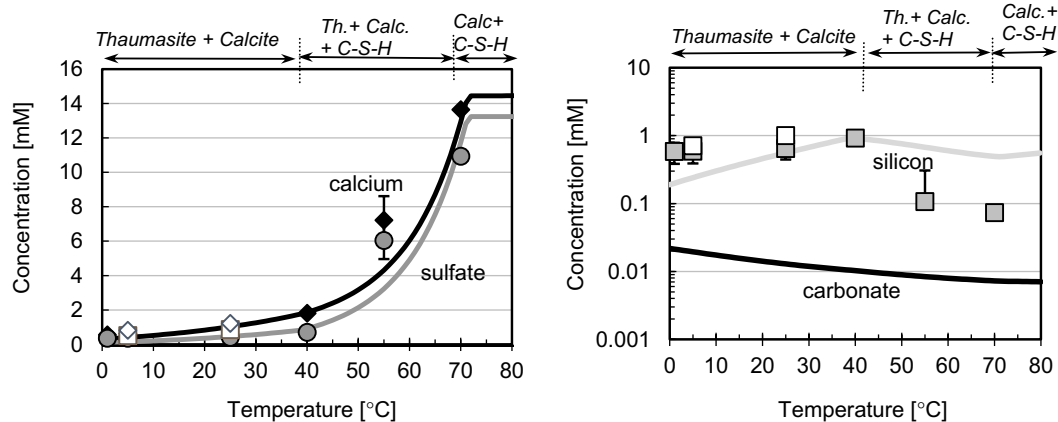


Fig. 3. Experimentally measured (markers) and re-calculated (lines) solubility data for thaumasite; (filled markers represent the experimental data for synthetic thaumasite, open markers – the data for natural thaumasite from [28]). Calculations are based on the new thermodynamic data for thaumasite complemented with the CSHQ data from Cemdata18 [1,7]. Predicted solid phases/phase assemblages are shown along the top.

2.3. Chloride-, nitrate-, and nitrite-Afm phases

Binding of chloride and the formation of chloride bearing cement hydrates has been widely studied due to its impact on the corrosion of steel in reinforced concrete. The first comprehensive solubility data for Friedel's salt ($\text{Ca}_4\text{Al}_2\text{Cl}_2(\text{OH})_{12}\cdot 4\text{H}_2\text{O}$) and Kuzel's salt ($\text{Ca}_4\text{Al}_2\text{Cl}(\text{SO}_4)_{0.5}(\text{OH})_{12}\cdot 6\text{H}_2\text{O}$) were provided in the late nineties. Birnin-Yauri [58] has described the dissolution of Friedel's salt as congruent and provided values of $\log K_{\text{so}}$ as -27.1 and -24.8 ($K_{\text{so}} = \{\text{Ca}^{2+}\}^4\{\text{Al(OH)}_4^-\}^2\{\text{Cl}^-\}^2\{\text{OH}^-\}^4\{\text{H}_2\text{O}\}^4$). Hobbs [59] estimated $\log K_{\text{so}}$ as -27.6 ± 0.9 and Bothe [60] has estimated via geochemical modelling that the solubility product of Friedel's salt should fall within the range $-28.8 < \log K_{\text{so}} < -27.6$. Balonis et al. [27] provided solubility data for Friedel's salt as a function of time and temperature with an estimated value of solubility product for an ideal composition and at room temperature to be -27.27 [34,36]. Compilation of the available solubility data is shown by triangles on Fig. 4.

The estimated thermodynamic data [36] ($\Delta_f G^\circ \sim -6810.9$ kJ/mol, $\Delta_f H^\circ \sim -7604$ kJ/mol, S° 731 J/mol K) have similar values (except the entropy) to the dataset published by Blanc et al. [16] ($\Delta_f G^\circ \sim -6815.44$ kJ/mol, $\Delta_f H^\circ \sim -7670.04$ kJ/mol, S° 527.70 J/mol K), and agree reasonably well with the data obtained by Grishchenko et al. [61] ($\Delta_f G^\circ$ estimated in a range between 6800 and 6860 kJ/mol, $S^\circ \sim 680$ J/mol K), though it should be kept in mind that Grishchenko's composition is reported to be slightly contaminated with carbonate ions. Attempts to synthesize Cl-AfT at temperatures above 0°C were unsuccessful [34], hence no thermodynamic data are available that can be used.

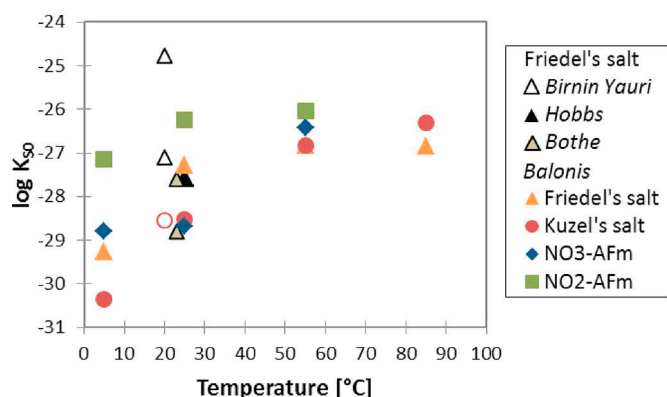


Fig. 4. Solubility products of Friedel's salt, Kuzel's salt, $\text{NO}_3\text{-AFm}$ and $\text{NO}_2\text{-AFm}$ (referring to reactions using Ca^{2+} , Cl^- , SO_4^{2-} , NO_3^- , NO_2^- , OH^- and H_2O as indicated in Table 2) as a function of temperature. Data for Friedel's salt from [27,58–60,62], data for other AFm are from Balonis and co-workers [27,34–36].

Glasser et al. [62] first measured the solubility of Kuzel's salt and noted that its dissolution is strongly incongruent, with ettringite precipitating as a secondary phase. From the solubility data given by Glasser et al. a $\log K_{s0}$ of Kuzel's salt -28.54 ($K_{s0} = \{\text{Ca}^{2+}\}^4\{\text{Al}(\text{OH})_4^-\}^2\{\text{Cl}^-\}\{\text{SO}_4^{2-}\}^{0.5}\{\text{OH}^-\}^4\{\text{H}_2\text{O}\}^6$) was estimated [27]. Balonis et al. [27] has also experimentally derived the solubility data and calculated solubility products for Kuzel's salt at different temperatures ranging from 5 to 85 °C for the period between 1 and 12 months, with the solubility product at room temperature determined to be $\log K_{s0} = -28.53$. Data for 12 months are shown by the filled circles in Fig. 4.

In recent years, the impact of soluble nitrate and nitrite corrosion inhibitors on the mineralogy of cement pastes has been studied [34,36,63], and it has been demonstrated that the AFm phase has the ability to accommodate NO_3^- and NO_2^- ions in the interlayer position. Solubility data along with thermodynamic parameters for the nitrate AFm ($\text{NO}_3\text{-AFm}$) and nitrite AFm ($\text{NO}_2\text{-AFm}$) published by Balonis et al. [34,35] are shown in Fig. 4. Similarly, as in the case of Cl-Aft , an attempted synthesis of $\text{NO}_3\text{-}$ or $\text{NO}_2\text{-Aft}$ at room temperature was not successful [34].

2.4. Iron containing hydrates

The main source of iron in cements is 5–15% ferrite clinker in Portland cements and slag in blended cements. In synthetic systems containing only water, C_2F , calcium sulfate, calcium carbonate or silica, different Fe-containing phases like ettringite, monosulfate,

monocarbonate, siliceous hydrogarnet can precipitate, as well as form solid solutions with their Al-containing analogues [8–10,21].

The stability of Fe-containing phases generally is only moderately affected by temperature, as shown in Fig. 5. At ambient temperature, Fe-ettringite ($\text{C}_6\text{FsH}_{32}$), Fe-monosulfate ($\text{C}_4\text{FsH}_{12}$), Fe-monocarbonate ($\text{C}_4\text{FCH}_{12}$), Fe-Friedel's salt ($\text{C}_4\text{FCl}_2\text{H}_{10}$), and Fe-siliceous hydrogarnet ($\text{C}_3\text{FS}_{0.95}\text{H}_{4.1}$, $\text{C}_3\text{FS}_{1.52}\text{H}_{2.96}$) are stable, while Fe-katoite (C_3FH_6) and Fe-hemicarbonate ($\text{C}_4\text{Fc}_{0.5}\text{H}_{10}$) are metastable [8–10,21,37]. Attempts to synthesize Fe-strätlingite (C_2FSH_8) failed, as only portlandite, C-S-H and iron hydroxide formed, indicating the instability of Fe-strätlingite at ambient conditions. $\text{C}_4\text{FsH}_{12}$, $\text{C}_4\text{FCH}_{12}$, and $\text{C}_4\text{FCl}_2\text{H}_{10}$ are also stable at 50 °C but not at 80 °C, while Fe-siliceous hydrogarnet is stable at up to 110 °C. The limited stability field of the Fe-containing AFm and Aft hydrates is related to the very high stability of goethite (FeOOH) and hematite (Fe_2O_3), which form at 50 °C within several months and at 80 °C within days [9]. Although hematite and portlandite would be more stable than the Fe-katoite, Aft and AFm phases between 0 and 100 °C, the formation of goethite and hematite at ambient temperatures is very slow, such that Fe-containing siliceous hydrogarnet, Aft and AFm phases can be synthesized instead. Fig. 3 shows the solubility products of Fe-containing phases calculated based on the measured composition of the liquid phase at 20, 50 and 80 °C; those data were used to derive the thermodynamic data for standard conditions (25 °C, 1 atm) given in Table 1. The formation of solid solutions between Al and Fe-containing endmembers has been observed for ettringite, siliceous hydrogarnet, monosulfate, and Friedel's salt, while no solid solution formed between the rhombohedral Fe-monocarbonate with the triclinic Al-monocarbonate due to the structural differences [8–10,21,37].

While different Fe-containing hydrates could be synthesized, only Fe-siliceous hydrogarnet is expected to occur in hydrated cements. The solubility product of Fe-siliceous hydrogarnet (given in Table 1) is 5 to 7 log units lower than that of Al-siliceous hydrogarnet indicating a high stabilization of Fe-siliceous hydrogarnet, while the solubility products of the Fe-containing hydrates are comparable or only somewhat more stable than their Al-containing analogues. In fact, in hydrated PC, Fe (III) precipitates as iron hydroxide during the first hours and as siliceous hydrogarnet ($\text{C}_3(\text{A},\text{F})\text{S}_{0.84}\text{H}_{4.32}$) after 1 day and longer [64–66]. The data for the $\text{C}_3\text{FS}_{0.84}\text{H}_{4.32}$ and for the mixed Al- and Fe-containing $\text{C}_3\text{A}_{0.5}\text{F}_{0.5}\text{S}_{0.84}\text{H}_{4.32}$ determined by Dilnesa et al. [9] are included in Cemdata18, but not the data for the Al-based $\text{C}_3\text{AS}_{0.84}\text{H}_{4.32}$ due to its formation being kinetically hindered at ambient conditions [9].

2.5. Effect of relative humidity

Cement hydrates are known to show varying water content as functions of temperature and relative humidity (RH). Some of these hydrates are crystalline phases with layered structure such as the AFm-phases or ettringite-type structures. The AFm and Aft phases have different hydration states (i.e. varying molar water content) depending on the exposure conditions, which can impact the volume stability, porosity and density of cement paste. The molar volume of some AFm phases can decrease by as much as 20% during drying [31], which may strongly influence the porosity and performance of some cementitious systems.

In gel-like phases such as C-S-H, water can be present within the intrinsic gel porosity, as well as in its interlayer. Unfortunately, until recently there was no thermodynamic model capable of assessing this varying water content.

The crystalline AFm phases have a layered structure and are known for their varying water content in the interlayer, which can be of two types. Firstly, the “space filling”, loosely integrated zeolitic water molecules, which are easily removed from the structure upon increase of temperature or at an initial small decrease of RH and have thermodynamic properties close to liquid water. Secondly, the “structural water” molecules, which are strongly bound to calcium cations of the

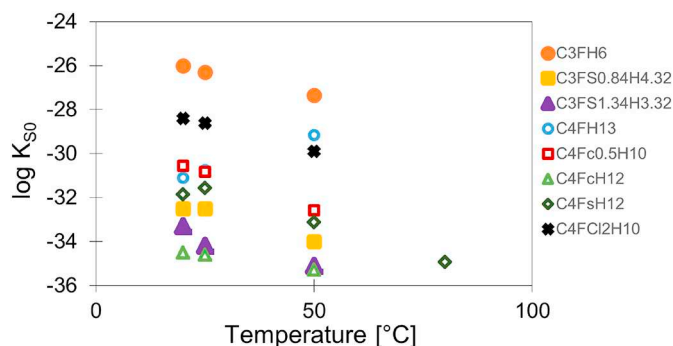


Fig. 5. Solubility product (K_{s0}) of Fe-containing hydrogarnet and AFm-phases at different temperatures, referring to reactions using Ca^{2+} , $\text{Fe}(\text{OH})_4^-$, $\text{SiO}(\text{OH})_3^-$, SO_4^{2-} , CO_3^{2-} , Cl^- , OH^- and H_2O as indicated in Table 2. Data from Dilnesa and co-workers [8–10,37].

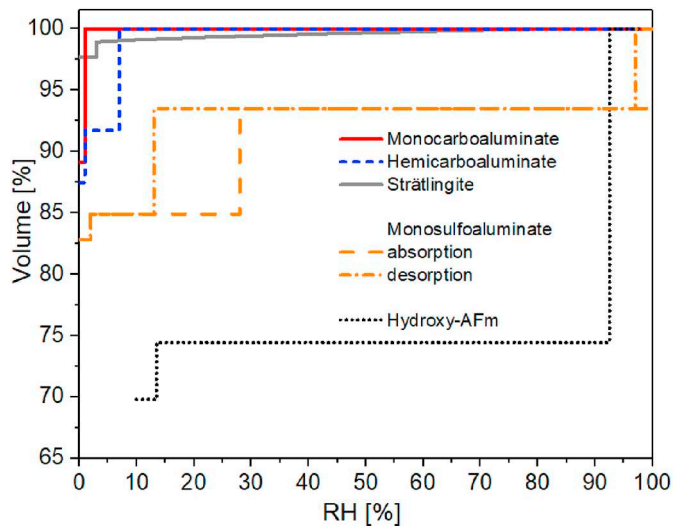


Fig. 6. Volume changes of the AFm phases studied as function of RH at 25 °C. 100% volume corresponds to the higher hydration state of each phase.

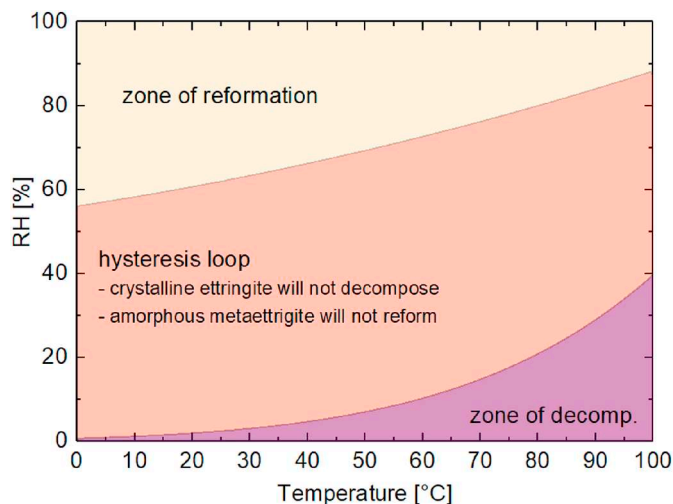


Fig. 7. Stability of ettringite as a function of relative humidity and temperature.

main layer and can only be removed at low water activities and/or high temperatures, typically accompanied by high enthalpies values. Recently, the thermodynamic properties of the different hydration states of the most important AFm phases were determined by Baquerizo et al. [31,32] and are listed in Table 1. A summary of the volume stability of AFm phases at 25 °C is shown in Fig. 6.

Ettringite, $C_6A_3H_{32}$, is also known to have varying water content. This hydrate is a common phase occurring during the hydration of PC. It is also the main hydration product in calcium sulfoaluminate cements and calcium aluminate cement blended with gypsum. Understanding the stability of ettringite during hydration and under different drying conditions is of great importance to assess the performance of systems containing large amounts of this phase. In general, ettringite contains 32 H_2O molecules per formula unit: 30 fixed in the columns and 2 H_2O of zeolitic water loosely bound in the channels. Removal of the two inter-channel water molecules takes place with decreasing relative humidity (RH) without any significant change of the structure. Nevertheless, a series of structural changes are observed when the water content is below 30 H_2O , resulting in an amorphous phase commonly known as metaettringite. The thermodynamic properties of crystalline ettringite, having 32 and 30 H_2O , and amorphous ettringite (or metaettringite) having 13 H_2O and 9 H_2O were recently derived by Baquerizo et al. [30] and are listed in Table 1. Something interesting to notice is that decomposition and reformation of ettringite takes place reversibly but with a marked hysteresis, which makes the estimation of thermodynamic properties difficult. The values presented in Table 1 corresponds to those derived using the desorption equilibrium properties. Fig. 7 shows the stability of ettringite at 25°, presenting three different zones:

- The zone of decomposition, which has to be reached in order to decompose ettringite into metaettringite.
- The hysteresis loop, where crystalline ettringite will not undergo decomposition unless the zone of decomposition is reached and amorphous metaettringite will not reform unless the zone of reformation is reached.
- The zone of reformation, which has to be reached in order to be convert metaettringite back to crystalline ettringite.

2.6. Mg-Al layered double hydroxide (hydrotalcite-like phase)

Mg-Al layered double hydroxide (LDH) type phases are structurally similar to hydrotalcite and typically occur as secondary reaction products in hydrated Portland cements [67] and in alkali-activated granulated blast furnace slag (GBFS) [68,69]. In hydrated or alkali-activated cementitious materials free from carbonation, Mg-Al LDH phases normally exhibit poor long-range structural order and are thought to significantly occur along the solid solution series $Mg_{(1-x)}Al_x(OH)_{(2+x)}(H_2O)_4$, where $0.2 \leq x \leq 0.33$ [70,71] due to the deficiency of CO_2 in the system. Mg-Al LDH formation is thus often difficult to observe by conventional X-ray diffraction, particularly at low MgO content.

Few solubility data for hydroxide containing hydrotalcite like Mg-Al LDH phases have been measured; the data at 25 °C are summarised in Fig. 8A and B. The samples studied by Bennet et al. [72] were

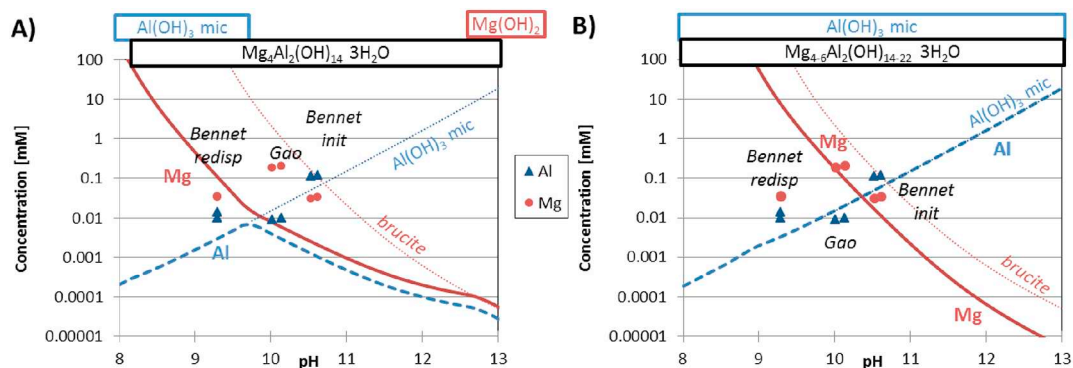


Fig. 8. Solubility of A) M_4AH_{10} (from Cemdata07 + 18) and B) of the MgAl-OH-LDH solid solution compared to the solubility of microcrystalline $Al(OH)_3$ and brucite (dotted lines) and to the experimental data (Mg: circles, Al: triangles) determined by Bennet et al. [72] and Gao and Li [73].

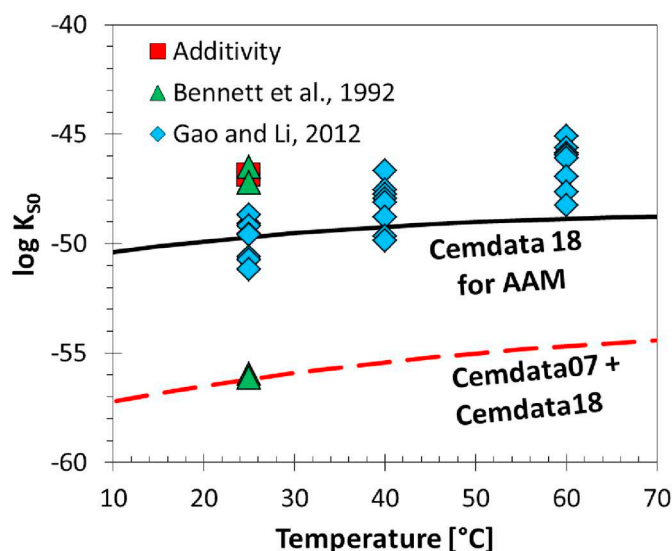


Fig. 9. Measured and calculated solubility products of M_4AH_{10} (reactions refer to Mg^{2+} , $Al(OH)_4^-$, OH^- and H_2O as indicated in Table 3) at different temperatures. Adapted from Myers et al. [74].

synthesized for 2 days at 80 °C, dried, and then re-dispersed in water for 4 weeks at 25 °C. This procedure resulted in a solubility product of 10^{-47} for M_4AH_{10} . Further re-dispersion steps lowered the solubility product of M_4AH_{10} to 10^{-56} . This lower solubility product of 10^{-56} for M_4AH_{10} was selected for use in Cemdata07 [1,29] (see Figs. 8A and 9), and by Bennet et al. [72].

Based on the solubility data of Gao and Li [73] for samples precipitated from oversaturated solutions (equilibration time 2 days), solubility data for hydrotalcite like Mg-Al LDH phases intercalated with OH^- (MgAl-OH-LDH) were recently recompiled and recalculated [74], as shown in Figs. 8B and 9. Solubility products for the end members of MgAl-OH-LDH solid solution model were defined using the available data [72,73] and guided using experimental observations in alkali activated slag cements with the high stability of MgAl-OH-LDH and absence of brucite in uncarbonated alkali-activated slag cements is widely documented and provides a reliable proxy for this task. An ideal (simple mixing) solid solution thermodynamic model (MA-OH-LDH_{ss}) was provisionally defined using these data for Mg/Al molar ratios between 2 and 4. The use of independent experimental observations to derive the solid solution model is important because solubility products derived from the available solubility data are scattered by up to $\sim 10 \log_{10}$ units at 25 °C, possibly due to the varied equilibration times used (2 days [73]

to 1 month [72]). We recommend using MgAl-OH-LDH_{ss} for alkali activated materials.

Usage of the MgAl-OH-LDH_{ss} model (describing hydrotalcite-like phases with variable Mg/Al ratio, and recommended for use in alkali activated material systems) does not lead to hydrotalcite formation under typical PC conditions due to the low aluminium concentrations in the pore solution [29] of PCs, for which brucite would be calculated to precipitate instead. As the formation of hydrotalcite like phases is reported in well hydrated PCs with dolomite [75], the use of a single phase, M_4AH_{10} , with a lower solubility product (see Table 3, Fig. 9) derived from the long-term experiments in [72] only, is recommended for hydrated PC. The necessity to use presently two different datasets and the large differences in the available data indicates that the solubility data selected for M_4AH_{10} and for MgAl-OH-LDH_{ss} are tentative and may require updating as more data become available. Therefore, we believe that additional solubility measurements for Mg-Al LDH phases are needed.

2.7. C-S-H solid solution models

The C-S-H gel-like phase is the major hydrate in PC and blended PC pastes. C-S-H is also the main “sorber” of alkali, alkali-earth, and hazardous cations (Sr^{2+} , UO_2^{2+} , Zn^{2+} , etc.) in hydrated cements used as waste matrices, including engineered barriers in nuclear waste repositories.

C-S-H phases have a variable composition that depends on the prevailing Ca/Si ratio in the system that can change by pozzolanic reaction, leaching caused by the ingress of water and/or chemical attack, such as carbonation. There are differences between properties of C-S-H samples prepared by (a) C_3S or C_2S hydration; (b) co-precipitation (double-decomposition) methods [76]. C-S-H has a ‘defect-tobermorite’ structure with a mean silicate chain length depending on the Ca/Si ratio, pH and the presence of aluminium [77]. It has variable “non-gel” water content (i.e. structural water and water present in the interlayer [78,79]), also depending on the Ca/Si ratio and the synthesis route, variable particle morphology, stacking, and “gel” water content, i.e. water present between C-S-H particles. Many C-S-H experimental solubility data sets available to date have been critically analyzed [80], including C-S-H type phases with variable aluminium and alkali contents [76,81–84].

C-S-H solubility can be reliably modelled using either solid solution models [11,80,85] or (to a limited extent) using a surface complexation approach [86,87]. Quantitative knowledge of C-S-H solubility is needed in essentially all studies of cement hydration and of waste-cement interactions, which explains why measuring and modelling the C-S-H solubility and water content is a major topic in cement chemistry [76].

Table 3

Standard thermodynamic properties at 25 °C and 1 atm for hydrotalcite-like phases (provided in separate modules of Cemdata18 database). The data are consistent with the GEMS version of the PSI/Nagra 12/07 TDB [22,23] and the data detailed in Tables 1 and 4.

	$\Delta_f G^\circ$ [kJ/mol]	$\Delta_f H^\circ$ [kJ/mol]	S° [J/K/mol]	a_0 [J/K/mol]	a_1 [J/mol/K ²]	a_2 [J/K/mol]	a_3 [J/K ^{0.5} /mol]	V° [cm ³ /mol]	Ref
$M_4AH_{10}^*$	−6394.6	−7196	549	−364	4.21	$3.75 \cdot 10^6$	629	220	[1,29]
MgAl-OH-LDH (ideal ternary solid solution)**									
M_4AH_{10}	−6358.5	−7160.2	548.9	547.6	−	−	−	219.1	[74]
M_6AH_{12}	−8022.9	−9006.7	675.2	803.1	−	−	−	305.4	[74]
M_8AH_{14}	−9687.4	−10,853.3	801.5	957.7	−	−	−	392.4	[74]
Mineral	$\log K_{so}$	Dissolution reactions used to calculate solubility products.							
$M_4AH_{10}^*$	−56.02 [*]	$Mg_4Al_2(OH)_{14} \cdot 3H_2O \rightarrow 4Mg^{2+} + 2Al(OH)_4^- + 6OH^- + 3H_2O$							
$M_4AH_{10}^{**}$	−49.7	$Mg_4Al_2(OH)_{14} \cdot 3H_2O \rightarrow 4Mg^{2+} + 2Al(OH)_4^- + 6OH^- + 3H_2O$							
$M_6AH_{12}^{**}$	−72.0	$Mg_6Al_2(OH)_{18} \cdot 3H_2O \rightarrow 6Mg^{2+} + 2Al(OH)_4^- + 10OH^- + 3H_2O$							
$M_8AH_{14}^{**}$	−94.3	$Mg_8Al_2(OH)_{22} \cdot 3H_2O \rightarrow 8Mg^{2+} + 2Al(OH)_4^- + 14OH^- + 3H_2O$							

a_0 , a_1 , a_2 , a_3 are the empirical coefficients of the heat capacity function: $C_p^\circ = a_0 + a_1T + a_2T^{-2} + a_3T^{-0.5}$.

* Tentative value; recommended for PC based systems.

** Tentative values; recommended for alkali activated materials.

Table 4
Solid solution models of C-S-H (provided in separate modules of Cemdata18 database).^a

Phase,	$\Delta_f G^\circ$	$\Delta_f H^\circ$	S°	a_0	a_1	a_2	V°	Ref
End member	[kJ/mol]	[kJ/mol]	[J/K/mol]	[J/K/mol]	[J/mol/K ²]	[J K/mol]	[cm ³ /mol]	
<u>C-S-H (CSH-II solid solution)</u>								
Tob: C _{0.83} SH _{1.3}	-1744.36	-1916	80	85	0.160		59	[1]
Jen: C _{1.67} SH _{2.1}	-2480.81	-2723	140	210	0.120	-3.07·10 ⁶	78	[1]
<u>C-S-H-K-N (ECSH-1 solid solution)</u>								
TobCa-1: C _{0.83} SH _{1.83}	-1863.62	-2059.5	114.6	170.4			68	[85]
SH: SH (SiO ₂ H ₂ O)	-1085.45	-1188.6	111.3	119.8			34	[85]
NaSH-1: N _{0.5} S _{0.2} H _{0.45}	-433.57	-480.4	41.2	37.9			10.5	[88]
KSH-1: K _{0.5} S _{0.2} H _{0.45}	-443.35	-490.0	48.4	40.6			12.4	[88]
SrSH-1: SrSH ₂	-2020.89 (-2017.47 ^b)	-2231.6 (-2228 ^b)	141.9	174.8			64	[88]
<u>C-S-H-K-N (ECSH-2 solid solution)</u>								
TobCa-2: C _{0.83} SH _{1.83}	-1863.62	-2059.5	114.6	170.4			68	[85]
JenCa: CS _{0.6} H _{1.1}	-1569.05	-1741.6	73.0	114.5			36	[85]
NaSH-2: N _{0.5} S _{0.2} H _{0.45}	-430.72	-477.6	41.2	37.9			10.5	[88]
KSH-2: K _{0.5} S _{0.2} H _{0.45}	-440.49	-487.2	48.4	40.6			12.4	[88]
SrSH-2: SrSH ₂	-2019.75 (-2016.33 ^b)	-2230.5 (-2227 ^b)	141.9	174.8			64	[88]
<u>C-S-H (CSHQ solid solution)</u>								
TobH Ca/Si = 0.67: C _{2/3} SH _{1.5}	-1668.56	-1841.5	89.9	141.6			55	[11]
TobD Ca/Si = 1.25: C _{5/6} S _{2/3} H _{1.83}	-1570.89	-1742.4	121.8	166.9			48	[11]
JenH Ca/Si = 1.33: C _{1.33} SH _{2.17}	-2273.99	-2506.3	142.5	207.9			76	[11]
JenD Ca/Si = 2.25: C _{1.5} S _{0.67} H _{2.5}	-2169.56	-2400.7	173.4	232.8			81	[11]
NaSH: N _{0.5} S _{0.2} H _{0.45}	-431.20	478.0	41.2	37.9			10.5	[88,89]
KSH: K _{0.5} S _{0.2} H _{0.45}	-440.80	-489.6	48.4	40.6			12.4	[88,89]
<u>C-S-H (CSH3T solid solution)</u>								
TobH Ca/Si = 0.67: C _{1/3} S _{2/3} H _{5/2}	-2561.53	-2832.97	152.8	231.2			85	[11]
T5C Ca/Si = 1.0: C _{5/4} S _{5/4} H _{5/2}	-2518.66	-2782.03	159.9	234.1			79	[11]
T2C Ca/Si = 1.5: C _{3/2} S ₁ H _{5/2}	-2467.08	-2722.40	167.0	237.0			81	[11]
<u>C-(N-)A-S-H (CNASH solid solution)</u>								
TobH ^c : C ₁ S _{3/2} H _{5/2}	-2560.00	-2831.4	152.8	231.2			85.0	[90]
INFCa: C ₁ A _{5/32} S _{38/32} H _{53/32}	-2342.90	-2551.3	154.5	180.9			59.3	[90]
INFCN: C ₁ N _{5/16} S _{3/2} H _{19/16}	-2452.46	-2642.0	185.6	183.7			71.1	[90]
INFCNA: C ₁ A _{5/32} N _{11/32} S _{38/32} H _{42/32}	-2474.28	-2666.7	198.4	179.7			69.3	[90]
T5C ^c : C _{5/4} S _{5/4} H _{5/2}	-2516.90	-2780.3	159.9	234.1			79.3	[90]
5CA: C _{5/4} A _{1/8} S ₁ H _{13/8}	-2292.82	-2491.3	163.1	177.1			57.3	[90]
5CNA: C _{5/4} N _{1/4} A _{1/8} S ₁ H _{11/8}	-2381.81	-2568.7	195.0	176.2			64.5	[90]
T2C ^c : C _{3/2} S ₁ H _{5/2}	-2465.40	-2720.7	167.0	237.0			80.6	[90]

a_0 , a_1 , a_2 , are the empirical coefficients of the heat capacity equation: $C_p^\circ = a_0 + a_1T + a_2T^{-2}$; no value = 0.

^a Only CSH-II solid solution included in Cemdata'07.03 database.

^b For the ACW conditions.

^c Thermodynamic properties were slightly modified relative to the T2C, T5C, and TobH end members of the downscaled CSH3T thermodynamic model [11].

In Table 4, five alternative C-S-H solid solution models are represented, in part for backward compatibility with previous versions of Cemdata (Cemdata07 and Cemdata14); they are provided in the Cemdata18 database. Here we provide a brief overview of those models with some recommendations for their use.

2.7.1. CSH-II model

This simple ideal C-S-H solid solution model [85] has been used for many years, and was included (with a modified stability to better describe the changes in the calcium concentrations with pH and less water to correspond to the composition of C-S-H present in cements) into Cemdata07 database [1,29]. The original model [85] consisted of two binary ideal solutions CSH-I and CSH-II. CSH-I used end-members of amorphous silica (SH; SiO₂) and a tobermorite-like C-S-H gel phase (Tob-I; (Ca(OH)₂)₂(SiO₂)_{2.4}·2H₂O). CSH-II used end-members of tobermorite-like (Tob-II; (Ca(OH)₂)_{0.8333}SiO₂·0.8333H₂O) and jennite-like (Jen; (Ca(OH)₂)_{1.6666}SiO₂·H₂O) C-S-H gel phases. The CSH-II phase co-exists with CH (portlandite) at Ca/Si ratios above 1.5 to 1.7. The CSH-I solid solution has been shown to be unrealistic ([80] and references therein) and amorphous SiO₂ co-exists with C-S-H gel of Ca/Si

ratios = 0.4–0.8. The water content in this C-S-H II is lower than in the other models discussed below, but corresponds well to the water present in the interlayer of C-S-H as measured by ¹H NMR [78,79]. In Cemdata18, we provide the CSH-II solid solution model only, covering the range of Ca/Si ratios from 0.83 to 1.67, for backward compatibility with the Cemdata07 database and as an alternative to the newer models.

2.7.2. ECSH-1 and ECSH-2 models

ECSH-1 and ECSH-2 models extend both CSH-I and CSH-II models with Na-, K- and Sr- containing end members. Aimed at pragmatic description of uptake of minor cations, these provisional ideal solid solution models [88] were constructed with help of the statistical dual-thermodynamic method [91] based on GEM-Selektor calculations. With this method, one can retrieve both the unknown stoichiometry and the standard molar Gibbs energy $\Delta_f G^\circ_{298}$ of ideal solid solution end members from the experimental bulk compositions of the aqueous solution and co-existing solid solution. In total, 13 possible end member stoichiometries with the general formula [(Ca(OH)₂)_{n_{Ca}}(Sr(OH)₂)_{n_{Sr}}(KOH)_{n_K}(NaOH)_{n_{Na}}SiO₂H₂O]_{n_{Si}} were considered for these

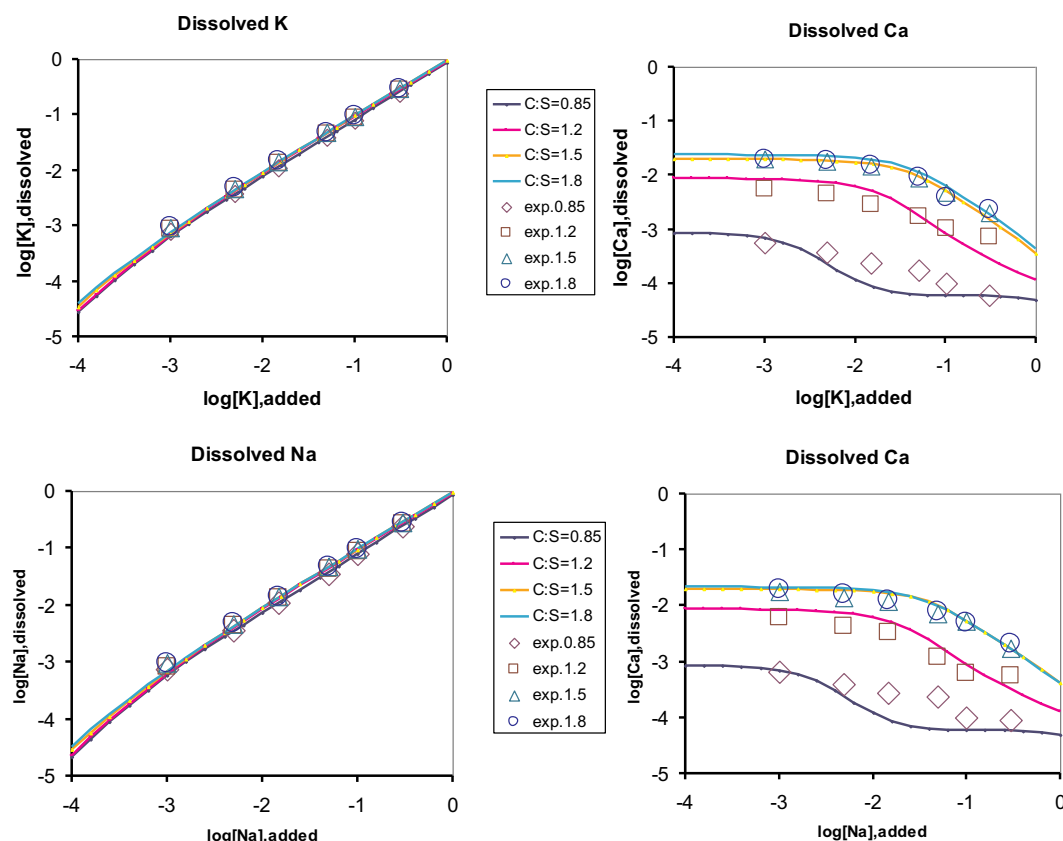


Fig. 10. Comparison of sorption isotherms for K or Na calculated using the ECSH-II Aq-SS model (curves) with the data for K and Na sorption [81] (scattered symbols). Abscissa: \log_{10} moles of added K or Na per 1 kg H_2O ; ordinate: \log_{10} molar.

models. To develop these models, the n_{Ca} , n_{Sr} , ... coefficients were adjusted in order to minimize the standard deviations of estimated G_{298}° values for model end members in trial GEM calculations for a number of experimental data points. These trial GEM calculations employed: (1) the Nagra-PSI database [24]; (2) many experimental data points at different Ca/Si, Sr/Si, Na/Si, K/Si ratios; and (3) varying stoichiometry coefficients of solid solution end members within the ranges of $0.1 < n_{\text{Si}} < 2$, $0 < n_{\text{Ca}} < 1.6$, $0 < n_{\text{Sr}} < 2$, $0 < n_{\text{K}} < 2$, and $0 < n_{\text{Na}} < 2$.

Followed by ‘forward GEM modelling’ of Sr uptake data in pure water and in artificial cement water (ACW), this procedure resulted in ideal ECSH-II and ECSH-I solid solution models that provided the optimal description of data (over 96 experiments published in [92] and additional in-house Sr uptake data on C-S-H in water and in ACW). $\Delta_r G_{298}^\circ$ values for Na- and K-containing end members were also fine-tuned using literature data [81] on Na and K uptake isotherms in C-S-H (Fig. 10). The ECSH-1 and ECSH-2 models can realistically describe the uptake of cations and the decrease of (maximum) Ca/Si ratios in equilibrium with portlandite upon increasing alkali concentration in aqueous solution. However, it was not possible to use the same $\Delta_r G_{298}^\circ$ of SrSH end member to model isotherms of Sr uptake in C-S-H prepared in water and in the artificial cement pore water (ACW with pH ≈ 13.3 at 25 °C, containing 0.18 M KOH, 0.114 M NaOH and 1.2 mM $\text{Ca}(\text{OH})_2$). We believe that the $\Delta_r G_{298}^\circ(\text{SrSH})$ difference (up to 3.4 kJ/mol) can probably be explained by different silica polymerization and cation exchange capacity of C-S-H due to the presence of alkali. We anticipate that ECSH-1 and ECSH-2 will be replaced by more accurate C-S-H-K-Na models in the near future.

With no known thermodynamic properties of structural analogues available, the standard entropy and heat capacity of the ECSH end members were estimated assuming linear dependencies of entropy and heat capacity effects of reactions on the Ca/Si ratio in C-S-H [11]:

$$(\text{CaO})_x(\text{SiO}_2)_y(\text{H}_2\text{O})_z = y\text{SiO}_2 + x\text{Ca}(\text{OH})_2 + (z - x)\text{H}_2\text{O} \quad (1)$$

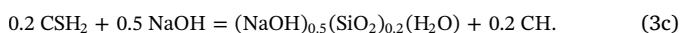
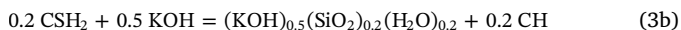
$$(\text{C} - \text{S} - \text{H} \text{ end member}) = y(\text{silica}) + x(\text{portlandite}) + (z - x)(\text{water})$$

$$\Delta_r S_{298}^\circ = y(61.054 + 5.357 x/y) \quad (2a)$$

$$\Delta_r C_{p,298}^\circ = y(31.881 - 11.905 x/y) \quad (2b)$$

Using Eqs. (2a) and (2b), $\Delta_r S_{298}^\circ$ and $\Delta_r C_{p,298}^\circ$ were calculated and rounded off to the nearest whole numbers. The $\Delta_r H_{298}^\circ$ values were calculated from $\log_{10} K_{298}^\circ$ and $\Delta_r S_{298}^\circ$ values together with the S° , C_p° , $\Delta_f H^\circ$ and $\Delta_f G^\circ$ values at $T_r = 298.15$ K using the ReacDC module of GEM-Selektor code and thermodynamic properties of water, portlandite and amorphous silica from the GEMS version of the PSI/Nagra 12/07 TDB [22,23] and Cemdata18 databases. The resulting thermodynamic properties (Table 4) are expected to suffice for temperatures between 0 and 90 °C within 0.5 pK units uncertainty.

Next, the S_{298}° , $C_{p,298}^\circ$ and values of the SrSH, NaSH and KSH end members of ECSH phases were evaluated. This was done by taking the properties of their reference calcium hydroxide counterpart $\text{C}_1\text{S}_1\text{H}_2$ and then either subtracting or adding respective properties of solid portlandite $\text{Ca}(\text{OH})_2$, as well as solid $\text{Sr}(\text{OH})_2$, solid NaOH or solid KOH from Wagman et al. [93]. This is equivalent to assuming $\Delta_r S_{298}^\circ = 0$ and $\Delta_r C_{p,298}^\circ = 0$ for the reactions:



For these calculations, $\Delta_f S_{298}^\circ$, and $\Delta_f Cp_{298}^\circ$, S_{298}° , Cp_{298}° of the reference compound CSH_2 were computed using Eqs. (1), (2a) and (2b). Note that the stoichiometries of the K and Na C-S-H end members defined by reactions 3b and 3c correspond to $\text{N}_{0.25}\text{S}_{0.2}\text{H}_{0.45}$ or $\text{K}_{0.25}\text{S}_{0.2}\text{H}_{0.45}$, but not $\text{N}_{0.25}\text{S}_{0.2}\text{H}_{0.3}$ or $\text{K}_{0.25}\text{S}_{0.2}\text{H}_{0.3}$ as defined in Kulik et al. [88]. The respective values for $\Delta_f G_{298}^\circ$, and $\Delta_f H_{298}^\circ$ are summarised in Table 4.

2.7.3. CSHQ model

CSHQ model [11] was developed in order to address some known shortcomings of the earlier CSH-I and CSH-II models [29,85], namely insufficient connection to the C-S-H structure and the unrealistic assumption of ideal mixing between tobermorite-like and amorphous silica end members. It was based on structural data supporting the defect-tobermorite model [94–96], represented as a solid solution model with four different structural sites (sublattices) [11]: $[\text{BTI}^{+2}]_1: [\text{IU}^-]_2: [\text{CU}^0]_2: [\text{IW}^0]_5$. The main assumption was that in BTI sites, the incorporation of Ca^{2+} ion in the interlayer occurs simultaneously with the removal of a bridging tetrahedron in the silica “dreierketten” chain, and this process is reversible. Excess calcium can also be incorporated as a $\text{Ca}(\text{OH})_2$ moiety, either interstitially in the tobermorite interlayer, or forming domains of jennite-like structure. This was accounted for by an exchange of a vacancy with $\text{Ca}(\text{OH})_2$ in CU sites. The occupation of TU and IW sublattices was fixed as $2\text{CaSiO}_{3.5}^-$ and $4\text{H}_2\text{O} + \text{vacancy}$, respectively. This led to four end members with stoichiometries depending on the assumed $\text{Ca}^{2+}/\text{H}^+$ ratio in BTI sites.

This solid solution model has a correct built-in dependence of the mean silica chain length (MCL) on Ca/Si ratios. By downscaling the end-member stoichiometries to Si = 1.0 and adjusting the G_{298}° values of end members, the CSHQ model could be fine-tuned to various C-S-H solubility data sets [11]. The downscaled ideal CSHQ model (Table 4) provides a reasonable fit to the variety of C-S-H solubility data in the [Ca]-[Si], [Ca]-C/S and [Si]-Ca/Si spaces as discussed in more detail in [11].

In this Cemdata18 database, two end members for K and Na (similar to those from the ESH model) were provisionally added to improve predictions of pH and composition of the PC porewater. The extension to cover the uptake of alkalis by C-S-H was based on an ideal solid solution model between jennite, tobermorite, $[(\text{KOH})_{2.5}\text{SiO}_2\text{H}_2\text{O}]_{0.2}$ and $[(\text{NaOH})_{2.5}\text{SiO}_2\text{H}_2\text{O}]_{0.2}$ as proposed by Kulik et al. [88] and using the thermodynamic data reported in [89]: $\Delta_f G^\circ = -440'800 \text{ J/mol}$ and $-431'200 \text{ J/mol}$ (at 20°C) for $[(\text{KOH})_{2.5}\text{SiO}_2\text{H}_2\text{O}]_{0.2}$ and $[(\text{NaOH})_{2.5}\text{SiO}_2\text{H}_2\text{O}]_{0.2}$, respectively.

2.7.4. CSH3T model

CSH3T model [11] was aimed at more consistency with the tobermorite-like structure of C-S-H phases at $\text{Ca/Si} < 1.5$. The evidence of interlayer ordering in tobermorite-like C-S-H with $0.9 < \text{C/S} < 1.25$ [96] has led to setting the CU sites always vacant, and to splitting the BTI sublattice into two ($[\text{BTI1}^{+}]_1: [\text{BTI2}^{+}]_1: [\text{IU}^-]_2: [\text{IW}^0]_4$) with substitutions of $\text{Si}_{0.5}\text{OH}^+$ by $\text{HO}_{0.5}\text{Ca}_{0.5}^{+}$. This yielded a solid solution model with end members TobH ($\text{C}_2\text{S}_3\text{H}_5$), T5C ($\text{C}_{2.5}\text{S}_{2.5}\text{H}_5$), T2C ($\text{C}_3\text{S}_2\text{H}_5$), connected by an ordering reaction $\frac{1}{2}\text{TobH} + \frac{1}{2}\text{T2C} = \text{T5C}$. The model has a built-in dependence of the mean chain length on the composition, consistent with measured values [95] for the co-precipitated tobermorite-like C-S-H. The CSH3T model [11] in its downscaled form (Table 4) can be computed just using a simple ideal mixing model. The CSH3T model has been later extended

with U(VI) end members [97] and with Al and Na end members [90]. The ideal CSH3T SS model [11] produces quite realistic curves for solubility of the synthetic C-S-H co-precipitation (double decomposition) data. More accurate C-S-H multi-site solid solution models are in development.

2.7.5. CNASH_{ss} model

CNASH_{ss} model [90] includes Al and Na and represents an extension of the CSH3T model that was optimised for alkali activated systems. The calcium (alkali) aluminosilicate hydrate (C-(N-)A-S-H) gel-like phase that precipitates in alkali-activated cements contains significantly less Ca, more Al and alkali and has a more densely packed structure than the C-(A-)S-H which forms in hydrated PC-based materials [98,99]. However, both phases are based on the same defect-tobermorite structure. In alkali-activated slag cements (an exemplary ‘high-Ca’ alkali-activated material [100]), the C-(N-)A-S-H phase typically has a $\text{Ca/Si} \approx 1$ and an $\text{Al/Si} \leq 0.25$ [90].

Many solubility and chemical composition data for the C-(N-)A-S-H system have been published. Much of this data was used to develop an ideal solid solution thermodynamic model (CNASH_{ss}), including configurational entropy terms, which explicitly includes mixing of Al and Na [90]. The CNASH_{ss} model enables Al incorporation into C-(N-)A-S-H gel to be explicitly considered in thermodynamic modelling simulations. The CNASH_{ss} model has been applied to simulate phase assemblages in NaOH, sodium silicate, Na_2CO_3 , and Na_2SO_4 -activated slag systems [74,101]. This model is also applicable to thermodynamic modelling of PC-based materials; however, it less closely represents the full body of available solubility data for the C-S-H phase [102] at $\text{Ca/Si} > \sim 1.3$ than other C-S-H thermodynamic models, e.g. [11,80]. CNASH_{ss} closely represents the full set of solubility data for the C-(N-)A-S-H gel phase down to $\text{Ca/Si} = 0.67$. Therefore, we recommend using CNASH_{ss} for alkali activated systems rather than hydrated PC systems, where we recommend the use of CSHQ or C-S-H-II.

Additional solubility data for C-(N-)A-S-H gel not used to validate CNASH_{ss} were recently published, including for C-(N-)A-S-H gels at synthesis temperatures of 7°C , 50°C and 80°C [103,104] and using K rather than Na [84,105]. Future refinement to the CNASH_{ss} thermodynamic model should include these data and formally extend the model to different temperatures and alkali type.

2.7.6. General remarks

During the last 20 years, ideal solid solution models of C-S-H have evolved starting from simple ideal solid solutions using full end-member mixing up to recent truly multi-site mixing models consistent with both solubility data and structural/spectroscopic data. Because end members in multi-site solid solutions are constructed of moieties substituting each other on different sublattices, such models have the best potential for: (1) extension by adding moieties for other elements of interest (e.g. K, Na, Al, U, Sr) in their respective sites; (2) generating all possible end members; and (3) parameterizing end members based on available solubility, element uptake, and spectroscopic data (e.g. using the GEMSFITS code [106]) and are the subjects of ongoing research.

For the calcium silicate hydrate complexes, $\text{CaH}_3\text{SiO}_4^+$ ($\text{CaHSiO}_3^+ + 2\text{H}_2\text{O}$) and $\text{CaH}_2\text{SiO}_4^0$ ($\text{CaSiO}_3^0 + 2\text{H}_2\text{O}$), the reported complex formation data show a significant scatter. In particular, complex formation constants for $\text{CaH}_2\text{SiO}_4^0$ vary by more than one log unit. While the PSI/Nagra TDB [22,23] reports a complex formation constant of $10^{4.6}$ for the reaction $\text{Ca}^{2+} + \text{SiO}_3^{2-} \rightarrow \text{CaSiO}_3^0$ (see Table 2), which has a large effect on the silicon concentrations in presence of C-S-H at $\text{Ca/Si} > 1$ [80], no such constant is defined in the PHREEQC database [18]. Walker et al. [80] recommended to use a constant of $10^{4.0}$, making the complex less important, while recently an even lower complex

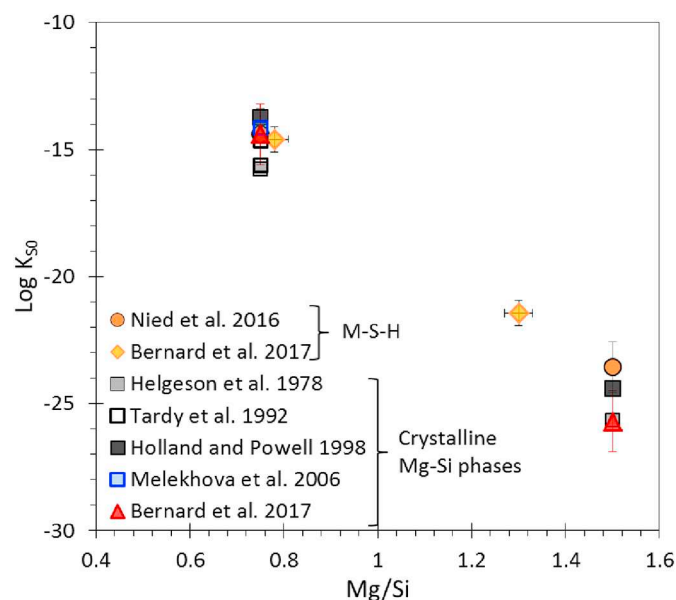


Fig. 11. Evolution of the solubility product (K_{s0}) of magnesium silicate hydrates at room temperature as a function of the total Mg/Si; referring to reactions using Mg^{2+} , SiO_2 and H_2O as indicated in Table 2. Adapted from [118].

formation constant of $10^{2.9}$ has been derived based on titration experiments [107]. This large scatter of data results in very diverging assessment of the importance of the CaSiO_3^0 complex at $\text{Ca}/\text{Si} > 1$ and has a significant impact on the C-S-H solubility as this complex accounts for about 90% of aqueous dissolved silicon in equilibrium with both C-S-H and portlandite. Dedicated investigations not only of calcium silicate hydrate complexes but also of other possible complexes between aluminium, calcium and silicate at high pH values are urgently needed.

2.8. Magnesium silicate hydrates

The formation of magnesium silicates hydrate (M-S-H) has been observed at the interfacial zone of cement paste with clays [67,108,109] and/or as secondary products from the degradation of cement pastes by groundwater or seawater [110–112]. The combination of leaching and carbonation of the cement paste decreases pH at the surface of the cement, decalcifies C-S-H and leads the formation of a Mg-enriched phase, M-S-H. M-S-H phases are poorly ordered but have a layered structure with tetrahedral silica arranged in sheets similar to clay minerals, have variable Mg/Si from ≈ 0.8 to $\text{Mg}/\text{Si} \approx 1.2$ and are stable at pH values between 7.5 and 11.5 [40,113–115]. Given the difference in structure and pH domains, most studies [114–117] observed the precipitation of distinct C-S-H and M-S-H phases and not of a mixed magnesium calcium silicate hydrate phase. Solubility measurements [40,113,118] indicated an only slightly higher solubility of the poorly ordered M-S-H in comparison to crystalline magnesium-silicates such as talc, antigorite or chrysotile as shown in Fig. 11. The ideal solid solution model for M-S-H published by Nied et al. [40] has been selected for the present version of the database. As several groups [113,114,118] are currently working on thermodynamic data for M-S-H, we expect that more sophisticated models will be published in the coming years.

2.9. Zeolites

Interactions of highly alkaline solutions in hydrated PC systems with service environments will likely result in the partial dissolution of

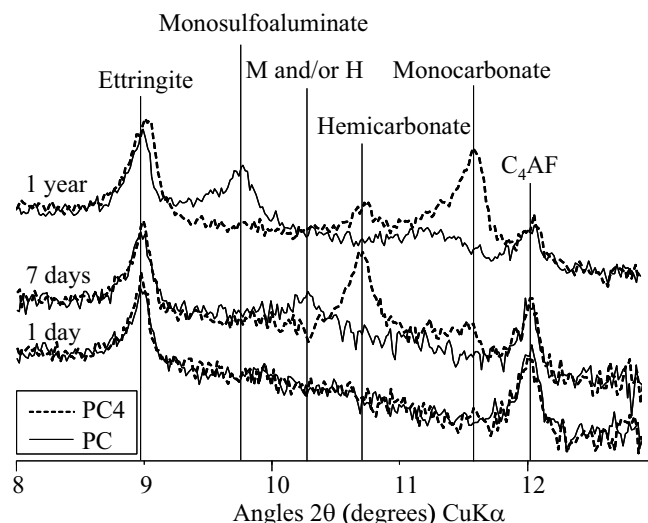


Fig. 12. Experimentally observed phase assemblage in a PC without additional limestone (PC) and with 4 wt% of limestone (PC4); reproduced from [123].

aluminosilicate minerals from adjacent rocks and the formation of secondary zeolite minerals [119] in the context of deep underground nuclear waste repositories. Zeolite formation also occurs in alkali activated cement systems. These zeolites are often related to the poorly crystalline N-A-S-H (sodium-aluminium-silicate-hydrate) and K-A-S-H (potassium-aluminium-silicate-hydrate) gels that form in these systems [74,103]; the type of gel formed depends on the presence of Na^+ or K^+ , cation concentrations, the relative degree of saturation of the liquid phase with respect to silica, pH and temperature [120]. Several papers in recent years estimated solubility data for different zeolites, based mainly on heat capacity and enthalpy measurements [47,74,121]. This may lead to considerable bias in the estimated solubility data in the range of several log units due to uncertainties associated with the measurements of enthalpy data. The determination of solubility data for zeolites has been hindered by variability in cation composition (Ca, Na, K), Al/Si ratios, H_2O contents and atomic structure, and also their slow reaction kinetics.

In 2017, two independent studies [41,103] reported very similar solubility products for zeolite Y and X (or for N-A-S-H gel with $\text{Al}/\text{Si} = 0.5$ and $\text{Al}/\text{Si} = 0.8$) based on experimental data. The data for zeolite X(Na), zeolite Y(Na) and chabazite [41] make it possible to predict zeolite formation in sodium activated cements; data for potassium-based zeolites are still missing in the Cemdata18 database. Also data for natrolite and zeolite P(Ca) have been included [41]. In experiments with high pH values their formation was kinetically hindered (although natrolite and zeolite P(Ca) were more stable than zeolite X (Na), zeolite Y(Na) and chabazite). Thus we recommend that natrolite and zeolite P(Ca) should be considered in modelling the interface between cement and adjacent rocks. However, their formation may be suppressed in models for alkali activated systems, where zeolite X(Na), zeolite Y(Na) and chabazite or their amorphous or nanocrystalline precursors are formed [122].

3. Comparison Cemdata07 with Cemdata18

The updates since the first cemdata version, cemdata07 (published in 2008), are significant. In particular, the distribution of iron and aluminium, the volume and Ca/Si in C-S-H as well as the alkali concentrations in the pore solution in PC can significantly affect thermodynamic modelling results. To illustrate these differences, the effect of

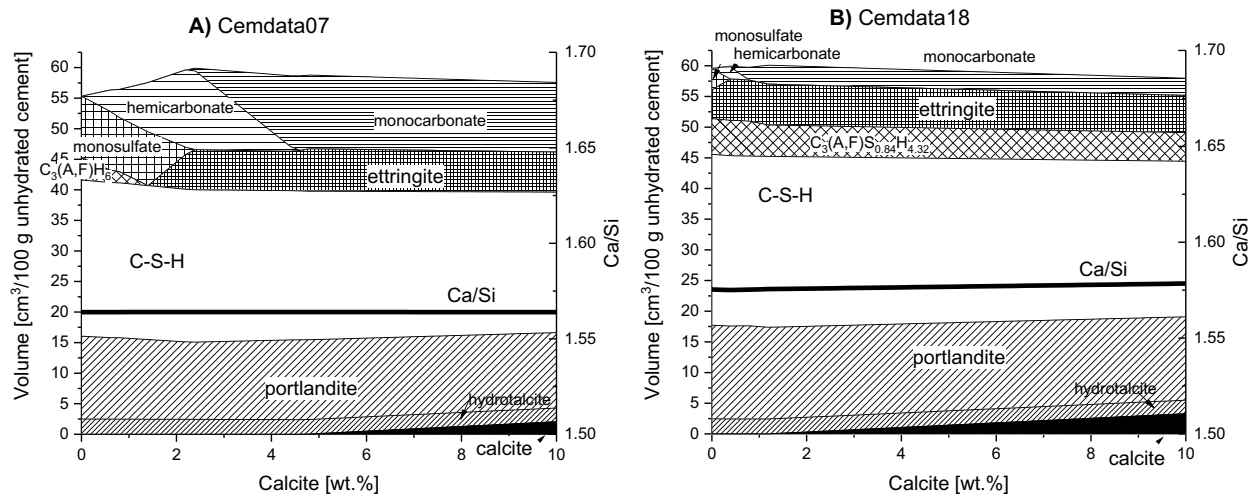


Fig. 13. Comparison of calculated solid phase assemblage using A) Cemdata07 and B) Cemdata18 assuming complete hydration of PC using the composition reported in [123].

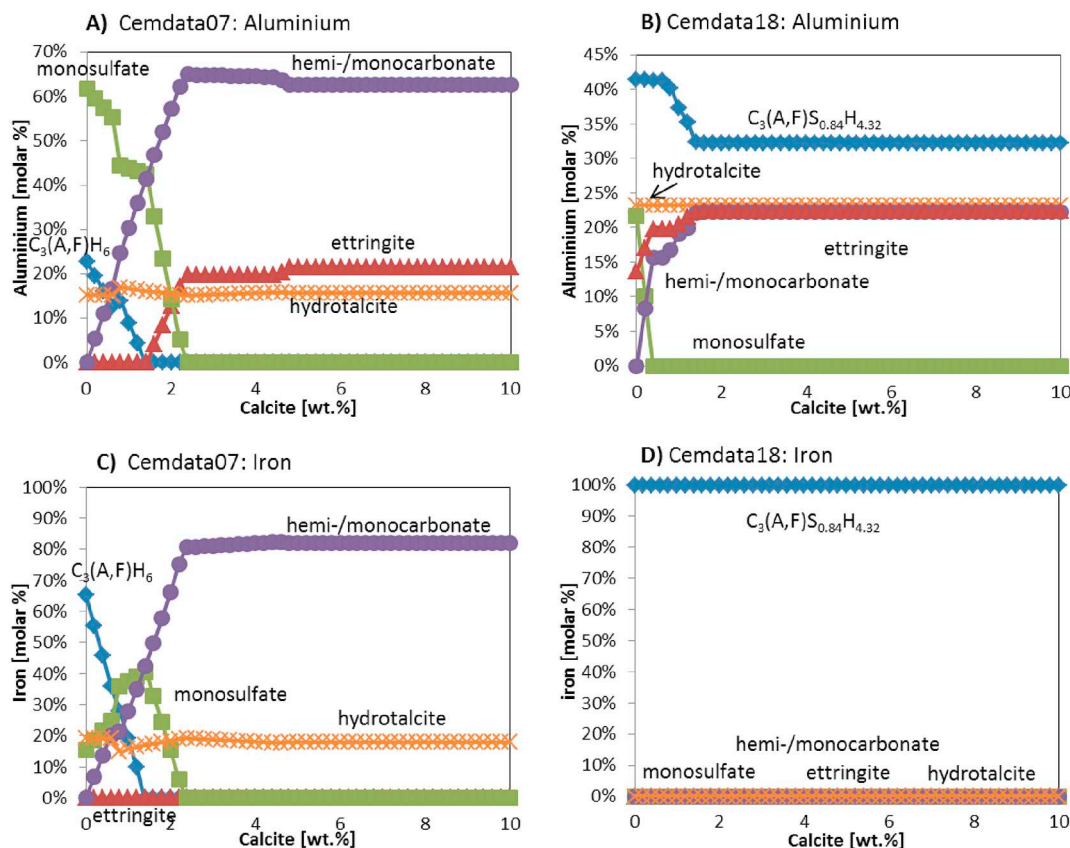


Fig. 14. Effect of the amount of limestone on the phase assemblage and the distribution of aluminium and iron in hydrated PC calculated using Cemdata07 (A, C) and Cemdata18 (B, D).

limestone on the same PC was calculated with Cemdata07 and Cemdata18 and compared below. The effect of relative humidity on calculated hydrates is used below as a second example. These comparisons concentrate on PC, as compiled specific data for alkali activated materials are only now available (in this paper).

3.1. Effect of limestone on solid and liquid phase composition

The influence of limestone on cement hydration has been widely studied and was the subject of several publications by the authors [2,20,123]. Experimental investigations showed that the presence of calcium carbonate prevents the destabilisation of ettringite to

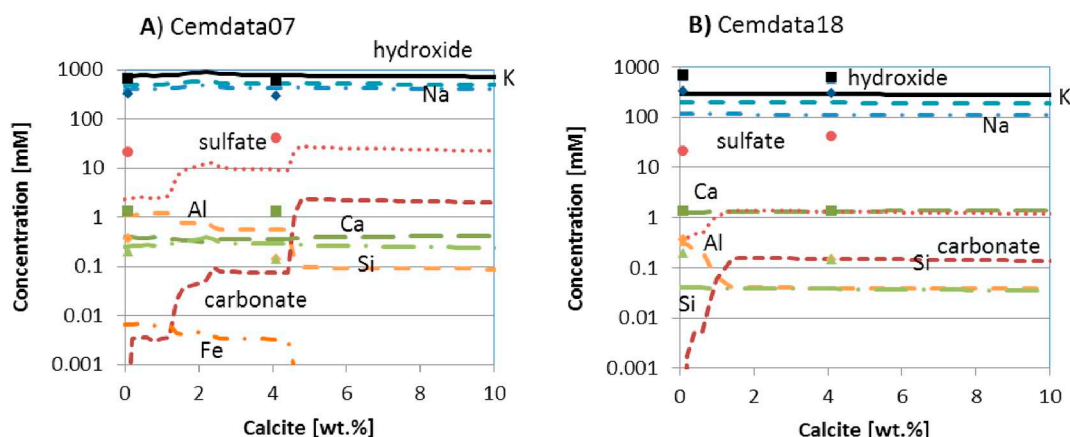


Fig. 15. Effect of the amount of limestone on the phase assemblage and the distribution of aluminium and iron in hydrated PC calculated using A) Cemdata07 and B) Cemdata18.

monosulfate at long hydration times and stabilises monocarbonate together with ettringite (see e.g. [123–125] and Fig. 12).

Also thermodynamic modelling [2,20,123] (mainly using the Cemdata2007 database) showed that the presence of small amounts of limestone significantly impacted the mineralogy of hydrated cements. In the absence of any limestone no ettringite but only monosulfate as well as of a small amount of katoite ($C_3(A,F)H_6$) was predicted as shown in Fig. 13A. The presence of a small amount of limestone was calculated to stabilise hemihydrogarnet and at higher dosages monocarbonate plus ettringite, resulting in an increase of the total volume. The higher volume in the presence of a small amount of limestone due to the stabilization of ettringite has been found to have a positive effect on the mechanical properties of PC and blended cements [20,124].

The stability of siliceous hydrogarnet was a matter of debate during the development of Cemdata07 and in most calculations with Cemdata07 the formation of siliceous hydrogarnet $C_3AS_{0.8}H_{4.4}$ had been suppressed assuming kinetic hindrance. Based on the data compiled in Cemdata07, which originated from measurements from [7,72,126], ettringite and siliceous hydrogarnet were calculated to be significantly more stable than monosulfate, hemi- or

monocarboaluminate thus theoretically preventing their presence. Since monosulfate, hemi- and monocarboaluminate are experimentally observed in hydrated PC, it was assumed that this was due to a kinetic hindrance in the formation of siliceous hydrogarnet and that possibly a later conversion of hemi- and monocarboaluminate to siliceous hydrogarnet could occur.

The new data for ($C_3A_{0.5}F_{0.5}S_{0.84}H_{4.32}$) by Dilnesa et al. [9], included in Cemdata18, suggest that mixed Al- and Fe-containing siliceous hydrogarnet can coexist with monosulfate, hemi- and monocarboaluminate at ambient conditions, which is in better agreement with the observed experimental data presented in Fig. 12 and elsewhere [123–125]. Fig. 13B displays the predicted phase assemblage of a hydrated PC with limestone using Cemdata18 as given in Tables 1–4; employing CSHQ and M_4AH_{10} . The formation of hemi- and monocarboaluminate accompanied by a stabilization of ettringite instead of monosulfoaluminate was correctly predicted by both datasets. As shown in Fig. 13 the biggest difference between the two datasets is the prediction of a katoite-type siliceous hydrogarnet phase ($C_3A_{0.5}F_{0.5}S_{0.84}H_{4.32}$), modelled as solid solution with a varying alumina and iron by using Cemdata18, together with hemi- and

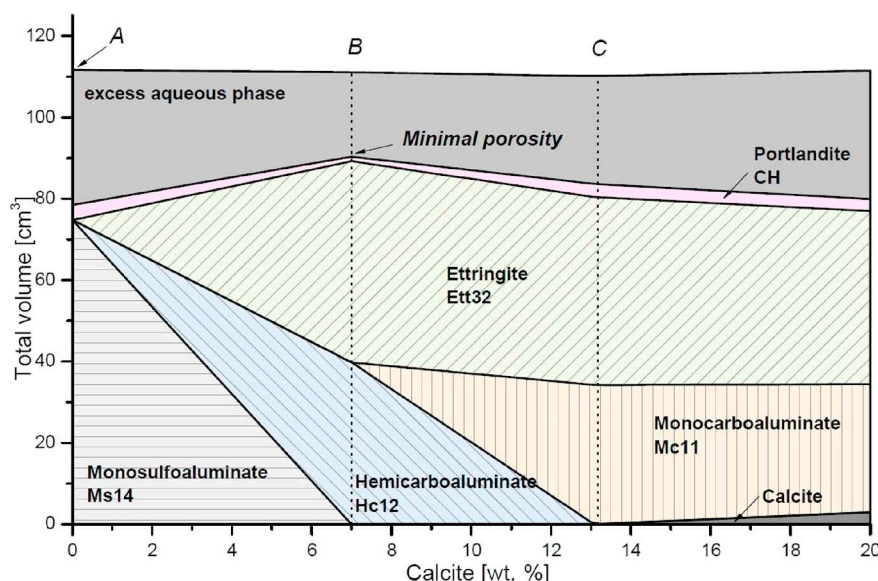


Fig. 16. Calculated specific volume changes of a hydrated model mixture consisting of C_3A , portlandite and with fixed sulfate ratio ($SO_3/Al_2O_3 = 1$, molar bulk ratio) in dependence of changing calcite content at 25 °C; calculated using Cemdata18.

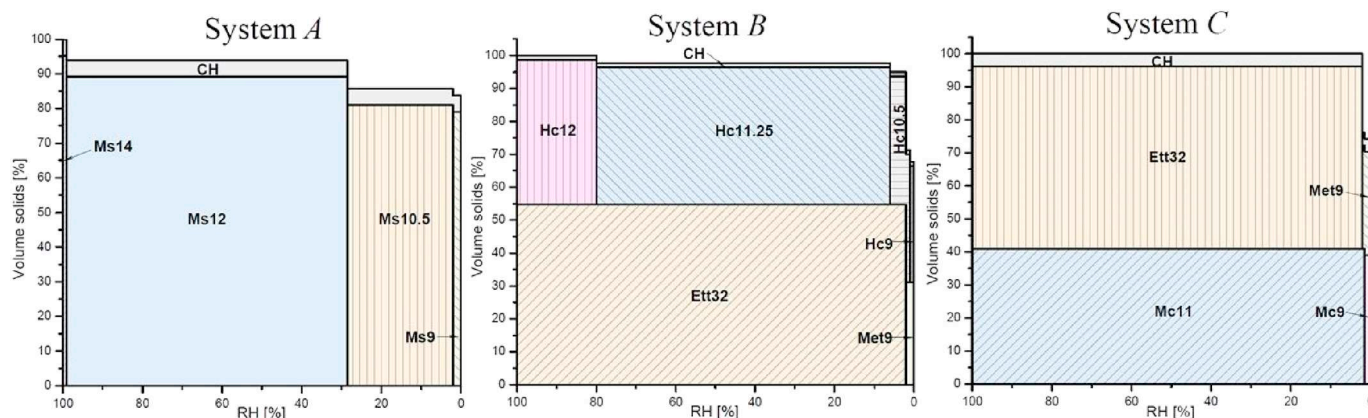


Fig. 17. Calculated specific volume changes of a hydrated model mixture consisting of C_3A , portlandite and with fixed sulfate ratio ($SO_3/Al_2O_3 = 1$, molar bulk ratio) in dependence of changing calcite content at 25 °C., as shown in Fig. 16 for the Systems A, B and C; calculated using Cemdata18.

monocarboaluminate and ettringite throughout the modelled composition range independently of the $CaCO_3$ content.

The consideration of the siliceous hydrogarnet solid solution in Cemdata18 led to a quite significant redistribution of alumina and iron within the phase assemblage. Whereas with Cemdata07 around 70% of the available alumina was bound in AFm phases (see Fig. 14A) the predictions based on Cemdata18 suggest that only about 25% of alumina is bound in AFm phases and ~30% in the hydrogarnet phase (Fig. 14B). For iron, the difference is even more drastic. The predictions with Cemdata18 suggest that close to 100% of the iron is bound by the siliceous hydrogarnet solid solution (Fig. 14D) which is also in agreement with experimental observations [64–66], where predominantly the formation of mixed aluminium and iron containing hydrogarnet phases in close proximity to the original ferrite phases was observed in hydrated cements.

The binding of alkalis in C-S-H lowers the alkali and hydroxide concentrations [81,84,88] in the pore solution of hydrated PC and thus the pH values from above 14 to ~13.5 [1,29,123,127]. The disregard of alkali binding by C-S-H would result in very high predicted pH values of 14 and above, which does not agree with measurements of the pore solution composition [5,29]. As in 2007 no thermodynamic models to describe the uptake of alkali in C-S-H were available, distribution coefficients (K_d values) were used together with Cemdata07 in most calculations of hydrated cements as described in details e.g. in [1,29,123]. The use of distribution coefficient allowed predicting the alkali concentrations in PC relatively well as shown in Fig. 15A, but the approach was not adequate to predict alkali uptake in low Ca/Si C-S-H present in blended cements. K_d values do not account for competitive sorption on specific sites which would be expected for the C-S-H gel, and also tend to be experiment-specific and so cannot generally be applied to other systems under different conditions. In the Cemdata18, the uptake of alkalis by C-S-H is modelled by introducing additional Na- and K-endmembers ($[(NaOH)_{2.5}SiO_2H_2O]_{0.2}$ and $[(KOH)_{2.5}SiO_2H_2O]_{0.2}$) in the CSHQ model, as described above (Section 2.7). The introduction of these provisional data simplify the modelling, as no additional K_d values have to be introduced in the models, and allows the calculation of alkali uptake over the whole range of Ca/Si ratios, although the agreement between measured and calculated alkali concentrations is only satisfactorily, as shown in Fig. 15B. Due to the lack of appropriate models for sodium and potassium uptake in C-S-H valid over the complete range of Ca/Si, the modelling of alkali and hydroxide concentrations in the pore solution remains a challenge.

The trends in the concentrations of calcium, sulfate, silicon and aluminium are generally correctly reproduced by both models (see e.g.

[1,29,123,127], Fig. 15) although there are differences between measured and calculated values, in particular for Ca and Al for Cemdata07 and for sulfate and silicon for Cemdata18.

3.2. Effect of relative humidity on hydrated cements

Using the thermodynamic properties of phases with different water contents described in Section 2.5 and Table 1 it was possible to predict the drying behaviour of hydrated systems.

Drying of the $CaO-Al_2O_3-SO_3-CO_2-H_2O$ was simulated because it is directly relevant to PC and limestone blended cements. The initial model mixture contained C_3A , portlandite (CH), calcium sulfate ($SO_3/Al_2O_3 = 1$ M bulk ratio), and varying amounts of calcite at 25 °C. The amount of solids was kept constant at 100 g and reacted with 90 g water. A diagram of the specific volume changes of the hydrated mixture with respect to calcite content is shown in Fig. 16.

Due to their differing AFm-AFt mineralogy hydrate phase assemblages A, B and C in Fig. 16, with 0%, 7% and 13.2% of calcite respectively, were selected as initial hydrated systems for the drying modelling. Drying was simulated by continuously removing water from the assemblages until a RH of zero was reached. The investigated systems were:

- System A: monosulfoaluminate (Ms14) and portlandite (CH)
- System B: ettringite (Ett32), hemicarboaluminate (Hc12) and portlandite (CH)
- System C: ettringite (Ett32), monocarboaluminate (Mc11) and portlandite (CH)

Fig. 17a, b and c present the evolution of specific solid volume as a function of RH. We can see that dehydration happens stepwise at critical RH stability limits of the phase assemblages, representing invariant points where the RH is fixed due to phase rule restrictions. At this critical RH two hydration states of the same cement hydrate coexist and buffer the humidity in a similar manner as conventional drying agents. Another important finding is that the addition of calcite and the formation of carboaluminates and ettringite will enhance the dimensional stability of hydrated cement paste and makes it less sensitive to humidity fluctuations, which appears to be relevant for limestone blended cements. Due to the presence of monocarboaluminate and ettringite system C is the most stable phase assemblage, which only decomposes at very low humidities (below 2% RH) whereas monosulfoaluminate quickly loses part of its interlayer water at < 99% RH.

Something important to keep in mind is that, although

experimentally we observe the changes shown in Fig. 17, several of these dehydration processes are metastable with respect to other phase assemblages. This has to be considered when predicting the drying behaviour of cementitious systems.

4. Conclusions

The Cemdata18 database summarised in this paper can reliably calculate the type, composition, amount and volume of hydrates formed and the pH and composition of the pore solution during hydration and degradation of cementitious systems. The Cemdata18 database, as compiled in Table 1 to Table 4, includes carefully selected thermodynamic data published in the literature based on critical reviews supplemented with new experimental data. Data for solids commonly encountered in cement systems in the temperature range 0–100 °C, including C-S-H, M-S-H, hydrogarnet, hydrotalcite-like phases, some zeolite, AFm and AFt phases and their respective solid solutions has been compiled. The Cemdata18 database is an update of the Cemdata07 and Cemdata14 databases, and is compatible with the GEMS version of the PSI/Nagra 12/07 TDB [22,23]. Cemdata18 TDB is freely downloadable (<http://www.empa.ch/cemdata>) in formats supporting the computer programs GEM-Selektor [13,14] and PHREEQC [18]. Further details are available in Appendices A and B.

The most important additions to the Cemdata18 TDB include:

- C-S-H:
 - CSHQ model for Portland and blended cements, the uptake of alkalis by C-S-H is modelled by additional Na- and K-containing end members
 - CSH3T model that corresponds to pure defect-tobermorite structure with ordering at Ca/Si ratio close to 1.0, and forms the basis for CNASH-ss model
 - C-(N)-A-S-H model for alkali activated materials (CNASH-ss), which calculates the uptake of aluminium and sodium in low Ca/Si C-S-H
- iron-containing hydrates, in particular for the mixed Fe-Al-hydrogarnet solid solution, $C_3FS_{0.84}H_{4.32}-C_3A_{0.5}F_{0.5}S_{0.84}H_{4.32}$, which takes up iron and a part of the aluminium in hydrated cements
- AFm and AFt-phases with different water contents to describe the effect of water activity and drying on hydrates
- amorphous, microcrystalline AH_3 and gibbsite to study the effect of AH_3 solubility on the hydrates in calcium aluminate and calcium sulfoaluminate cements
- chloride, nitrate and nitrate-containing AFm phases
- thaumasite and the uptake of carbonates in SO_4 -ettringite.
- description of the variation in Mg/Al in layered double hydroxides (hydrotalcite-like phases) observed in alkali activated materials
- data for M-S-H and some Na- and Ca-based zeolites, which can form at the interaction zone of cement with clays, rocks or seawater and in alkali activated materials.

Appendix A. Cemdata18 dataset in GEMS format

Cemdata18 database in GEM-Selektor v.3 format can be freely downloaded (<http://www.empa.ch/cemdata>) and is fully compatible with the GEMS version of the PSI/Nagra 12/07 TDB [22,23] (<http://gems.web.psi.ch>). As several alternative C-S-H models, as well as two models for hydroxide-hydrotalcite are available, the user needs to select the appropriate models during the generation of new projects, as illustrated in Fig. A.1. The CSHQ and the OH-hydrotalcite with Mg/Al = 2 are well adapted for Portland cement systems (select cemdata, pc, ht. and cshq as indicated at the left hand side of Fig. A.1).

For alkali activated binders, the CNASH model has been developed for C-S-H type calcium (alkali) aluminosilicate hydrate gels with lower calcium but higher aluminium and alkali content. An Mg-Al layered double hydroxide model with variable Mg/Al ratio is also available for use in alkali activated cement systems. For alkali activated binders, the selection of cemdata and aam and deselection of pc, including ht and csh is recommended as illustrated at the right hand side of Fig. A.1.

These additions improve the reliability of thermodynamic modelling of cement systems, in particular for alkali activated materials and for processes at cement/environment interfaces, where hydrates such as thaumasite, Friedel's salt, M-S-H, and zeolites may form.

The consideration of siliceous hydrogarnet solid solution in Cemdata18 leads to a quite significant redistribution of alumina and iron within the phase assemblage in PC; the predictions based on Cemdata18 suggest that alumina is bound not only in AFt, AFm phases and hydrotalcite but also in siliceous hydrogarnet phase while all hydrated iron is present in siliceous hydrogarnet.

Several C-S-H solubility models as well two models for hydroxide-hydrotalcite are available (Table 4, Appendices A and B). The CSHQ and the OH-hydrotalcite with Mg/Al = 2 are well adapted for PC systems. Although CSHQ is able to describe the entire range of Ca/Si ratios encountered, it is best used for high Ca/Si C-S-H as it lacks the ability to predict aluminium uptake, however, this is less important in PC where the aluminium content is relatively low. For alkali activated binders, the CNASH model has been developed for C-S-H type calcium (alkali) aluminosilicate hydrate gels with lower calcium but higher aluminium and alkali content. An Mg-Al layered double hydroxide model with variable Mg/Al ratio is also available for use in alkali activated cement systems.

Despite significant additions to the Cemdata18 TDB, several important gaps still exist in the database. In particular, reliable thermodynamic data for alkali, aluminium and water uptake in C-S-H applicable to high and low Ca/Si C-S-H and M-S-H, data for hydrotalcite-like phases of variable composition and for different interlayer ions, data for further zeolites derived from experimental solubility measurements, data for aqueous complexes which possibly form at high pH values as well as data for the reaction products of alkali silica reaction are needed. However, these data gaps should be viewed as possible future improvements rather than barriers to use thermodynamic modelling: Cemdata18 database has already been successfully applied to model hydrated PC, calcium aluminate, calcium sulfoaluminate and blended cements, and also alkali activated materials. Cemdata18, therefore, enables improved characterisation and understanding of the chemistry and related in-service performance properties of a wide range of cement systems, including the most common types.

Acknowledgements

The partial financial support from the NANOCER consortium (www.nanocem.org), the Swiss National Foundation (SNF grants No. 117605, 132559, 130419 and 200021_169014), from Nagra, Wettingen, Switzerland, and from the BMBF ThermAc3 Verbundprojekt (Germany) are gratefully acknowledged. The authors thank also Tres Thoenen, Ravi Patel and Andres Idriart for their support on the PHREEQC version.

Built-in Database	Version
<input checked="" type="checkbox"/> support	
<input checked="" type="checkbox"/> template	
<input type="checkbox"/> supcrt	
<input checked="" type="checkbox"/> psi-nagra	
<input checked="" type="checkbox"/> 3rdparty	
<input type="checkbox"/> cemdata	18.01
<input checked="" type="checkbox"/> .	
<input type="checkbox"/> pc	18.01
<input checked="" type="checkbox"/> .	
<input checked="" type="checkbox"/> ht	18.01
<input checked="" type="checkbox"/> csh	
<input checked="" type="checkbox"/> cshq	18.01
<input type="checkbox"/> cshkn	18.01
<input type="checkbox"/> csh3t	18.01
<input type="checkbox"/> csh2o	18.01
<input type="checkbox"/> aam	18.01
<input type="checkbox"/> .	
<input type="checkbox"/> csh+ht	18.01
<input checked="" type="checkbox"/> ss	18.01
<input checked="" type="checkbox"/> ss-fe3	18.01

Fig. A.1. Selection of modules of Cemdata18 and related databases in GEM-Selektor to model PC (Portland-cement) systems (left) and to model AAM (alkali-activated materials). For PC systems, one of four alternative solid solution models of C-S-H should be selected (see Section 2.7); selection of Fe-containing solid solutions (“ss-fe3+” module) is also optional.

Appendix B. Cemdata18 dataset in PHREEQC format

To enable users to model cementitious systems using the Cemdata18 dataset with the popular PHREEQC geochemical speciation code [18], a PHREEQC “.dat” format database of the Cemdata18 dataset (CEMDATA18.dat) is provided for download from <http://www.empa.ch/cemdata>. This LMA (Law of Mass Action) type dataset has been generated using the reaction generator module of the ThermoMatch code (Miron et al. in preparation) and exported into the PHREEQC format “.dat” file using the ThermoMatch database export module. The reaction generator algorithm is based on the matrix “row reduce” method described by Smith and Missen [128]. In this process, all aqueous and solid species from the Cemdata18 GEM-Selektor database were considered. The supplementary data for aqueous, gaseous and solid species corresponding to the list of elements covered by Cemdata18 were selected from the GEMS version of the PSI/Nagra TDB [22,23]. The latter and the Cemdata18 GEM database are mutually consistent, and should be used together in GEMS codes for modelling cementitious systems.

To generate PHREEQC-style reactions for product species, firstly the following master species were selected based on their generic predominance: Ca^{+2} , Mg^{+2} , Sr^{+2} , Na^{+} , K^{+} , H^{+} , CO_3^{-2} , SO_4^{-2} , Cl^{-} , NO_3^{-} , AlO_2^{-} , FeO_2^{-} , SiO_2^0 , H_2O^0 , and e^{-} (electron). Using selected master species, the reactions were automatically generated for the remaining (product) species, and their properties at 25 °C and 1 bar were calculated. Formation reactions were generated for aqueous product species, and dissolution reactions - for gaseous and solid product species. The LMA dataset of reactions was then exported into a PHREEQC “.dat” file (CEMDATA18.dat) using the ThermoMatch database export module. Parameters for the $\log K^\circ = f(T)$ analytical expressions were calculated for the 3-term extrapolation method that assumes the $\Delta_r C_p^\circ$ to be not zero and independent of temperature. These reported parameters are used by PHREEQC for calculating the $\log_{10} K^\circ$ as a function of temperature. Such temperature extrapolations of $\log_{10} K^\circ$ should be valid at least up to 100 °C.

Table B.1 contains the generated formation reactions for the aqueous product species, together with the values for reaction standard effects at 25 °C and 1 bar. Table B.2 contains the generated dissolution reactions for gaseous and solid product species, together with the reaction standard effects at 25 °C and 1 bar. Table B.2 contains, in addition to the Cemdata18 database as detailed in Table 1 to Table 4, also the thermodynamic data of all solids composed of Al, C, Ca, Cl, Fe, H, K, Mg, N, Na, S, Si or Sr compiled in the GEMS version of the PSI/Nagra 12/07 TDB [22,23], needed to allow the generation of a compatible dataset in PHREEQC. Figs. B.1, B.2, and B.3 show comparisons of cement-related modelling problems between GEM-Selektor (using GEM-type Cemdata18) and PHREEQC (using LMA-type Cemdata18 CEMDATA18.dat). For the PHREEQC calculations, PHREEQC for Windows version 2.18.00 (uses PHREEQC-2 source version 2.18.3-5570) was used. In all three cases, the considered solid solutions were modelled in PHREEQC using the simple ideal mixing model.

Table B.1
Product aqueous species reactions from master species, together with their reaction properties at 25 °C and 1 bar.

Product Substance	Reaction	$\log_{10}K_{298}^{\circ}$	$\Delta_r G_{298}^{\circ}$ [J/mol]	$\Delta_r H_{298}^{\circ}$ [J/mol]	$\Delta_r S_{298}^{\circ}$ [J/K/mol]	$\Delta_r Cp_{298}^{\circ}$ [J/K/mol]	$\Delta_r V_{298}^{\circ}$ [J/bar]
Al(SO ₄) ⁺	Si[6]O ₄ -2 + AlO ₂ - + 4H ⁺ + = Al(SO ₄) ⁺ + 2H ₂ O@	26.8	-152,857	-159,164	-21.2	261.8	0.8
Al(SO ₄) ₂ ⁻	2Si[6]O ₄ -2 + AlO ₂ - + 4H ⁺ + = Al(SO ₄) ₂ ⁻ + 2H ₂ O@	28.8	-164,272	-165,197	-3.1	463.6	3.2
Al ⁺ 3	AlO ₂ - + 4H ⁺ + = Al ⁺ 3 + 2H ₂ O@	22.9	-130,595	-176,821	-155.0	71.1	-1.9
AlHSiO ₃ + 2	AlO ₂ - + 3H ⁺ + + SiO ₂ = AlHSiO ₃ + 2 + H ₂ O	20.5	-116,839	-106,764	33.8	-136	3.3
AlO ⁺	AlO ₂ - + 2H ⁺ + = AlO ⁺ + H ₂ O@	12.3	-70,124	-73,951	-12.8	-0.7	0.9
AlO ₂ H@	AlO ₂ - + H ⁺ + = AlO ₂ H@	6.4	-36,798	-21,554	51.1	-160.2	0.4
AlOH + 2	AlO ₂ - + 3H ⁺ + = Al(OH) + 2 + H ₂ O@	17.9	-102,299	-127,582	-84.8	180.4	0.6
AlSiO ₅ -3	AlO ₂ - + H ₂ O@ + SiO ₂ @ = AlSiO ₅ -3 + 2H ⁺	-22.6	129,059	71,975	-191.5	0.0	-7.8
Ca(CO ₃)@	CO ₃ -2 + Ca + 2 = CaCO ₃ @	3.2	-18,405	16,462	116.9	196.4	0.9
Ca(HCO ₃) ⁺	CO ₃ -2 + Ca + 2 + H ⁺ + = Ca(HCO ₃) ⁺	11.4	-65,269	-13,562	173.4	554.0	3.8
Ca(HSiO ₃) ⁺	Ca + 2 + H ₂ O@ + SiO ₂ @ = Ca(HSiO ₃) ⁺ + H ⁺	-8.6	49,143	30,328	-63.1	48.9	-2.2
Ca(SO ₄)@	Ca + 2 + Si[6]O ₄ -2 = CaSO ₄ @	2.3	-13,128	4336	58.6	192.4	1.0
CaOH ⁺	Ca + 2 + H ₂ O@ = Ca(OH) ⁺ + H ⁺	-12.8	72,950	77,301	14.6	-38.4	0.6
CaSiO ₃ @	Ca + 2 + H ₂ O@ + SiO ₂ @ = CaSiO ₃ @ + 2H ⁺	-18.5	105,827	48,743	-191.5	0.0	-1.6
CH ₄ @	CO ₃ -2 + 8e ⁻ + 10H ⁺ + = C[4]H ₄ @ + 3H ₂ O@	38.2	-217,923	-270,138	-175.1	677.3	9.8
ClO ₄ ⁻	Cl ⁻ + 4H ₂ O@ = Cl[7]O ₄ - + 8e ⁻ + 8H ⁺	-187.7	1,071,500	1,181,308	368.3	-87.6	-4.6
CO ₂ @	CO ₃ -2 + 2H ⁺ + = CO ₂ @ + H ₂ O@	16.7	-95,216	-24,408	237.5	607.8	5.7
Fe(CO ₃)@	CO ₃ -2 + e ⁻ + 4H ⁺ + Fe[3]O ₂ - = FeCO ₃ @ + 2H ₂ O@	39.0	-222,615	-216,144	21.7	537.5	2.5
Fe(HCO ₃) ⁺	CO ₃ -2 + e ⁻ + 5H ⁺ + Fe[3]O ₂ - = FeHCO ₃ ⁺ + 2H ₂ O@	46.9	-267,988	-246,735	71.3	892.0	5.0
Fe(HSO ₄) ⁺	Si[6]O ₄ -2 + e ⁻ + 5H ⁺ + Fe[3]O ₂ - = FeHSO ₄ ⁺ + 2H ₂ O@	37.7	-215,125	-208,704	21.5	975.6	4.2
Fe(HSO ₄) ₂ + 2	Si[6]O ₄ -2 + 5H ⁺ + Fe[3]O ₂ - = Fe[3]HSO ₄ +2 + 2H ₂ O@	26.1	-148,798	-200,163	-172.3	1078.5	2.5
Fe(SO ₄)@	Si[6]O ₄ -2 + e ⁻ + 4H ⁺ + Fe[3]O ₂ - = Fe(SO ₄)@ + 2H ₂ O@	36.9	-210,456	-212,106	-5.5	535.7	2.4
Fe(SO ₄) ⁺	Si[6]O ₄ -2 + 4H ⁺ + Fe[3]O ₂ - = Fe[3](SO ₄) ⁺ + 2H ₂ O@	25.6	-146,355	-160,671	-48.0	505.8	2.0
Fe(SO ₄) ₂ ⁻	2Si[6]O ₄ -2 + 4H ⁺ + Fe[3]O ₂ - = Fe[3](SO ₄) ₂ ⁻ + 2H ₂ O@	27.0	-154,003	-162,930	-29.9	707.5	4.0
Fe + 2	e ⁻ + 4H ⁺ + Fe[3]O ₂ - = Fe + 2 + 2H ₂ O@	34.6	-197,613	-220,183	-75.7	338.8	1.3
Fe + 3	4H ⁺ + Fe[3]O ₂ - = Fe[3] ⁺ + 3 + 2H ₂ O@	21.6	-123,295	-177,529	-181.9	308.9	-0.2
FeHSiO ₃ + 2	FeO ₂ - + 3H ⁺ + SiO ₂ = Fe[3]HSiO ₃ + 2 + H ₂ O@	21.5	-122,665	-148,472	-86.5	101.9	3.5
FeCl ⁺	Cl ⁻ + e ⁻ + 4H ⁺ + Fe[3]O ₂ - = FeCl ⁺ + 2H ₂ O@	34.8	-198,413	-218,887	-68.7	580.2	1.9
FeCl ₂ + 2	Cl ⁻ + 4H ⁺ + Fe[3]O ₂ - = Fe[3]Cl ₂ + 2 + 2H ₂ O@	23.1	-131,742	-173,502	-140.1	523.0	-0.5
FeCl ₃ + 2	2Cl ⁻ + 4H ⁺ + Fe[3]O ₂ - = Fe[3]Cl ₃ + 2 + 2H ₂ O@	23.7	-135,453	-179,471	-147.6	931.3	1.1
FeCl ₃ @	3Cl ⁻ + 4H ⁺ + Fe[3]O ₂ - = Fe[3]Cl ₃ @ + 2H ₂ O@	22.7	-129,649	-190,999	-205.8	1121.3	2.0
FeO ⁺	2H ⁺ + Fe[3]O ₂ - = Fe[3]O ⁺ + H ₂ O@	15.9	-90,930	-97,152	-20.9	109.3	-2.4
FeO ₂ H@	H ⁺ + Fe[3]O ₂ - = Fe[3]O ₂ H@	9.0	-51,601	-37,130	48.5	-77.2	0.7
FeOH ⁺	e ⁻ + 3H ⁺ + Fe[3]O ₂ - = FeOH ⁺ + H ₂ O@	25.1	-143,387	-167,718	-81.6	358.9	0.1
FeOH + 2	3H ⁺ + Fe[3]O ₂ - = Fe[3](OH) ₂ + 2 + H ₂ O@	19.4	-110,794	-134,855	-80.7	276.6	-0.8
Fe ₂ (OH) ₂ + 4	2FeO ₂ - + 6H ⁺ + = Fe[3/2](OH) ₂ + 4 + 2H ₂ O@	40.3	-229,747	-298,572	-230.8	617.9	7.5
Fe ₃ (OH) ₄ + 5	3FeO ₂ - + 8H ⁺ + = Fe[3/3](OH) ₄ + 5 + 2H ₂ O@	58.5	-333,918	-472,753	-465.6	926.8	7.6

(continued on next page)

Table B.1 (continued)

Product Substance	Reaction	$\log_{10}K_{298}^{\circ}$	ΔG_{298}° [J/mol]	ΔH_{298}° [J/mol]	ΔS_{298}° [J/K/mol]	ΔG_{298}° [J/K/mol]	ΔV_{298}° [J/bar]
H ₂ @	2e ⁻ + 2H ⁺ = H ₂ O 2@	-3.1	17,729	-4018	-72.9	138.0	2.5
H ₂ S@	Si ₆ O ₄ -2 + 8e ⁻ + 10H ⁺ = H ₂ S -2 @ + 4H ₂ O@	40.7	-232,203	-272,852	-136.3	631.4	9.4
HCN@	CO ₃ -2 + NO ₃ - + 10e ⁻ + 13H ⁺ = HC -1 N O @ + 6H ₂ O@	117.4	-669,854	-729,336	-199.5	664.1	8.6
HCO ₃ -	CO ₃ -2 + H ⁺ = HCO ₃ -	10.3	-58,959	-14,699	148.4	254.5	3.0
HS-	Si ₆ O ₄ -2 + 8e ⁻ + 9H ⁺ = HS -2 + 4H ₂ O@	33.7	-192,305	-250,044	-193.7	358.3	8.0
HSiO ₃ -	H ₂ O@ + SiO ₂ @ = HSiO ₃ - + H ⁺	-9.8	55,992	29,057	-90.3	-207.0	-3.0
HSO ₄ -	Si ₆ O ₄ -2 + 2e ⁻ + 3H ⁺ = HS 4 O ₃ - + H ₂ O@	3.8	-11,822	-3885	60.2	307.2	3.8
K(SO ₄)-	Si ₆ O ₄ -2 + H ⁺ = HS 6 O ₄ -	2.0	-11,346	20,464	106.7	288.8	2.2
KOH@	Si ₆ O ₄ -2 + K ⁺ = KSO ₄ -	0.9	-4851	3070	26.6	212.6	0.6
Mg(CO ₃)@	H ₂ O@ + K ⁺ = KOH@ + H ⁺	-14.5	82,538	63,874	-62.6	-168.8	-1.2
Mg(HCO ₃) +	CO ₃ -2 + Mg + 2 = Mg(CO ₃)@	3.0	-17,009	9124	87.7	194.5	1.1
Mg(HSiO ₃) +	CO ₃ -2 + Mg + 2 + H ⁺ = Mg(HCO ₃) +	11.4	-65,056	-12,725	175.5	565.4	3.7
MgOH +	Mg + 2 + H ₂ O@ = Mg(OH) + + H ⁺	-8.3	47,429	25,758	-72.7	60.5	-2.3
MgSiO ₃ @	Mg + 2 + H ₂ O + SiO ₂ = MgSiO ₃ @ + 2H ⁺	-11.4	65,300	61,792	-11.8	75.5	0.6
MgSO ₄ @	Si ₆ O ₄ -2 + Mg + 2 = Mg(SO ₄)@ + 2H ⁺	-17.4	99,548	85,125	-48.4	-363.0	1.0
N ₂ @	2NO ₃ - + 10e ⁻ + 12H ⁺ = N ₂ O 2@ + 6H ₂ O@	2.4	-13,529	6855	68.4	197.4	1.1
Na(CO ₃)-	CO ₃ -2 + Na ⁺ = NaCO ₃ -	207.3	-1,183,095	-1,311,876	-431.9	675.7	8.4
Na(HCO ₃)@	CO ₃ -2 + Na ⁺ + H ⁺ = NaHCO ₃ @	1.3	-7251	-22,969	-52.7	199.9	0.7
Na(SO ₄)-	Si ₆ O ₄ -2 + Na ⁺ = Na(SO ₄)-	10.1	-57,533	-13,909	146.3	451.5	4.0
NaOH@	Na ⁺ + H ₂ O@ = NaOH@ + H ⁺	0.7	-3996	3314	24.5	197.9	0.7
NH ₃ @	NO ₃ - + 8e ⁻ + 9H ⁺ = N -3 H ₃ @ + 3H ₂ O@	-14.2	80,940	56,026	-83.6	-126.9	-1.3
NH ₄ +	NO ₃ - + 8e ⁻ + 10H ⁺ = N -3 H ₄ + + 3H ₂ O@	109.9	-627,314	-732,284	-352.1	254.4	5.0
O ₂ @	2H ₂ O@ = O O 2@ + 4e ⁻ + 4H ⁺	119.1	-680,039	-784,011	-348.7	244.6	4.4
OH-	H ₂ O@ = OH- + H ⁺	-86.0	490,812	559,525	230.5	141.1	-0.6
S-2	H ₂ O@ = OH- + H ⁺	-14.0	79,913	55,872	-80.6	-211.7	-2.3
S ₂ O ₃ -2	Si ₆ O ₄ -2 + 8e ⁻ + 8H ⁺ = S -2 2 + 4H ₂ O@	14.7	-83,851	-250,044	-557.4	358.3	5.9
SCN-	2S -6 O ₄ -2 + 8e ⁻ + 10H ⁺ = S 2 2O ₃ -2 + 5H ₂ O@	38.0	-216,987	-259,866	-143.8	555.2	9.2
Si ₄ O ₁₀ -4	CO ₃ -2 + NO ₃ - + Si ₆ O ₄ -2 + 16e ⁻ + 20H ⁺ = S O C O N -1 - + 10H ₂ O@	156.9	-895,711	-990,513	-318.0	1105.5	18.1
SiO ₃ -2	2H ₂ O@ + 4SiO ₂ @ = Si ₄ O ₁₀ -4 + 4H ⁺	-36.3	207,202	207,202	0.0	0.0	-10.0
SiO ₃ -2	H ₂ O@ + SiO ₂ @ = SiO ₃ -2 + 2H ⁺	-23.1	132,084	75,000	-191.5	0.0	-3.4
Sr(CO ₃)@	Si ₆ O ₄ -2 + 2e ⁻ + 2H ⁺ = S 4 O ₃ -2 + H ₂ O@	-3.4	19,390	-13,070	-108.9	31.6	0.1
Sr(HCO ₃) +	CO ₃ -2 + Sr + 2 = Sr(CO ₃)@	2.8	-16,013	18,891	117.1	196.6	0.9
Sr(SO ₄)@	CO ₃ -2 + Sr + 2 + H ⁺ = SrHCO ₃ +	11.5	-65,721	-12,816	177.4	541.0	3.8
SrOH +	Si ₆ O ₄ -2 + Sr + 2 = Sr(SO ₄)@	2.3	-13,072	9071	74.3	197.1	1.0
SrSiO ₃ @	Sr + 2 + H ₂ O@ = Sr(OH) + + H ⁺	-13.3	75,860	82,619	22.7	-65.5	0.7
	Sr + 2 + H ₂ O@ + SiO ₂ @ = SrSiO ₃ @ + 2H ⁺	-18.8	107,136	107,184	0.2	0.1	0.0

e⁻ - represents one electron.

|| - is used for specifying a different valence for the element.

@ - is used to represent a neutral aqueous species.

Table B.2
Product solid and gaseous species reactions from master species, together with their reaction properties at 25 °C and 1 bar.

Product Substance	Reaction	$\log 10^{\circ}$ 298	A_f° 298 [J/mol]	A_f^H 298 [J/mol]	A_f° 298 [J/K/ mol]	A_f^{cp} 298 [J/K/ mol]	A_f° 298 [J/ bar]
5CA	(CaO)1.25(SiO ₂)1(Al ₂ O ₃)0.125(H ₂ O)1.625 + 2.25H ⁺ = 0.25AlO ₂ ⁻ + 1.25Ca + 2 + 2.75H ₂ O@ + SiO ₂ @	15.9	-90709	-92987	-7.6	23.7	-1.2
5CNA	(CaO)1.25(SiO ₂)1(Al ₂ O ₃)0.125(Na ₂ O)0.25(H ₂ O)1.375 + 2.75H ⁺ = 0.25AlO ₂ ⁻ + 1.25Ca + 2 + 0.5Na + 2.75H ₂ O@ + SiO ₂ @	23.2	-132663	-135750	-10.4	43.6	-2.0
AlOHam	Al(OH)3 = AlO ₂ ⁻ + H ⁺ + H ₂ O@	-13.8	78536	69482	-30.4	-66.8	-0.4
AlOHmic	Al(OH)3 = AlO ₂ ⁻ + H ⁺ + H ₂ O@	-14.7	83730	53830	-100.3	-66.8	-0.4
Amor-Sl	SiO ₂ = SiO ₂ @	-2.7	15492	15492	0.0	0.0	-1.3
Anh	CaSO ₄ = Ca + 2 + S[6]O4-2	-4.4	24872	-18165	-144.3	-396.7	-5.1
Arg	CaCO ₃ = CO ₃ -2 + Ca + 2	-8.3	47583	-11060	-196.7	-401.5	-5.9
Brc	Mg(OH)2 + 2H ⁺ = Mg + 2 + 2H ₂ O@	16.8	-96124	-114419	-61.4	51.8	-1.1
C12A7	(CaO)12(Al ₂ O ₃)7 + 10H ⁺ = 14AlO ₂ ⁻ + 12Ca + 2 + 5H ₂ O@	167.2	-954361	-1489798	-1795.9	-1765.7	-51.6
C2ACIH5	Ca ₂ AlCl(OH)6(H ₂ O)2 + 2H ⁺ = AlO ₂ ⁻ + 2Ca + 2 + Cl ⁻ + 6H ₂ O@	14.4	-82445	-92106	-32.4	-195.7	-3.8
C2AH65	Ca ₂ Al(OH)7(H ₂ O)3 + 3H ⁺ = AlO ₂ ⁻ + 2Ca + 2 + 8H ₂ O@	29.4	-167699	-167567	0.4	-79.0	-2.0
C2AH7.5	Ca ₂ Al ₂ (OH)10(H ₂ O)2.5 + 2H ⁺ = 2AlO ₂ ⁻ + 2Ca + 2 + 8.5H ₂ O@	14.2	-81085	-89743	-29.0	-55.2	-4.4
C2S	(CaO)2SiO ₂ + 4H ⁺ = 2Ca + 2 + 2H ₂ O@ + SiO ₂ @	38.5	-219567	-237276	-59.4	4.7	-3.6
C3A	(CaO)3Al ₂ O ₃ + 4H ⁺ = 2AlO ₂ ⁻ + 3Ca + 2 + 2H ₂ O@	70.7	-403436	-491527	-295.5	-249.5	-8.9
C3AFS0.84H4.32	(AlFe[3]O3)[Ca ₃ O ₃ (SiO ₂)0.84(H ₂ O)4.32] + 4H ⁺ = AlO ₂ ⁻ + 3Ca + 2 + 6.32H ₂ O@ + 0.84SiO ₂ @ + Fe[3]O ₂ -	22.3	-127203	-215980	-297.8	-286.9	-6.3
C3AH6	Ca ₃ Al ₂ O ₆ (H ₂ O)6 + 4H ⁺ = 2AlO ₂ ⁻ + 3Ca + 2 + 8H ₂ O@	35.5	-202666	-230152	-92.2	-33.6	-4.2
C3AS0.41H5.18	Ca ₃ Al ₂ O ₆ (SiO ₂)0.41(H ₂ O)5.18 + 4H ⁺ = 2AlO ₂ ⁻ + 3Ca + 2 + 7.18H ₂ O@ + 0.41SiO ₂ @	28.9	-165175	-197973	-110.0	-61.6	-4.6
C3AS0.84H4.32	Ca ₃ Al ₂ O ₆ (SiO ₂)0.84(H ₂ O)4.32 + 4H ⁺ = 2AlO ₂ ⁻ + 3Ca + 2 + 6.32H ₂ O@ + 0.84SiO ₂ @	25.8	-147182	-185475	-128.4	-90.9	-5.1
C3FH6	Ca ₃ Fe ₁₃ 206(H ₂ O)6 + 4H ⁺ = 3Ca + 2 + 8H ₂ O@ + 2Fe[3]O ₂ -	29.7	-169558	-286244	-391.4	-426.6	-6.5
C3FS0.84H4.32	(Fe[3]Fe[3]O3)[Ca ₃ O ₃ (SiO ₂)0.84(H ₂ O)4.32] + 4H ⁺ = 3Ca + 2 + 6.32H ₂ O@ + 0.84SiO ₂ @ + 2Fe[3]O ₂ -	20.0	-114074	-246486	-444.1	-482.9	-7.5
C3FS1.34H3.32	Ca ₃ Fe[3]2O6(SiO ₂)1.34(H ₂ O)3.32 + 4H ⁺ = 3Ca + 2 + 5.32H ₂ O@ + 1.34SiO ₂ @ + 2Fe[3]O ₂ -	16.2	-92409	-233544	-473.4	-516.4	-8.5
C3S	(CaO)3SiO ₂ + 6H ⁺ = 3Ca + 2 + 3H ₂ O@ + SiO ₂ @	73.3	-418180	-444107	-87.0	6.2	-5.8
C4ACIH10	Ca ₄ Al ₂ Cl ₂ (OH)12(H ₂ O)4 + 4H ⁺ = 2AlO ₂ ⁻ + 4Ca + 2 + 2Cl ⁻ + 12H ₂ O@	28.9	-164890	-184212	-64.8	-391.5	-7.6
C4AF	(CaO)4(Al ₂ O ₃)(Fe[3]2O3) + 4H ⁺ = 2AlO ₂ ⁻ + 4Ca + 2 + 2H ₂ O@ + 2Fe[3]O ₂ -	50.5	-288060	-402597	-384.2	-937.0	-14.8
C4AH11	Ca ₄ Al ₂ (OH)14(H ₂ O)4 + 6H ⁺ = 2AlO ₂ ⁻ + 4Ca + 2 + 14H ₂ O@	60.5	-345302	-369182	-80.1	-228.6	-5.9
C4AH13	Ca ₄ Al ₂ (OH)14(H ₂ O)6 + 6H ⁺ = 2AlO ₂ ⁻ + 4Ca + 2 + 16H ₂ O@	58.8	-335407	-335144	0.9	-158.0	-4.0
C4AH19	Ca ₄ Al ₂ (OH)14(H ₂ O)12 + 6H ⁺ = 2AlO ₂ ⁻ + 4Ca + 2 + 22H ₂ O@	58.6	-334271	-294930	132.0	53.7	-2.6
C4AsCIH12	Ca ₄ Al ₂ Cl(SO ₄)0.5(OH)12(H ₂ O)6 + 4H ⁺ = 2AlO ₂ ⁻ + 4Ca + 2 + Cl ⁻ + 0.5S[6]O4-2 + 14H ₂ O@	27.6	-157430	-175702	-61.3	-351.3	-6.7
C4FH13	Ca ₄ Fe[3]2(OH)14(H ₂ O)6 + 6H ⁺ = 4Ca + 2 + 16H ₂ O@ + 2Fe[3]O ₂ -	53.3	-304002	-199193	351.5	-343.7	-7.0
CA	CaOAl ₂ O ₃ = 2AlO ₂ ⁻ + Ca + 2	-0.3	1756	-67154	-231.1	-254.7	-5.3
CA2	CaO(Al ₂ O ₃)2 + H ₂ O@ = 4AlO ₂ ⁻ + Ca + 2 + 2H ⁺	-30.1	171600	44867	-425.1	-502.0	-8.8
CAH10	CaOAl ₂ O ₃ (H ₂ O)10 = 2AlO ₂ ⁻ + Ca + 2 + 10H ₂ O@	-7.6	43348	35098	-27.7	-43.2	-1.3
Cal	CaCO ₃ = CO ₃ -2 + Ca + 2	-8.5	48404	-10975	-199.2	-402.1	-6.1
CH4	Cl ⁻ 4[H ₄ + 3H ₂ O@ = CO ₃ -2 + 10H ⁺ + 8e-	-41.0	234277	257142	76.7	-435.8	-
Cls	SrSO ₄ = S[6]O4-2 + Sr + 2	-6.6	37855	-854	-129.8	-415.5	-5.1

(continued on next page)

Table B.2 (continued)

Product	Substance	Reaction	$\log 10^{-\circ}$ 298	A_f^G 298 [J/mol]	A_f^H 298 [J/mol]	A_f^S 298 [J/K/ mol]	A_f^{Cp} 298 [J/K/ mol]	A_f° 298 [J/ bar]
CO2		$CO_2 + H_2O@ = CO_3^{2-} + 2H^+$	-18.1	103560	4079	-333.7	-401.8	-
CSH3T-T2C		$((CaO)0.75(SiO_2)0.5(H_2O)1.25)_2 + 3H^+ = 1.5Ca + 2 + 4H_2O@ + SiO_2@$	25.3	-144257	-123574	69.4	62.5	-2.0
CSH3T-T5C		$((CaO)1(SiO_2)1(H_2O)2)1.25 + 2.5H^+ = 1.25Ca + 2 + 3.75H_2O@ + 1.25SiO_2@$	18.1	-103538	-78676	83.4	65.4	-1.4
CSH3T-TobH		$(CaO)1(SiO_2)1.5(H_2O)2.5 + 2H^+ = Ca + 2 + 3.5H_2O@ + 1.5SiO_2@$	12.5	-71524	-42463	97.5	68.4	-1.6
CSHQ-JenD		$(CaO)1.5(SiO_2)0.6667(H_2O)2.5 + 3H^+ = 1.5Ca + 2 + 4H_2O@ + 0.6667SiO_2@$	28.7	-164004	-149357	49.1	51.9	-2.6
CSHQ-JenH		$(CaO)1.3333(SiO_2)1(H_2O)2.1667 + 2.6666H^+ = 1.3333Ca + 2 + 3.5H_2O@ + SiO_2@$	22.2	-126609	-106258	68.3	59.1	-2.1
CSHQ-TobD		$((CaO)1.25(SiO_2)1(H_2O)2.75)0.6667 + 1.66675H^+ = 0.833375Ca + 2 + 2.6668H_2O@ + 0.6667SiO_2@$	13.7	-77952	-64488	45.2	37.9	-0.4
CSHQ-TobH		$(CaO)0.6667(SiO_2)1(H_2O)1.5 + 1.3334H^+ = 0.6667Ca + 2 + 2.1667H_2O@ + SiO_2@$	8.3	-47306	-27842	65.3	45.5	-1.2
Dis-Dol		$CaMg(CO_3)_2 = 2CO_3^{2-} + Ca + 2 + Mg + 2$	-16.5	94412	43108	-461.2	-789.0	-11.7
ECSH1-KSH		$((KOH)2.5SiO_2H_2O)0.2 + 0.5H^+ = 0.7H_2O@ + 0.2SiO_2@ + 0.5K^+$	5.5	-31394	-13703	59.3	25.2	0.8
ECSH1-NaSH		$((NaOH)2.5SiO_2H_2O)0.2 + 0.5H^+ = 0.5Na^+ + 0.7H_2O@ + 0.2SiO_2@$	5.4	-30883	-17398	45.2	42.8	0.5
ECSH1-SH		$(SiO_2H_2O)1 = H_2O@ + SiO_2@$	-2.6	14839	14839	0.0	0.0	0.0
ECSH1-SrSH		$((Sr(OH)2)1SiO_2H_2O)1 + 2H^+ = Sr + 2 + 3H_2O@ + SiO_2@$	15.4	-87911	-64744	77.7	54.2	-1.1
ECSH1-TobCa		$((Ca(OH)2)0.8333SiO_2H_2O)1 + 1.6666H^+ = 0.8333Ca + 2 + 2.6666H_2O@ + SiO_2@$	11.0	-62909	-43194	66.1	49.3	-1.9
ECSH2-JenCa		$((Ca(OH)2)1.6667SiO_2H_2O)0.6 + 2.00004H^+ = 1.00002Ca + 2 + 2.60004H_2O@ + 0.6SiO_2@$	17.6	-100489	-77495	77.1	77.2	0.2
ECSH2-KSH		$((KOH)2.5SiO_2H_2O)0.2 + 0.5H^+ = 0.7H_2O@ + 0.2SiO_2@ + 0.5K^+$	6.0	-34250	-16559	59.3	25.2	0.8
ECSH2-NaSH		$((NaOH)2.5SiO_2H_2O)0.2 + 0.5H^+ = 0.5Na^+ + 0.7H_2O@ + 0.2SiO_2@$	5.9	-33732	-20247	45.2	42.8	0.5
ECSH2-SrSH		$((Sr(OH)2)1SiO_2H_2O)1 + 2H^+ = Sr + 2 + 3H_2O@ + SiO_2@$	16.2	-92473	-69306	77.7	54.2	-1.1
ECSH2-TobCa		$((Ca(OH)2)0.8333SiO_2H_2O)1 + 1.6666H^+ = 0.8333Ca + 2 + 2.6666H_2O@ + SiO_2@$	11.0	-62909	-43194	66.1	49.3	-1.9
ettringite		$((H_2O)2)Ca_6Al_2(SO_4)3(OH)12(H_2O)24 + 4H^+ = 2AlO_2^- + 6Ca + 2 + 3S[6]O_4^{2-} + 34H_2O@$	11.2	-63708	-23594	134.5	-694.0	-14.6
ettringite03_ss		$(SO_4)Ca_2Al_0.6666667(OH)4(H_2O)8.6666667 + 1.3333332H^+ = 0.6666667AlO_2^- + 2Ca + 2 + S[6]O_4^{2-} + 11.333333H_2O@$	3.7	-21231	-7860	44.8	-231.3	-4.9
ettringite05		$Ca_3Al(SO_4)1.5(OH)6(H_2O)13 + 2H^+ = AlO_2^- + 3Ca + 2 + 1.5S[6]O_4^{2-} + 17H_2O@$	5.6	-31852	-11795	67.3	-347.0	-7.3
ettringite13		$Ca_6Al_2(SO_4)3(OH)12(H_2O)7 + 4H^+ = 2AlO_2^- + 6Ca + 2 + 3S[6]O_4^{2-} + 15H_2O@$	39.0	-222527	-596572	-1254.6	-1364.4	-19.3
Ettringite13_des		$Ca_6Al_2(SO_4)3(OH)12(H_2O)7 + 4H^+ = 2AlO_2^- + 6Ca + 2 + 3S[6]O_4^{2-} + 15H_2O@$	39.0	-222527	-596572	-1254.6	-1364.4	-19.3
ettringite30		$Ca_6Al_2(SO_4)3(OH)12(H_2O)24 + 4H^+ = 2AlO_2^- + 6Ca + 2 + 3S[6]O_4^{2-} + 32H_2O@$	11.8	-67136	-36633	102.3	-764.6	-18.3
ettringite9		$Ca_6Al_2(SO_4)3(OH)12(H_2O)3 + 4H^+ = 2AlO_2^- + 6Ca + 2 + 3S[6]O_4^{2-} + 11H_2O@$	48.0	-273943	-339631	-220.3	-1505.6	-21.5
Ettringite9_des		$Ca_6Al_2(SO_4)3(OH)12(H_2O)3 + 4H^+ = 2AlO_2^- + 6Ca + 2 + 3S[6]O_4^{2-} + 11H_2O@$	48.0	-273943	-339631	-220.3	-1505.6	-21.5
Fe		$Fe[0] + 2H_2O@ = 4H^+ + 3e^- + Fe[3]O_2^-$	-18.6	106109	127947	73.2	-367.4	-4.3
Fe-ettringite		$Ca_6Fe[3]2(SO_4)3(OH)12(H_2O)26 + 4H^+ = 6Ca + 2 + 3S[6]O_4^{2-} + 34H_2O@ + 2Fe[3]O_2^-$	12.1	-68843	4803	247.0	-1091.4	-17.4
Fe-ettringite05		$Ca_3Fe[3](SO_4)1.5(OH)6(H_2O)13 + 2H^+ = 3Ca + 2 + 1.5S[6]O_4^{2-} + 17H_2O@ + Fe[3]O_2^-$	6.0	-34420	2403	123.5	-545.7	-8.7
Fe-hemicarbonate		$Ca_3O_3Fe[3]2O_3(CaCO_3)0.5(CaO_2H_2)0.5(H_2O)9.5 + 5H^+ = 0.5CO_3^{2-} + 4Ca + 2 + 12.5H_2O@ + 2Fe[3]O_2^-$	39.2	-223627	-390054	-558.2	-637.4	-12.3
Femonocarbonate		$Ca_4O_4Fe[3]2O_3CO_2(H_2O)12 + 4H^+ = CO_3^{2-} + 4Ca + 2 + 14H_2O@ + 2Fe[3]O_2^-$	21.4	-122258	-252941	-438.3	-778.2	-11.8
Fe-monosulph05		$Ca_2Fe[3]SO_5O_5(H_2O)6 + 2H^+ = 2Ca + 2 + 0.5S[6]O_4^{2-} + 7H_2O@ + Fe[3]O_2^-$	12.2	-69792	-154688	-284.7	-386.3	-6.4
Fe-monosulphate		$Ca_4Fe[3]2SO_{10}(H_2O)12 + 4H^+ = 4Ca + 2 + S[6]O_4^{2-} + 14H_2O@ + 2Fe[3]O_2^-$	24.5	-139576	-309368	-569.5	-772.7	-12.8
FeOOHmic		$Fe[3]OOH = H^+ + Fe[3]O_2^-$	-19.6	111875	65468	-155.7	-309.3	-3.4
Gbs		$Al(OH)3 = AlO_2^- + H^+ + H_2O@$	-15.1	86323	77269	-30.4	-66.8	-0.4

(continued on next page)

Table B.2 (continued)

Product	Substance	Reaction	$\log 10^{\circ}$ 298	A_f^G 298 [J/mol]	A_f^H 298 [J/mol]	A_f^S 298 [J/K/ mol]	A_f^{Cp} 298 [J/K/ mol]	A_f° 298 [J/ bar]
Gp		$\text{CaSO}_4(\text{H}_2\text{O})_2 = \text{Ca} + 2 + \text{S}[6 \text{O}_4\text{-}2 + 2\text{H}_2\text{O}@$	-4.6	26147	-1167	-91.6	-332.5	-4.4
Gr		$\text{C} 0 + 3\text{H}_2\text{O}@ = \text{CO}_3\text{-}2 + 6\text{H} + + 4\text{e-}$	-32.2	183569	182332	-4.1	-466.4	-6.6
Gt		$\text{Fe}[3 \text{O}(\text{OH}) = \text{H} + + \text{Fe}[3 \text{O}_2\text{-}$	-22.6	128995	124419	-15.4	-309.2	-2.0
H2		$\text{H}[0 2 = 2\text{H} + + 2\text{e-}$	0.0	0	0	0.0	0.0	-
H2O		$\text{H}_2\text{O} = \text{H}_2\text{O}@$	1.5	-8500	-43481	-117.3	35.3	-
H2S		$\text{H}_2\text{S}[-2 + 4\text{H}_2\text{O}@ = \text{S}[6 \text{O}_4\text{-}2 + 10\text{H} + + 8\text{e-}$	-41.7	237742	254458	56.1	-486.4	-
Hem		$\text{Fe}[3 2\text{O}_3 + \text{H}_2\text{O}@ = 2\text{H} + + 2\text{Fe}[3 \text{O}_2\text{-}$	-42.1	240195	219672	-68.8	-650.0	-4.7
hemicarbonat10.5		$(\text{CaO})3\text{Al}_2\text{O}_3(\text{CaCO}_3)0.5(\text{CaO}_2\text{H}_2)0.5(\text{H}_2\text{O})10 + 5\text{H} + = 2\text{AlO}_2\text{-} + 0.5\text{CO}_3\text{-}2 + 4\text{Ca} + 2 + 13\text{H}_2\text{O}@$	42.6	-243220	-264276	-70.6	-232.4	-8.4
hemicarbonat		$(\text{CaO})3\text{Al}_2\text{O}_3(\text{CaCO}_3)0.5(\text{CaO}_2\text{H}_2)0.5(\text{H}_2\text{O})11.5 + 5\text{H} + = 2\text{AlO}_2\text{-} + 0.5\text{CO}_3\text{-}2 + 4\text{Ca} + 2 + 14.5\text{H}_2\text{O}@$	40.9	-233337	-236348	-10.1	-179.5	-8.0
hemicarbonat9		$(\text{CaO})3\text{Al}_2\text{O}_3(\text{CaCO}_3)0.5(\text{CaO}_2\text{H}_2)0.5(\text{H}_2\text{O})8.5 + 5\text{H} + = 2\text{AlO}_2\text{-} + 0.5\text{CO}_3\text{-}2 + 4\text{Ca} + 2 + 11.5\text{H}_2\text{O}@$	45.6	-260338	-299005	-129.7	-285.4	-9.9
hemihydrate		$\text{CaSO}_4(\text{H}_2\text{O})0.5 = \text{Ca} + 2 + \text{S}[6 \text{O}_4\text{-}2 + 0.5\text{H}_2\text{O}@$	-3.6	20413	-20432	-137.0	-383.4	-5.8
hydrotalcite		$\text{Mg}_4\text{Al}_2(\text{OH})_2(\text{H}_2\text{O})10 + 6\text{H} + = 2\text{AlO}_2\text{-} + 4\text{Mg} + 2 + 13\text{H}_2\text{O}@$	28.0	-159755	-235072	-252.6	146.4	-5.4
INPCA		$(\text{CaO})1(\text{SiO}_2)1.1875(\text{Al}_2\text{O}_3)0.15625(\text{H}_2\text{O})1.65625 + 1.6875\text{H} + = 0.3125\text{AlO}_2\text{-} + \text{Ca} + 2 + 2.5\text{H}_2\text{O}@ + 1.1875\text{SiO}_2@$	9.0	-51116	-50080	3.5	14.1	-1.1
INFCN		$(\text{CaO})1(\text{SiO}_2)1.5(\text{Na}_2\text{O})0.3125(\text{H}_2\text{O})1.1875 + 2.625\text{H} + = \text{Ca} + 2 + 0.625\text{Na} + + 2.5\text{H}_2\text{O}@ + 1.5\text{SiO}_2@$	18.8	-107089	-97770	31.3	64.3	-2.1
INFCNA		$(\text{CaO})1.25(\text{SiO}_2)1(\text{Al}_2\text{O}_3)0.125(\text{Na}_2\text{O})0.25(\text{H}_2\text{O})1.375 + 2.75\text{H} + = 0.25\text{AlO}_2\text{-} + 1.25\text{Ca} + 2 + 0.5\text{Na} + + 2.75\text{H}_2\text{O}@ + \text{SiO}_2@$	23.2	-132663	-135750	-10.4	43.6	-2.0
Jennite		$(\text{SiO}_2)1(\text{CaO})1.666667(\text{H}_2\text{O})2.1 + 3.333334\text{H} + = 1.666667\text{Ca} + 2 + 3.766667\text{H}_2\text{O}@ + \text{SiO}_2@$	29.3	-167347	-146306	70.6	66.0	-2.5
K2O		$\text{K}_2\text{O} + 2\text{H} + = \text{H}_2\text{O}@ + 2\text{K} +$	84.1	-480020	-426988	177.9	8.0	-0.4
K2SO4		$\text{K}_2\text{SO}_4 = \text{S}[6 \text{O}_4\text{-}2 + 2\text{K} +$	-1.8	10214	23725	45.3	-379.3	-3.5
Kln		$\text{Al}_2\text{Si}_2\text{O}_5(\text{OH})_4 = 2\text{AlO}_2\text{-} + 2\text{H} + + \text{H}_2\text{O}@ + 2\text{SiO}_2@$	-38.3	218758	185703	-110.9	-173.4	-3.0
*KSiOH		$((\text{KOH})2.5\text{SiO}_2\text{H}_2\text{O})0.2 + 0.5\text{H} + = 0.7\text{H}_2\text{O}@ + 0.2\text{SiO}_2@ + 0.5\text{K} +$	5.8	-32604	-13463	65.3	20.7	0.8
Lim		$\text{CaO} + 2\text{H} + = \text{Ca} + 2 + \text{H}_2\text{O}@$	32.6	-186017	-193861	-26.3	1.6	-1.7
M4A-OH-LDH		$\text{Mg}_4\text{Al}_2(\text{OH})14(\text{H}_2\text{O})3 + 6\text{H} + = 2\text{AlO}_2\text{-} + 4\text{Mg} + 2 + 13\text{H}_2\text{O}@$	34.3	-195826	-271137	-252.6	147.4	-5.3
M6A-OH-LDH		$\text{Mg}_6\text{Al}_2(\text{OH})18(\text{H}_2\text{O})3 + 10\text{H} + = 2\text{AlO}_2\text{-} + 6\text{Mg} + 2 + 17\text{H}_2\text{O}@$	68.0	-388083	-499991	-375.3	250.0	-11.1
M8A-OH-LDH		$\text{Mg}_8\text{Al}_2(\text{OH})22(\text{H}_2\text{O})3 + 14\text{H} + = 2\text{AlO}_2\text{-} + 8\text{Mg} + 2 + 21\text{H}_2\text{O}@$	101.7	-580340	-728838	-498.1	353.5	-17.0
Mag		$\text{FeFe}[3 2\text{O}_4 + 2\text{H}_2\text{O}@ = 4\text{H} + + \text{e-} + 3\text{Fe}[3 \text{O}_2\text{-}$	-67.8	387007	361013	-87.2	-992.8	-7.9
Melanterite		$\text{FeSO}_4(\text{H}_2\text{O})7 = \text{S}[6 \text{O}_4\text{-}2 + 4\text{H} + + \text{e-} + 5\text{H}_2\text{O}@ + \text{Fe}[3 \text{O}_2\text{-}$	-36.8	210222	230774	68.9	-109.8	-4.3
Mg2AlCO.5OH		$\text{Mg}_2\text{Al}(\text{OH})6(\text{CO}_3)0.5(\text{H}_2\text{O})2 + 2\text{H} + = \text{AlO}_2\text{-} + 0.5\text{CO}_3\text{-}2 + 2\text{Mg} + 2 + 6\text{H}_2\text{O}@$	5.9	-33755	-100890	-225.2	-182.5	-4.0
Mg2FeCO.5OH		$\text{Mg}_2\text{Fe}[3 (\text{OH})6(\text{CO}_3)0.5(\text{H}_2\text{O})2 + 2\text{H} + = 0.5\text{CO}_3\text{-}2 + 2\text{Mg} + 2 + 6\text{H}_2\text{O}@ + \text{Fe}[3 \text{O}_2\text{-}$	5.8	-33224	-81424	-161.7	-377.1	-5.6
Mg3AlCO.5OH		$\text{Mg}_3\text{Al}(\text{OH})8(\text{CO}_3)0.5(\text{H}_2\text{O})2.5 + 4\text{H} + = \text{AlO}_2\text{-} + 0.5\text{CO}_3\text{-}2 + 3\text{Mg} + 2 + 8.5\text{H}_2\text{O}@$	22.7	-129680	-215112	-286.5	-130.7	-2.1
Mg3FeCO.5OH		$\text{Mg}_3\text{Fe}[3 (\text{OH})8(\text{CO}_3)0.5(\text{H}_2\text{O})2.5 + 4\text{H} + = 0.5\text{CO}_3\text{-}2 + 3\text{Mg} + 2 + 8.5\text{H}_2\text{O}@ + \text{Fe}[3 \text{O}_2\text{-}$	22.4	-127660	-194156	-223.0	-325.3	-3.4
Mgs		$\text{MgCO}_3 = \text{CO}_3\text{-}2 + \text{Mg} + 2$	-8.3	47310	-28349	-253.8	-386.8	-5.6
monocarbonate		$\text{Ca}_4\text{Al}_2\text{CO}_9(\text{H}_2\text{O})11 + 4\text{H} + = 2\text{AlO}_2\text{-} + \text{CO}_3\text{-}2 + 4\text{Ca} + 2 + 13\text{H}_2\text{O}@$	24.5	-140067	-165182	-84.2	-412.8	-8.8
monocarbonate05		$\text{Ca}_2\text{AlCO}_5\text{O}_4.5(\text{H}_2\text{O})5.5 + 2\text{H} + = \text{AlO}_2\text{-} + 0.5\text{CO}_3\text{-}2 + 2\text{Ca} + 2 + 6.5\text{H}_2\text{O}@$	12.3	-70033	-82591	-42.1	-206.4	-4.4
monocarbonate9		$\text{Ca}_4\text{Al}_2\text{CO}_9(\text{H}_2\text{O})9 + 4\text{H} + = 2\text{AlO}_2\text{-} + \text{CO}_3\text{-}2 + 4\text{Ca} + 2 + 11\text{H}_2\text{O}@$	28.5	-162891	-224860	-207.8	-483.4	-9.6
mononitrate		$\text{Ca}_4\text{Al}_2(\text{OH})12\text{N}[5 2\text{O}_6(\text{H}_2\text{O})4 + 4\text{H} + = 2\text{AlO}_2\text{-} + 4\text{Ca} + 2 + 2\text{NO}_3\text{-} + 12\text{H}_2\text{O}@$	27.3	-156023	-148389	25.6	-356.1	-7.7
mononitrite		$\text{Ca}_4\text{Al}_2(\text{OH})12\text{N}[3 2\text{O}_4(\text{H}_2\text{O})4 = 2\text{AlO}_2\text{-} + 4\text{Ca} + 2 + 2\text{NO}_3\text{-} + 4\text{e-} + 10\text{H}_2\text{O}@$	-25.7	146749	197173	169.1	-420.1	-9.2

(continued on next page)

Table B.2 (continued)

Product Substance	Reaction	$\log 10^{-\circ}$ 298	A_{f}^{C} 298 [J/mol]	A_{f}^{H} 298 [J/mol]	A_{f}^{S} 298 [J/K/ mol]	A_{f}^{CP} 298 [J/K/ mol]	A_{f}° 298 [J/ bar]
monosulphate10.5	$\text{Ca}_4\text{Al}_2\text{SO}_{10}(\text{H}_2\text{O})_{10.5} + 4\text{H}^+ = 2\text{AlO}_2^- + 4\text{Ca} + 2 + \text{S}[6 \text{O}_4-2 + 12.5\text{H}_2\text{O}@$	28.1	-160590	-194728	-114.5	-434.2	-9.8
monosulphate12	$\text{Ca}_4\text{Al}_2\text{SO}_{10}(\text{H}_2\text{O})_{12} + 4\text{H}^+ = 2\text{AlO}_2^- + 4\text{Ca} + 2 + \text{S}[6 \text{O}_4-2 + 14\text{H}_2\text{O}@$	26.8	-152912	-176816	-80.2	-381.2	-7.1
monosulphate1205	$\text{Ca}_2\text{AlSO}_5(\text{H}_2\text{O})_6 + 2\text{H}^+ = \text{AlO}_2^- + 2\text{Ca} + 2 + 0.5\text{S}[6 \text{O}_4-2 + 7\text{H}_2\text{O}@$	13.4	-76454	-88406	-40.1	-190.6	-6.0
monosulphate14	$\text{Ca}_4\text{Al}_2\text{SO}_{10}(\text{H}_2\text{O})_{14} + 4\text{H}^+ = 2\text{AlO}_2^- + 4\text{Ca} + 2 + \text{S}[6 \text{O}_4-2 + 16\text{H}_2\text{O}@$	26.8	-152768	-185449	-109.6	-310.6	-8.4
monosulphate16	$\text{Ca}_4\text{Al}_2\text{SO}_{10}(\text{H}_2\text{O})_{16} + 4\text{H}^+ = 2\text{AlO}_2^- + 4\text{Ca} + 2 + \text{S}[6 \text{O}_4-2 + 18\text{H}_2\text{O}@$	26.9	-153259	-184873	16.1	-246.2	-6.7
monosulphate9	$\text{Ca}_4\text{Al}_2\text{SO}_{10}(\text{H}_2\text{O})_9 + 4\text{H}^+ = 2\text{AlO}_2^- + 4\text{Ca} + 2 + \text{S}[6 \text{O}_4-2 + 11\text{H}_2\text{O}@$	30.2	-172114	-232353	-202.0	-487.1	-11.8
N2	$\text{N}[0]_2 + 6\text{H}_2\text{O}@ = 2\text{NO}_3^- + 12\text{H}^+ + 10\text{e}^-$	-210.5	1201289	1301508	336.1	-470.7	-
Na2O	$\text{Na}_2\text{O} + 2\text{H}^+ = 2\text{Na}^+ + \text{H}_2\text{O}@$	67.4	-384943	-351639	111.7	82.7	-0.9
Na2SO4	$\text{Na}_2\text{SO}_4 = \text{S}[6 \text{O}_4-2 + 2\text{Na}^+$	-0.3	1703	-2457	-14.0	-254.9	-4.3
*NaSiOH	$((\text{NaOH})_2.5\text{SiO}_2\text{H}_2\text{O})_{0.2} + 0.5\text{H}^+ = 0.5\text{Na}^+ + 0.7\text{H}_2\text{O}@ + 0.25\text{SiO}_2@$	5.7	-32021	-19201	43.7	34.7	0.5
O2	$\text{O}[0]_2 + 4\text{H}^+ + 4\text{e}^- = 2\text{H}_2\text{O}@$	83.1	-474371	-571762	-326.7	63.7	-
Ord-Dol	$\text{CaMg}(\text{CO}_3)_2 = 2\text{CO}_3-2 + \text{Ca} + 2 + \text{Mg} + 2$	-17.1	97552	-36538	-449.7	-789.0	-11.7
Portlandite	$\text{Ca}(\text{OH})_2 + 2\text{H}^+ = \text{Ca} + 2 + 2\text{H}_2\text{O}@$	22.8	-130145	-130156	0.0	32.3	-1.5
Py	$\text{FeS}[0 \text{S} -2] + 10\text{H}_2\text{O}@ = 2\text{S}[6 \text{O}_4-2 + 20\text{H}^+ + 15\text{e}^- + \text{Fe}[3 \text{O}_2-$	-120.5	687822	780233	309.9	-1366.5	-17.8
Qtz	$\text{SiO}_2 = \text{SiO}_2@$	-3.7	21386	21386	0.0	0.0	-0.7
Sd	$\text{FeCO}_3 + 2\text{H}_2\text{O}@ = \text{CO}_3-2 + 4\text{H}^+ + \text{e}^- + \text{Fe}[3 \text{O}_2-$	-45.5	259775	204566	-185.2	-742.7	-7.1
Str	$\text{SrCO}_3 = \text{CO}_3-2 + \text{Sr} + 2$	-9.3	52918	-324	-178.6	-413.3	-6.3
straetlingite	$\text{Ca}_2\text{Al}_2\text{Si}_7\text{O}_{17}(\text{H}_2\text{O})_8 + 2\text{H}^+ = 2\text{AlO}_2^- + 2\text{Ca} + 2 + 9\text{H}_2\text{O}@ + \text{SiO}_2@$	4.1	-23479	-38065	-48.9	-39.9	-5.5
straetlingite5.5	$\text{Ca}_2\text{Al}_2\text{Si}_5\text{O}_{17}(\text{H}_2\text{O})_{5.5} + 2\text{H}^+ = 2\text{AlO}_2^- + 2\text{Ca} + 2 + 6.5\text{H}_2\text{O}@ + \text{SiO}_2@$	7.1	-40503	-79963	-132.3	-128.1	-9.7
straetlingite7	$\text{Ca}_2\text{Al}_2\text{Si}_7\text{O}_{17}(\text{H}_2\text{O})_7 + 2\text{H}^+ = 2\text{AlO}_2^- + 2\text{Ca} + 2 + 8\text{H}_2\text{O}@ + \text{SiO}_2@$	4.8	-27477	-45434	-60.2	-75.2	-7.3
Sulfur	$\text{S}[0] + 4\text{H}_2\text{O}@ = \text{S}[6 \text{O}_4-2 + 8\text{H}^+ + 6\text{e}^-$	-35.8	204198	233827	99.4	-503.8	-7.5
syngenite	$\text{K}_2\text{Ca}(\text{SO}_4)_2\text{H}_2\text{O} = \text{Ca} + 2 + 2\text{S}[6 \text{O}_4-2 + \text{H}_2\text{O}@ + 2\text{K}^+$	-7.2	41078	19412	-72.7	-743.9	-8.4
T2C-CNASHss	$(\text{CaO})_{1.5}(\text{SiO}_2)_1(\text{H}_2\text{O})_{2.5} + 3\text{H}^+ = 1.5\text{Ca} + 2 + 4\text{H}_2\text{O}@ + \text{SiO}_2@$	25.6	-145938	-125275	69.3	62.5	-2.0
T5C-CNASHss	$(\text{CaO})_{1.25}(\text{SiO}_2)_{1.25}(\text{H}_2\text{O})_{2.5} + 3\text{H}^+ = 1.25\text{Ca} + 2 + 3.75\text{H}_2\text{O}@ + 1.25\text{SiO}_2@$	18.4	-105297	-80438	83.4	65.4	-1.5
thaumasite	$(\text{CaSiO}_3)(\text{CaSO}_4)(\text{CaCO}_3)(\text{H}_2\text{O})_{15} + 2\text{H}^+ = \text{CO}_3-2 + 3\text{Ca} + 2 + \text{S}[6 \text{O}_4-2 + 16\text{H}_2\text{O}@ + \text{SiO}_2@$	-0.9	5236	23833	62.4	-468.7	-7.3
TobH-CNASHss	$(\text{CaO})_1(\text{SiO}_2)_{1.5}(\text{H}_2\text{O})_{2.5} + 2\text{H}^+ = \text{Ca} + 2 + 3.5\text{H}_2\text{O}@ + 1.5\text{SiO}_2@$	12.8	-73056	-44000	97.5	68.3	-1.6
Tob-I	$(\text{SiO}_2)_{2.4}(\text{CaO})_2(\text{H}_2\text{O})_{3.2} + 4\text{H}^+ = 2\text{Ca} + 2 + 5.2\text{H}_2\text{O}@ + 2.4\text{SiO}_2@$	26.7	-152677	-105616	157.8	119.1	-4.5
Tob-II	$(\text{SiO}_2)_1(\text{CaO})_{0.833333}(\text{H}_2\text{O})_{1.333333} + 1.666666\text{H}^+ = 0.833333\text{Ca} + 2 + 2.166666\text{H}_2\text{O}@ + \text{SiO}_2@$	11.1	-63617	-44009	65.8	49.6	-1.9
tricarboal03	$(\text{CO}_3)\text{Ca}_2\text{Al}_0.6666667(\text{OH})_4(\text{H}_2\text{O})_{8.6666667} + 1.3333332\text{H}^+ = 0.6666667\text{AlO}_2^- + \text{CO}_3-2 + 2\text{Ca} + 2 + 11.333333\text{H}_2\text{O}@$	3.2	-18115	-21090	-10.0	-236.8	-4.9
Tro	$\text{Fe}[2 \text{S} -2] + 6\text{H}_2\text{O}@ = \text{S}[6 \text{O}_4-2 + 12\text{H}^+ + 9\text{e}^- + \text{Fe}[3 \text{O}_2-$	-73.6	420228	471331	171.4	-873.9	-11.3

* - reaction properties at 20 °C 1 bar.

e- - represents one electron.

|| - is used for specifying a different valence for the element.

@ - is used to represent a neutral aqueous species.

Standard molar volumes for ideal gases are not listed because they are all equal to 2479 J/bar at 1 bar, 298.15 K.

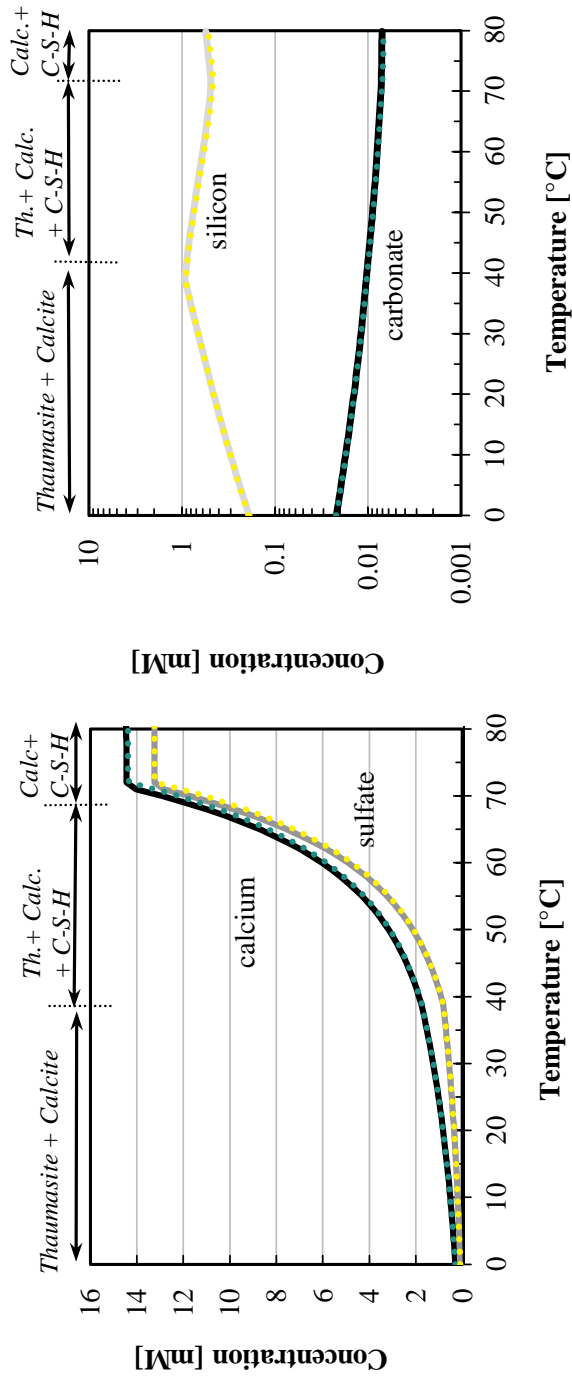


Fig. B.1. Calculated (curves) solubility data for thaumasite, based on the new thermodynamic data for thaumasite complemented with the CSHQ data from Cemdata18 [1,7] in GEM format; Calculated (dotted lines) solubility data for thaumasite, based on data Cemdata18 [1,7] in PHREEQC format.

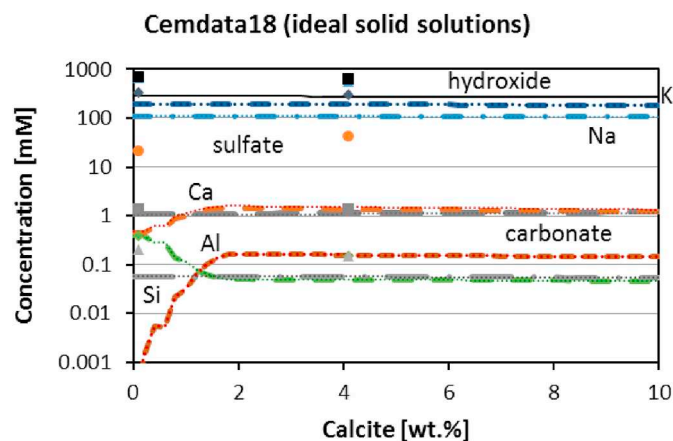


Fig. B.2. Effect of the amount of limestone on the phase assemblage and the distribution of aluminium and iron in hydrated Portland cement calculated using Cemdata18 GEM format (dashed lines) and Cemdata18 PHREEQC format (dotted lines), in both cases using ideal solid solutions.

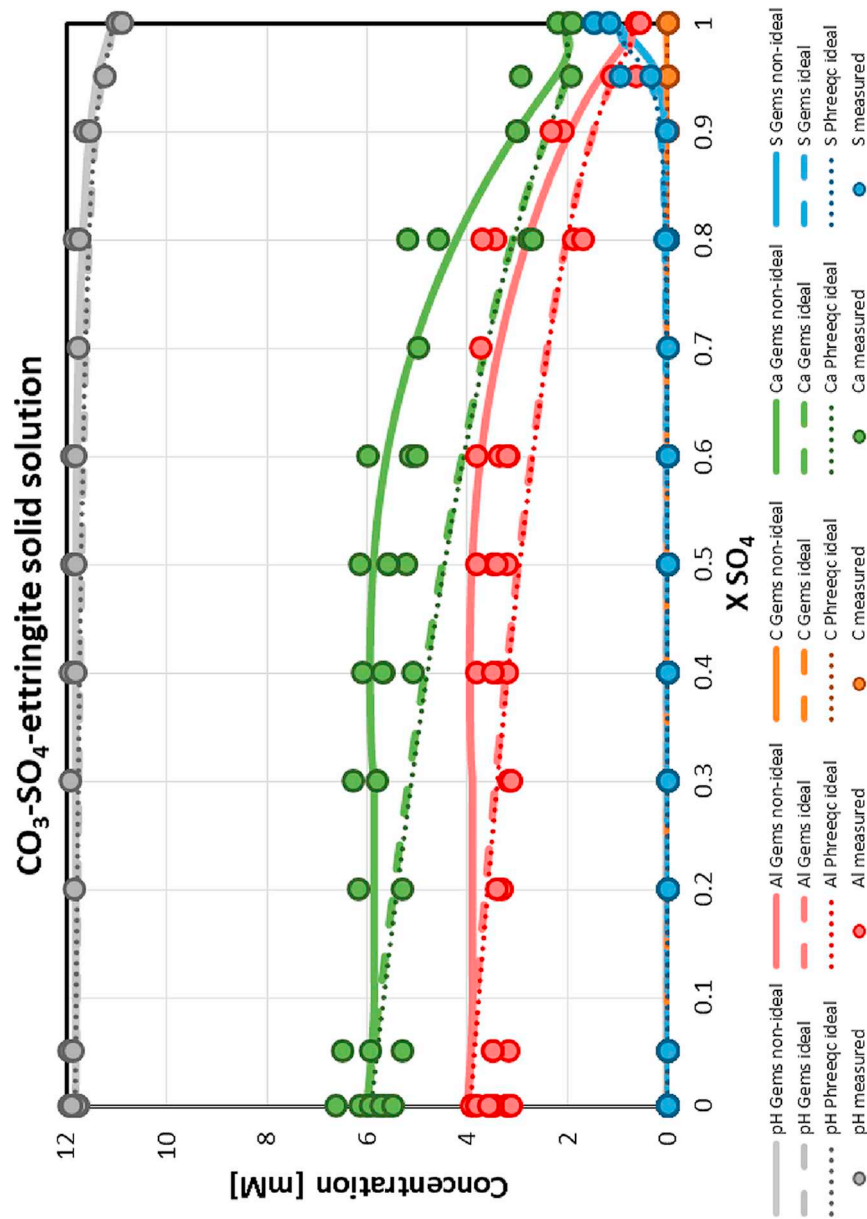


Fig. B.3. Calculated aqueous composition in equilibrium with CO₃-SO₄-ettringite solid solution as a function of SO₄ in the solid. Solid lines calculated using the Cemdata18 GEM format using non ideal solid solution; Dashed lines calculated using the Cemdata18 GEM format using ideal solid solution; Dotted lines calculated using the Cemdata18 PHREEQC format using ideal solid solution; Circles: experimental data [7,129].

Appendix C. Thermodynamic equations and assumptions

The solubility products compiled in Cemdata18 have generally been derived from solutions composition measured at different temperatures, as documented in detail in [1,7–10,12,27,28,30,31,34–37,39–41]. The activity of a species i , a_i , has been calculated with GEMS from the measured concentrations considering the formation of aqueous complexes. By definition $a_i = \gamma_i \cdot m_i$, where γ_i is the activity coefficient and m_i the concentration in mol/kg H₂O. Activity coefficients of aqueous species γ_i were computed using the built-in extended Debye-Hückel equation with the common ion-size parameter a_i of 3.67 Å for KOH and 3.31 Å for NaOH solutions and the common third parameter b_y according to the Eq. (C.1):

$$\log \gamma_i = \frac{-A_y z_i^2 \sqrt{I}}{1 + B_y a_i \sqrt{I}} + b_y I \quad (\text{C.1})$$

where z_i denotes the charge of species i , I is the effective molal ionic strength, b_y is a semi-empirical parameter (~ 0.123 for KOH and ~ 0.098 for NaOH electrolyte at 25 °C), and A_y and B_y are P, T -dependent coefficients. For uncharged species, Eq. (C.1) reduces to $\log \gamma_i = b_y I$. This extended Debye-Hückel activity correction is applicable up to approx. 1 m ionic strength [130].

From the solubility products K of solids calculated at different temperatures T , the Gibbs free energy of reaction, $\Delta_r G^\circ$, the Gibbs free energy of formation, $\Delta_f G^\circ$, and the absolute entropy, S° , at $T_0 = 298.15$ K were obtained according to Eqs. (C.2) and (C.3):

$$\Delta_r G^\circ = \sum_i \nu_i \Delta_f G^\circ = -RT \ln K \quad (\text{C.2})$$

$$\Delta_a G_T^\circ = \Delta_f G_{T_0}^\circ - S_{T_0}^\circ (T - T_0) + \int_{T_0}^T C_p^0 dT - \int_{T_0}^T \frac{C_p^0}{T} dT \quad (\text{C.3})$$

Using $C_p^0 = a_0 + a_1 T + a_2 T^{-2} + a_3 T^{0.5}$ [131], where a_{0-3} are the empirical parameters defined for each mineral, the two integral terms of Eq. (C.3) can be solved to give Eq. (C.4):

$$\Delta_a G_T^\circ = \Delta_f G_{T_0}^\circ - S_{T_0}^\circ (T - T_0) - a_0 \left(T \ln \frac{T}{T_0} - T + T_0 \right) - 0.5 a_1 (T - T_0)^2 - a_2 \frac{(T - T_0)^2}{2T \cdot T_0^2} - a_3 \frac{2(\sqrt{T} - \sqrt{T_0})^2}{\sqrt{T_0}} \quad (\text{C.4})$$

where ν_i are the stoichiometric reaction coefficients, $R = 8.31451$ J/mol/K, T is the temperature in K, and C_p^0 is the heat capacity at constant pressure. The apparent Gibbs free energy of formation, $\Delta_a G_T^\circ$, refers to standard Gibbs energies of elements at 298.15 K. A more detailed description of the derivation of the dependence of the Gibbs free energy on temperature is available in [131,132].

Dependence of the solubility product on temperature, consistent to Eq. (C.4) can be expressed as:

$$\log K_T = A_0 + A_1 T + \frac{A_2}{T} + A_3 \ln T + \frac{A_4}{T^2} + A_5 T^2 + A_6 \sqrt{T} \quad (\text{C.5})$$

[131], where A_0, \dots, A_6 are empirical coefficients. If the entropy (S°), the enthalpy ($\Delta_f H^\circ$), and the coefficients (a_0, a_1, \dots) of the heat capacity equation ($C_p^0 = a_0 + a_1 T + a_2 T^{-2} + a_3 T^{0.5} + a_4 T^2$) of the species are available, the coefficients A_0, \dots, A_6 can be calculated directly (see [131]). These calculations involving Eqs. (C.4) and (C.5) are all implemented in the GEM-Selektor.

The heat capacity function, $C_p = f(T)$ is usually obtained from calorimetry experiments. In many cases, the heat capacity has to be estimated by using a reference reaction with a solid having a known heat capacity and similar structure, as described in publications [1,7–10,12,27,28,30,31,34–37,39–41]. Helgeson et al. [43] applied this principle successfully to estimate heat capacities of silicate minerals by formulating reactions involving structurally-related minerals with known heat capacity functions. This method has limitations due to the differing thermodynamic properties of “water” varieties, bound loosely as a hydration water, or structurally as OH-groups. To minimize errors associated with the varying strengths of bonding for “water”, reference reactions had been formulated to involve no “free” water as a substituent in reactions, wherever appropriate.

The value of $\Delta_r C_p^0$ has little influence on the calculated $\log K$ value in the temperature range 0–100 °C and is thus often assumed to be constant in a narrow temperature range: $\Delta_r C_p^0 = \Delta_r C_{p_{T_0}}^0 = \Delta a_0$. This simplifies Eq. (C.5) to the so called 3-term approximation of the temperature dependence, see Eq. (C.6), which can be used to compute the standard thermodynamic properties of each solid [132] to obtain a temperature-dependent “log K” function using Eqs. (C.6)–(C.12) (implemented in GEMS).

$$\log K_T = A_0 + A_2 T^{-1} + A_3 \ln T \quad (\text{C.6})$$

and

$$A_0 = \frac{0.4343}{R} \cdot [\Delta_r S_{T_0}^0 - \Delta_r C_{p_{T_0}}^0 (1 + \ln T_0)] \quad (\text{C.7})$$

$$A_2 = \frac{0.4343}{R} \cdot (\Delta_r H_{T_0}^0 - \Delta_r C_{p_{T_0}}^0 T_0) \quad (\text{C.8})$$

$$A_3 = \frac{0.4343}{R} \cdot \Delta_r C_{p_{T_0}}^0 \quad (\text{C.9})$$

$$\Delta_r S_T^0 = \Delta_r S_{T_0}^0 + \Delta_r C_{p_{T_0}}^0 \ln \frac{T}{T_0} \quad (\text{C.10})$$

$$\Delta_r H_T^0 = \Delta_r H_{T_0}^0 + \Delta_r C_{p_{T_0}}^0 (T - T_0) \quad (\text{C.11})$$

$$\Delta_r G_T^0 = \Delta_r H_T^0 - T \Delta_r S_T^0 \quad (\text{C.12})$$

Within the relatively narrow temperature range of 0 to 100 °C, where the Cemdata18 database is valid, this simplification has a negligible influence on the resulting solubility products, also for non-isoelectric reactions as exemplified for ettringite in [20].

Appendix D. Thermodynamic data for aqueous and gaseous species

The thermodynamic data for aqueous and gaseous species compatible with Cemdata18 are summarised in Tables D.1 and D.2.

Table D.1

Standard (partial molal) thermodynamic properties and equation of state parameters of aqueous species at 25 °C, 1 bar used in GEM calculations, as detailed in the GEMS version of the PSI/Nagra 12/07 TDB [22,23]. Numbers referring to the charge of aqueous species are written after the plus or minus signs to avoid any ambiguity; “@” is used to represent a neutral aqueous species.

Species	ΔG^0 (kJ/mol)	ΔH^0 (kJ/mol)	S^0 (J/ mol·K)	C_p^0 (J/mol·K)	V^0 (J/bar)	$a_1 \cdot 10^*$ (cal/mol/ bar)	$a_2 \cdot 10^{-2*}$ (cal/mol)	a_3^* (cal·K/mol/ bar)	$a_4 \cdot 10^{-4*}$ (cal·K/ mol)	c_1^* (cal/mol/ K)	$c_2 \cdot 10^{-4*}$ (cal·K/ mol)	$\omega_0 \cdot 10^{-5*}$ (cal/mol)
$Al(SO_4)^+$	–1250.43	–1422.67	–172.38	–204.01	–6.02	1.3869	–4.3920	7.4693	–2.5974	–11.6742	–12.9914	1.1729
$Al(SO_4)^{2-}$	–2006.30	–2338.40	–135.50	–268.37	31.11	6.8275	8.8925	2.2479	–3.1466	–12.0220	–16.1447	2.1199
Al^{+3}	–483.71	–530.63	–325.10	–128.70	–45.24	–3.3802	–17.0071	14.5185	–2.0758	10.7000	–8.0600	2.7530
AlO^+	–660.42	–713.64	–112.97	–125.11	0.31	2.1705	–2.4811	6.7241	–2.6763	–2.5983	–9.1455	0.9570
AlO_2^-	–827.48	–925.57	–30.21	–49.04	9.47	3.7221	3.9954	–1.5879	–2.9441	15.2391	–5.4585	1.7418
AlO_2H^0	–864.28	–947.13	20.92	–209.21	13.01	3.5338	0.8485	5.4132	–2.8140	–23.4129	–13.2195	–0.0300
$AlOH^{+2}$	–692.60	–767.27	–184.93	55.97	–2.73	2.0469	–2.7813	6.8376	–2.6639	29.7923	–0.3457	1.7247
$Ca(CO_3)@$	–1099.18	–1201.92	10.46	–123.86	–15.65	–0.3907	–8.7325	9.1753	–2.4179	–11.5309	–9.0641	–0.0380
$Ca(HCO_3)^+$	–1146.04	–1231.94	66.94	233.70	13.33	3.7060	1.2670	5.2520	–2.8310	41.7220	8.3360	0.3080
$Ca(HSiO_3)^+$	–1574.24	–1686.48	–8.33	137.80	–6.74	1.0647	–5.1787	7.7785	–2.5649	30.8048	3.6619	0.5831
$Ca(SO_4)@$	–1310.38	–1448.43	20.92	–104.60	4.70	2.4079	–1.8992	6.4895	–2.7004	–8.4942	–8.1271	–0.0010
Ca^{+2}	–552.79	–543.07	–56.48	–30.92	–18.44	–0.1947	–7.2520	5.2966	–2.4792	9.0000	–2.5220	1.2366
$CaOH^+$	–717.02	–751.65	28.03	6.05	5.76	2.7243	–1.1303	6.1958	–2.7322	11.1286	–2.7493	0.4496
$CH_4@$	–34.35	–87.81	87.82	277.26	37.40	6.7617	8.7279	2.3212	–3.1397	42.0941	10.4707	–0.3179
Cl^-	–131.29	–167.11	56.74	–122.49	17.34	4.0320	4.8010	5.5630	–2.8470	–4.4000	–5.7140	1.4560
ClO_4^-	–8.54	–129.33	182.00	–24.00	43.90	8.1411	15.5654	–7.8077	–3.4224	16.4500	–6.5700	0.9699
$CO_2@$	–386.02	–413.84	117.57	243.08	32.81	6.2466	7.4711	2.8136	–3.0879	40.0325	8.8004	–0.0200
CO_3^{-2}	–527.98	–675.31	–50.00	–289.33	–6.06	2.8524	–3.9844	6.4142	–2.6143	–3.3206	–17.1917	3.3914
e^-	0	0	65.34	14.42	0	0	0	0	0	0	0	0
$Fe(CO_3)@$	–644.49	–763.51	–58.45	–123.03	–17.23	–0.6069	–9.2604	9.3828	–2.3961	–11.4137	–9.0233	–0.0380
$Fe(HCO_3)^+$	–689.86	–794.10	–8.87	231.41	8.18	3.1064	–0.1934	5.8191	–2.7710	43.9175	8.2195	0.5831
$Fe(HSO_4)^+$	–853.48	–990.45	10.21	338.23	18.81	4.5330	3.2897	4.4500	–2.9149	58.2305	13.4217	0.5121
$Fe(HSO_4)^{+2}$	–787.15	–981.91	–248.95	426.71	2.32	2.8251	–0.8804	6.0891	–2.7426	83.8315	17.6994	1.9551
$Fe(SO_4)@$	–848.81	–993.86	–16.86	–101.60	1.67	1.9794	–2.9454	6.9007	–2.6572	–8.4131	–7.9804	–0.0380
$Fe(SO_4)^+$	–784.71	–942.42	–124.68	–145.93	–2.64	1.7837	–3.4232	7.0885	–2.6374	–5.1341	–10.1600	0.9986
$Fe(SO_4)_2^-$	–1536.81	–1854.38	–87.78	–210.37	30.49	6.6756	8.5215	2.3937	–3.1312	–5.4923	–13.3173	1.9457
Fe^{+2}	–91.50	–92.24	–105.86	–32.44	–22.64	–0.7867	–9.6969	9.5479	–2.3780	14.7860	–4.6437	1.4382
Fe^{+3}	–17.19	–49.58	–277.40	–76.71	–37.79	–2.4256	–13.6961	11.1141	–2.2127	19.0459	–6.8233	2.5812
$FeCl^+$	–223.59	–258.05	–42.09	86.49	0.85	2.1468	–2.5367	6.7401	–2.6741	24.6912	1.1617	0.7003
$FeCl^{+2}$	–156.92	–212.67	–178.82	14.83	–22.86	–0.7164	–9.5277	9.4878	–2.3851	23.8149	–2.3482	1.7013
$FeCl_2^+$	–291.92	–385.75	–129.66	300.72	10.27	3.5610	0.9165	5.3828	–2.8168	57.6940	11.5846	1.0276
$FeCl_3@$	–417.51	–564.39	–131.06	368.22	35.94	6.6686	8.5038	2.4024	–3.1304	57.3959	14.8930	–0.0380

(continued on next page)

Table D.1 (continued)

Species	ΔG^0 (kJ/mol)	ΔH^0 (kJ/mol)	S^0 (J/ mol·K)	C_p^0 (J/mol·K)	V^0 (J/bar)	$a_1 \cdot 10^*$ (cal/mol/ bar)	$a_2 \cdot 10^{-2*}$ (cal/mol)	a_3^* (cal·K/mol/ bar)	$a_4 \cdot 10^{-4*}$ (cal·K/ mol)	c_1^* (cal/mol/ K)	$c_2 \cdot 10^{-4*}$ (cal·K/ mol)	$\omega_0 \cdot 10^{-5*}$ (cal/mol)
FeO^+	-222.00	-255.09	-46.44	-200.94	-42.02	-3.7118	-16.8408	12.3595	-2.0827	-15.3982	-12.8325	0.7191
FeO_2^-	-368.26	-443.82	44.35	-234.93	0.45	2.3837	-1.9602	6.5182	-2.6979	-13.3207	-14.5028	1.4662
$\text{FeO}_2\text{H}^\oplus$	-419.86	-480.95	92.88	-312.14	7.21	2.7401	-1.0905	6.1776	-2.7338	-37.8300	-18.2305	-0.0300
FeOH^+	-274.46	-325.65	-41.84	63.06	-16.71	-0.2561	-8.4029	9.0457	-2.4315	21.4093	0.0209	0.7003
FeOH^{+2}	-241.87	-292.79	-106.27	-33.69	-25.34	-1.1562	-10.6009	9.9077	-2.3407	14.6102	-4.7048	1.4382
H^+	0	0	0	0	0	0	0	0	0	0	0	0
H_2^\oplus	17.73	-4.02	57.74	166.85	25.26	5.1427	4.7758	3.8729	-2.9764	27.6251	5.0930	-0.2090
$\text{H}_2\text{O}^\oplus$	-237.18	-285.88	69.92	75.36	18.07	0	0	0	0	0	0	0
$\text{H}_2\text{S}^\oplus$	-27.93	-39.03	125.52	179.17	34.95	6.5097	6.7724	5.9646	-3.0590	32.3000	4.7300	-0.1000
HCN^\oplus	114.37	103.75	131.30	0	0	0	0	0	0	0	0	0
HCO_3^-	-586.94	-690.01	98.45	-34.85	24.21	7.5621	1.1505	1.2346	-2.8266	12.9395	-4.7579	1.2733
HS^-	11.97	-16.22	68.20	-93.93	20.21	5.0119	4.9799	3.4765	-2.9849	3.4200	-6.2700	1.4410
HSiO_3^-	-1014.60	-1144.68	20.92	-87.20	4.53	2.9735	-0.5181	5.9467	-2.7575	8.1489	-7.3123	1.5511
HSO_3^-	-529.10	-627.70	139.75	-5.38	32.96	6.7014	8.5816	2.3771	-3.1338	15.6949	-3.3198	1.1233
HSO_4^-	-755.81	-889.23	125.52	22.68	34.84	6.9788	9.2590	2.1108	-3.1618	20.0961	-1.9550	1.1748
$\text{K(SO}_4)_-$	-1031.77	-1158.77	146.44	-45.13	27.46	5.9408	6.7274	3.0989	-3.0571	9.9089	-5.2549	1.0996
K^+	-282.46	-252.14	101.04	8.39	9.01	3.5590	-1.4730	5.4350	-2.7120	7.4000	-1.7910	0.1927
KOH^\oplus	-437.11	-474.15	108.37	-85.02	14.96	3.7938	1.4839	5.1619	-2.8402	-6.1240	-7.2104	-0.0500
$\text{Mg(CO}_3)_^\oplus$	-998.98	-1132.12	-100.42	-116.50	-16.78	-0.5450	-9.1130	9.3320	-2.4020	-10.4990	-8.7060	-0.0380
$\text{Mg(HCO}_3)_+$	-1047.02	-1153.97	-12.55	254.42	9.34	3.2710	0.2060	5.6690	-2.7880	47.2840	9.3400	0.5990
$\text{Mg(HSiO}_3)_+$	-1477.15	-1613.91	-99.50	158.65	-10.85	0.6289	-6.2428	8.1967	-2.5209	36.7882	4.6702	0.9177
Mg^{+2}	-453.99	-465.93	-138.07	-21.66	-22.01	-0.8217	-8.5990	8.3900	-2.3900	20.8000	-5.8920	1.5372
MgOH^+	-625.87	-690.02	-79.91	129.23	1.64	2.3105	-2.1365	6.5827	-2.6906	32.0008	3.2394	0.8449
MgSO_4^\oplus	-1211.97	-1368.77	-50.88	-90.31	1.81	1.9985	-2.8987	6.8823	-2.6591	-6.8307	-7.4304	-0.0380
N_2^\oplus	18.19	-10.37	95.81	234.16	33.41	6.2046	7.3685	2.8539	-3.0836	35.7911	8.3726	-0.3468
$\text{Na(CO}_3)_-$	-797.11	-938.56	-44.31	-51.28	-0.42	2.3862	-1.9521	6.5103	-2.6982	15.3395	-5.5686	1.7870
$\text{Na(HCO}_3)_^\oplus$	-847.39	-929.50	154.72	200.33	32.32	6.1730	7.2943	2.8760	-3.0805	33.8790	6.7193	-0.0380
$\text{Na(SO}_4)_-$	-1010.34	-1146.66	101.75	-30.09	18.64	4.7945	3.9284	4.1990	-2.9414	13.4899	-4.5256	1.2606
Na^+	-261.88	-240.28	58.41	38.12	-1.21	1.8390	-2.2850	3.2560	-2.7260	18.1800	-2.9810	0.3306
NaOH^\oplus	-418.12	-470.14	44.77	-13.40	3.51	2.2338	-2.3287	6.6683	-2.6826	4.0146	-3.6863	-0.0300
NH_3^\oplus	-26.67	-81.53	107.82	76.89	24.45	5.0911	2.7970	8.6248	-2.8946	20.3000	-1.1700	-0.0500
NH_4^+	-79.40	-133.26	111.17	67.11	18.08	3.8763	2.3448	8.5605	-2.8759	17.4500	-0.0210	0.1502
NO_3^-	-110.91	-206.89	146.94	-66.80	28.66	7.3161	6.7824	-4.6838	-3.0594	7.7000	-6.7250	1.0977
O_2^\oplus	16.45	-12.24	108.95	234.13	30.50	5.7889	6.3536	3.2528	-3.0417	35.3530	8.3726	-0.3943
OH^-	-157.27	-230.01	-10.71	-136.34	-4.71	1.2527	0.0738	1.8423	-2.7821	4.1500	-10.3460	1.7246
$\text{S}_2\text{O}_3^{-2}$	-519.99	-649.86	66.94	-238.47	27.59	6.6685	12.4951	-7.7281	-3.2955	-0.0577	-14.7066	2.9694
SCN^-	92.70	76.40	144.01	-39.69	35.36	7.0244	9.3687	2.0708	-3.1662	10.7414	-4.9900	1.1073

(continued on next page)

Table D.1 (continued)

Species	ΔG^0	ΔH^0	S^0	C_p^0	V^0	$a_1 \cdot 10^{*}$	$a_2 \cdot 10^{-2*}$	a_3^{*}	$a_4 \cdot 10^{-4*}$	c_1^{*}	$c_2 \cdot 10^{-4*}$	$\omega_0 \cdot 10^{-5*}$
	(kJ/mol)	(kJ/mol)	(J/ mol·K)	(J/mol·K)	(J/bar)	(cal/mol/ bar)	(cal/mol)	(cal·K/mol/ bar)	(cal·K/ mol)	(cal/mol/ K)	(cal·K/ mol)	(cal/mol)
SO_3^{-2}	-487.89	-636.89	-29.29	-280.99	-4.12	2.4632	-1.7691	6.4494	-2.7058	-2.7967	-16.7843	3.3210
SO_4^{-2}	-744.46	-909.70	18.83	-266.09	12.92	8.3014	-1.9846	-6.2122	-2.6970	1.6400	-17.9980	3.1463
$Sr(CO_3)^@$	-1107.83	-1207.29	35.56	-134.32	-15.23	-0.3332	-8.5922	9.1201	-2.4237	-12.9961	-9.5733	-0.0380
$Sr(HCO_3)^+$	-1157.54	-1239.00	95.94	210.07	14.08	3.7702	1.4274	5.1820	-2.8380	37.4746	7.1883	0.2058
$Sr(SO_4)^@$	-1321.37	-1451.50	61.59	-110.60	5.02	2.4382	-1.8251	6.4604	-2.7035	-9.6731	-8.4183	-0.0380
Sr^{+2}	-563.84	-550.87	-31.51	-41.56	-17.76	0.7071	-10.1508	7.0027	-2.3594	10.7452	-5.0818	1.1363
$SrOH^+$	-725.16	-754.14	61.09	-31.66	7.10	2.8620	-0.7922	6.0586	-2.7462	4.7576	-4.5826	0.3306
Temperature correction using $C_p(T)$ integration												
$SiO_2^{@**}$	-833.41	-887.86 [*]	41.34	44.47	1.61	46.94	0.034	a_2	$(C_p^0 = a_0 + a_1 T + a_2 T^{-2})$			
Temperature correction using $\log K(T)$												
SiO_3^{-2**}	-938.51	-1098.74	-80.20	119.83	0	-10.0006	0	A_2	$(\log K_T = A_0 + A_1 T + A_2 T^{-1})$			
$Si_4O_{10}^{-4***}$	-3600.81	-3915.99	305.20	328.58	0	0	0	-3917.5				
$CaSiO_3^{@**}$	-1517.56	-1668.06	-136.68	88.90	0	0	0	-10,822.8				
$MgSiO_3^@$	-1425.03	-1554.54	-75.17	-264.79	0	5.7	0	1371.49				
$AlSiO_5^{-3***}$	-1769.01	-2027.33	-110.41	70.78	-3.41	0	0	0				
$AlHSiO_3^{+2*V}$	-1540.55	-1634.31	-24.99	-215.896	0	14.5828	0	158.02				
$FeHSiO_3^{+2*V}$	-1087.15	-1194.26	-70.77	-163.91	0	9.7	0	-2141.57				
$Fe_2(OH)_2^{+4*V}$	-491.9	-614.44	-281.97	-2.71	0	6.94586	0	0				
$Fe_3(OH)_4^{+5*V}$	-964.33	-1232.44	-472.43	71.30	0	4.1824	0	-2950.45				
$SrSiO_3^{@***}$	-1527.29	-1617.43	79.92	78.39	1.64	0	0	-3125.33				
S^{-2}	120.42	-16.22	-295.55	-93.93	0	-19	0	1302.92				

*Parameters of the HKF-equation of state; given in original calorimetric units (see [25,26,133]) as used in GEM.

Calculated in Matschei et al. [7] assuming $\Delta_f S^0 = \Delta_f C_p^0 = 0$ using S^0 and C_p^0 from SiO_2 (quartz) $\Delta_f G^0 = \Delta_f H^0 - 2H^0 - > SiO_2 + H_2O \Delta_f G^0 = 132.08$, $\Delta_f H^0 = 75$, $\Delta_f S^0 = -191.46$, $\Delta_f C_p^0$.*Calculated in this paper assuming $\Delta_f S^0 = \Delta_f C_p^0 = 0$ using S^0 and C_p^0 from SiO_2 (quartz) $\Delta_f G^0 = \Delta_f H^0 - 2H^0 - > 4SiO_2 + 2H_2O \Delta_f G^0 = \Delta_f H^0 = 207.2$, $\Delta_f S^0 = 0$, $\Delta_f C_p^0$. $= 0$; $SiO_3^{2-} + Ca^{2+} - > CaSiO_3 \Delta_f G^0 = \Delta_f H^0 = -26.257$, $\Delta_f S^0 = 0$, $\Delta_f C_p^0 = 0$
 $SiO_3^{2-} + AlO_2^- - > AlSiO_3 \Delta_f G^0 = \Delta_f H^0 = -3.025$, $\Delta_f S^0 = 0$, $\Delta_f C_p^0 = 0$; $Si_4O_{10}^{4-} + 4H^+ - > 4SiO_2 + 2H_2O \Delta_f G^0 = \Delta_f H^0 = 207.2$, $\Delta_f S^0 = 0$, $\Delta_f C_p^0$. $= 0$; $SiO_3^{2-} + Mg^{2+} - > MgSiO_3 \Delta_f G^0 = -32.54$, $\Delta_f H^0 = 0$, $\Delta_f S^0 = 109.126$, $\Delta_f C_p^0 = 0$; $SiO_3^{2-} - > Sr^{2+} - > SrSiO_3 \Delta_f G^0 = \Delta_f H^0 = -29.944$, $\Delta_f S^0 = 0$, $\Delta_f C_p^0 = 0$ *^VFrom the GEMS version of the PSI/Nagra 12/07 TDB [22,23]; $Al^{+3} + HSiO_3^- - > AlHSiO_3 \Delta_f G^0 = -42.24$, $\Delta_f H^0 = 41$, $\Delta_f S^0 = 279.19$, $\Delta_f C_p^0 = 0$; $Fe^{+3} + HSiO_3^- - > FeHSiO_3 \Delta_f G^0 = -55.37$, $\Delta_f H^0 = 0$, $\Delta_f S^0 = 185.7$, $\Delta_f C_p^0$. $= 0$; $2Fe^{+3} + 2H_2O - > Fe_2(OH)_2^{+4} + 2H^+ \Delta_f G^0 = 16.84$, $\Delta_f H^0 = 56.486$, $\Delta_f S^0 = 132.98$, $\Delta_f C_p^0$ $= 0$; $3Fe^{+3} + 4H_2O - > Fe_3(OH)_4^{+5} + 4H^+ \Delta_f G^0 = 35.96$, $\Delta_f H^0 = 59.834$, $\Delta_f S^0 = 80.07$, $\Delta_f C_p^0 = 0$

Table D.2

Standard (partial molal) thermodynamic properties and heat capacity coefficients ($C_p^0 = a_0 + a_1T + a_2T^{-2}$) of gaseous species at 25 °C, 1 bar used in GEM calculations, as used in the GEMS version of the PSI/Nagra 12/07 TDB [22,23]. Standard molar volumes for ideal gases are not listed because they are all equal to 2479 J/bar at 1 bar, 298.15 K.

Species	ΔG^0	ΔH^0	S^0	C_p^0	a_0	a_1	a_2
	(kJ/mol)	(kJ/mol)	(J/mol K)	(J/mol K)	(J/mol/K)	(J/mol/K ²)	(J·K/mol)
CH ₄	−50.66	−74.81	186.26	35.75	23.64	0.0479	−192,464
CO ₂	−394.39	−393.51	213.74	37.15	44.22	0.0088	−861,904
H ₂	0	0	130.68	28.82	27.28	0.0033	50,208
H ₂ O	−228.68	−242.40	187.25	40.07	52.99	−0.0435	5472
H ₂ S	−33.75	−20.63	205.79	34.20	32.68	0.0124	−192,464
N ₂	0	0	191.61	29.13	28.58	0.0038	−50,208
O ₂	0	0	205.14	29.32	29.96	0.0042	−167,360

References

- [1] B. Lothenbach, T. Matschei, G. Möschner, F.P. Glasser, Thermodynamic modelling of the effect of temperature on the hydration and porosity of Portland cement, *Cem. Concr. Res.* 38 (2008) 1–18.
- [2] T. Matschei, B. Lothenbach, F.P. Glasser, The role of calcium carbonate in cement hydration, *Cem. Concr. Res.* 37 (2007) 551–558.
- [3] M. Moesgaard, D. Herfort, M. Steenberg, L.F. Kirkegaard, Y. Yue, Physical performance of blended cements containing calcium aluminosilicate glass powder and limestone, *Cem. Concr. Res.* 41 (2011) 359–364.
- [4] T. Matschei, F.P. Glasser, Temperature dependence, 0 to 40 °C, of the mineralogy of Portland cement paste in the presence of calcium carbonate, *Cem. Concr. Res.* 40 (2010) 763–777.
- [5] B. Lothenbach, F. Winnefeld, C. Alder, E. Wieland, P. Lunk, Effect of temperature on the pore solution, microstructure and hydration products of Portland cement pastes, *Cem. Concr. Res.* 37 (2007) 483–491.
- [6] F. Deschner, B. Lothenbach, F. Winnefeld, J. Neubauer, Effect of temperature on the hydration Portland cement blended with siliceous fly ash, *Cem. Concr. Res.* 52 (2013) 169–181.
- [7] T. Matschei, B. Lothenbach, F.P. Glasser, Thermodynamic properties of Portland cement hydrates in the system CaO–Al₂O₃–SiO₂–CaSO₄–CaCO₃–H₂O, *Cem. Concr. Res.* 37 (2007) 1379–1410.
- [8] B.Z. Dilnesa, B. Lothenbach, G. Le Saout, G. Renaudin, A. Mesbah, Y. Filinchuk, A. Wichser, E. Wieland, Iron in carbonate containing AFm phases, *Cem. Concr. Res.* 41 (2011) 311–323.
- [9] B.Z. Dilnesa, B. Lothenbach, G. Renaudin, A. Wichser, D. Kulik, Synthesis and characterization of hydrogarnet Ca₃(Al_xFe_{1-x})₂(SiO₄)_y(OH)_{4(3-y)}, *Cem. Concr. Res.* 59 (2014) 96–111.
- [10] B.Z. Dilnesa, B. Lothenbach, G. Renaudin, A. Wichser, E. Wieland, Stability of monosulfate in the presence of iron, *J. Am. Ceram. Soc.* 95 (2012) 3305–3316.
- [11] D.A. Kulik, Improving the structural consistency of C-S-H solid solution thermodynamic models, *Cem. Concr. Res.* 41 (2011) 477–495.
- [12] B. Lothenbach, L. Pelletier-Chaignat, F. Winnefeld, Stability in the system CaO–Al₂O₃–H₂O, *Cem. Concr. Res.* 42 (2012) 1621–1634.
- [13] D. Kulik, T. Wagner, S. Dmytrieva, G. Kosakowski, F. Hingerl, K. Chudnenko, U. Berner, GEM-Selektor geochemical modeling package: revised algorithm and GEMS3K numerical kernel for coupled simulation codes, *Comput. Geosci.* 17 (2013) 1–24.
- [14] T. Wagner, D.A. Kulik, F.F. Hingerl, S.V. Dmytrieva, GEM-Selektor geochemical modeling package: TSolMod library and data interface for multicomponent phase models, *Can. Mineral.* 50 (2012) 1173–1195.
- [15] P. Blanc, X. Bourbon, A. Lassin, E. Gaucher, Chemical model for cement-based materials: Temperature dependence of thermodynamic functions for nanocrystalline and crystalline C-S-H phases, *Cem. Concr. Res.* 40 (2010) 851–866.
- [16] P. Blanc, X. Bourbon, A. Lassin, E. Gaucher, Chemical model for cement-based materials: thermodynamic data assessment for phases other than CSH, *Cem. Concr. Res.* 40 (2010) 1360–1374.
- [17] C.M. Bethke, *Geochemical and Biogeochemical Reaction Modeling*, 2nd Ed., Cambridge University Press, New York, NY, USA, 2008.
- [18] D.J. Parkhurst, C.A.J. Appelo, Description of Input and Examples for PHREEQC Version 3 - A Computer Program for Speciation, Batch-reaction, One-dimensional Transport, and Inverse Geochemical Calculations, 6 USGS, Denver, CO, USA, 2013.
- [19] J.E. Cross, F.T. Ewart, HATCHES - a thermodynamic database and management system, *Radiochim. Acta* 52/53 (1991) 421–422.
- [20] D. Damidot, B. Lothenbach, D. Herfort, F.P. Glasser, Thermodynamics and cement science, *Cem. Concr. Res.* 41 (2011) 679–695.
- [21] G. Möschner, B. Lothenbach, J. Rose, A. Ulrich, R. Figi, R. Kretzschmar, Solubility of Fe-ettringite (Ca₆[Fe(OH)₆]₂(SO₄)₃·26H₂O), *Geochim. Cosmochim. Acta* 72 (2008) 1–18.
- [22] T. Thoenen, W. Hummel, U. Berner, E. Curti, The PSI/Nagra Chemical Thermodynamic Data Base 12/07, PSI Report 14-04, Villigen PSI, Switzerland, 2014.
- [23] T. Thoenen, D.A. Kulik, Nagra/PSI Chemical Thermodynamic Data Base 01/01 for the GEM-Selektor (V.2- PSI) Geochemical Modeling Code: Release 28-02-03. Internal Report TM-44-03-04, available from <http://gems.web.psi.ch/TDB/doc/pdf/TM-44-03-04-web.pdf>, (2003) (checked 2018-04-19).
- [24] W. Hummel, U. Berner, E. Curti, F.J. Pearson, T. Thoenen, Nagra/PSI Chemical Thermodynamic Data Base 01/01, Universal Publishers/uPUBLISH.com, USA, Also Published as Nagra Technical Report NTB 02-16, Wettingen, Switzerland, 2002.
- [25] E. Shock, D. Sassani, M. Willis, D. Sverjensky, Inorganic species in geologic fluids: Correlations among standard molal thermodynamic properties of aqueous ions and hydroxide complexes, *Geochim. Cosmochim. Acta* 61 (1997) 907–950.
- [26] D. Sverjensky, E. Shock, H. Helgeson, Prediction of the thermodynamic properties of aqueous metal complexes to 1000 °C and 5 kb, *Geochim. Cosmochim. Acta* 61 (1997) 1359–1412.
- [27] M. Balonis, B. Lothenbach, G. Le Saout, F.P. Glasser, Impact of chloride on the mineralogy of hydrated Portland cement systems, *Cem. Concr. Res.* 40 (2010) 1009–1022.
- [28] T. Matschei, F.P. Glasser, The thermal stability of thaumasite, *Mater. Struct.* 48 (2015) 2277–2289.
- [29] B. Lothenbach, F. Winnefeld, Thermodynamic modelling of the hydration of Portland cement, *Cem. Concr. Res.* 36 (2006) 209–226.
- [30] L.G. Baquerizo, T. Matschei, K.L. Scrivener, Impact of water activity on the stability of ettringite, *Cem. Concr. Res.* 76 (2016) 31–44.
- [31] L.G. Baquerizo, T. Matschei, K.L. Scrivener, Hydration states of AFm cement phases, *Cem. Concr. Res.* 73 (2015) 143–157.
- [32] L.G. Baquerizo, T. Matschei, K.L. Scrivener, M. Saeidpour, A. Thorell, L. Wadsö, Methods to determine hydration states of minerals and cement hydrates, *Cem. Concr. Res.* 65 (2014) 85–95.
- [33] M. Balonis, F.P. Glasser, The density of cement phases, *Cem. Concr. Res.* 39 (2009) 733–739.
- [34] M. Balonis, The Influence of Inorganic Chemical Accelerators and Corrosion Inhibitors on the Mineralogy of Hydrated Portland Cement Systems, Thesis University of Aberdeen, Aberdeen, UK, 2010.
- [35] M. Balonis, M. Medala, F.P. Glasser, Influence of calcium nitrate and nitrite on the constitution of AFm and Aft cement hydrates, *Adv. Cem. Res.* 23 (2011) 129–143.
- [36] M. Balonis, F.P. Glasser, Calcium nitrite corrosion inhibitor in portland cement: influence of nitrite on chloride binding and mineralogy, *J. Am. Ceram. Soc.* 94 (2011) 2230–2241.
- [37] B.Z. Dilnesa, Fe-containing Hydrates and Their Fate During Cement Hydration: Thermodynamic Data and Experimental Study, Thesis EPFL, Lausanne, 2012.
- [38] D. Garvin, V.B. Parker, H.J. White, CODATA Thermodynamic Tables. Selections for Some Compounds of Calcium and Related Mixtures: A Prototype Set of Tables, Springer Verlag, Berlin, 1987.
- [39] K.B. Rozov, U. Berner, D.A. Kulik, L.W. Diamond, Solubility and thermodynamic properties of carbonate-bearing hydrotalcite-pyroaurite solid solutions with a 3:1 Mg/(Al + Fe) mole ratio, *Clay Clay Miner.* 59 (2011) 215–232.
- [40] D. Nied, K. Enemark-Rasmussen, E. L'Hôpital, J. Skibsted, B. Lothenbach, Properties of magnesium silicate hydrates (M-S-H), *Cem. Concr. Res.* 79 (2016) 323–332.
- [41] B. Lothenbach, E. Bernard, U. Mäder, Zeolite formation in the presence of cement hydrates and albite, *Phys. Chem. Earth* 99 (2017) 77–94.
- [42] V.J. Babushkin, G.M. Matveyev, O.P. Mchedlov-Petrosyan, Thermodynamics of Silicates, Springer-Verlag, Berlin, H, 1985.
- [43] H.C. Helgeson, J.M. Delany, H.W. Nesbitt, D.K. Bird, Summary and critique of the thermodynamic properties of rock-forming minerals, *Am. J. Sci.* 278-A (1978) 1–229.

- [44] R.A. Robie, B.S. Hemingway, Thermodynamic properties of minerals and related substances at 298.15 K and 1 bar (105 Pascals) pressures and at higher temperatures, U.S. Geol. Surv. Bull. 2131 (1995) 1–461.
- [45] G. Möschner, B. Lothenbach, A. Ulrich, R. Figi, R. Kretschmar, Solid solution between Al-ettringite and Fe-ettringite ($\text{Ca}_6[\text{Al}_{1-x}\text{Fe}_x(\text{OH})_6]_2(\text{SO}_4)_3 \cdot 26\text{H}_2\text{O}$), Cem. Concr. Res. 39 (2009) 482–489.
- [46] E. Corazza, C. Sabelli, The crystal structure of syngenite, $\text{K}_2\text{Ca}(\text{SO}_4)_2 \cdot \text{H}_2\text{O}$, Z. Kristallogr. 124 (1967) 398–408.
- [47] P. Blanc, P. Vieillard, H. Gailhanou, S. Gaboreau, N. Marty, F. Claret, B. Made, E. Giffaut, ThermoChimie database developments in the framework of cement/clay interactions, Appl. Geochem. 55 (2015) 95–107.
- [48] R.M. Milton, Molecular sieve adsorbents, US Patent No (1959) 2,882,244.
- [49] G. Gottardi, E. Galli, Natural Zeolites, Mineral and Rocks, 18 (1985).
- [50] H. Boysen, M. Lerch, A. Stys, A. Senyshyn, Structure and oxygen mobility in mayenite ($\text{Ca}_{12}\text{Al}_{14}\text{O}_{33}$): a high-temperature neutron powder diffraction study, Acta Crystallogr. B63 (2007) 675–682.
- [51] W. Hörkner, H. Müller-Buschbaum, Zur Kristallstruktur von CaAl_2O_4 , J. Inorg. Nucl. Chem. 38 (1976) 983–984.
- [52] D.W. Goodwin, A.J. Lindop, The crystal structure of $\text{CaO} \cdot 2\text{Al}_2\text{O}_3$, Acta Crystallogr. B 26 (1970) 1230–1235.
- [53] F. Winnefeld, B. Lothenbach, Phase equilibria in the system $\text{Ca}_4\text{Al}_6\text{O}_{12}\text{SO}_4 - \text{Ca}_2\text{SiO}_4 - \text{CaSO}_4 - \text{H}_2\text{O}$ referring to the hydration of calcium sulfoaluminate cements, RILEM Tech. Lett. 1 (2016) 10–16.
- [54] D. Damidot, S.J. Barnett, F.P. Glasser, D.E. Macphee, Investigation of the $\text{CaO} - \text{Al}_2\text{O}_3 - \text{SiO}_2 - \text{CaSO}_4 - \text{CaCO}_3 - \text{H}_2\text{O}$ system at 25 °C by thermodynamic calculation, Adv. Cem. Res. 16 (2004) 69–76.
- [55] T. Schmidt, B. Lothenbach, M. Romer, K.L. Scrivener, D. Rentsch, R. Figi, A thermodynamic and experimental study of the conditions of thaumasite formation, Cem. Concr. Res. 38 (2008) 337–349.
- [56] D.E. Macphee, S.J. Barnett, Solution properties of solids in the ettringite-thaumasite solid solution series, Cem. Concr. Res. 34 (2004) 1591–1598.
- [57] F. Bellmann, On the formation of thaumasite $\text{CaSiO}_3 \cdot \text{CaSO}_4 \cdot \text{CaCO}_3 \cdot 15\text{H}_2\text{O}$: part I, Adv. Cem. Res. 16 (2004) 55–60.
- [58] U.A. Birnin-Yauri, F.P. Glasser, Friedel's salt, $\text{Ca}_2\text{Al}(\text{OH})_6(\text{Cl},\text{OH}) \cdot 2\text{H}_2\text{O}$: its solid solutions and their role in chloride binding, Cem. Concr. Res. 28 (1998) 1713–1723.
- [59] M.Y. Hobbs, Solubilities and Ion Exchange Properties of Solid Solutions Between OH^- , Cl^- and CO_3^{2-} End Members of the Monocalcium Aluminate Hydrates, Thesis University of Waterloo, Ontario, Canada, 2001.
- [60] J.V. Bothe Jr, P.W. Brown, PhreeQC modeling of Friedel's salt equilibria at 23 ± 1 °C, Cem. Concr. Res. 34 (2004) 1057–1063.
- [61] R.O. Grishchenko, A.L. Emelina, P.Y. Makarov, Thermodynamic properties and thermal behavior of Friedel's salt, Thermochim. Acta 570 (2013) 74–79.
- [62] F.P. Glasser, A. Kindness, S.A. Stronach, Stability and solubility relationships in AFm phases. Part I. Chloride, sulfate and hydroxide, Cem. Concr. Res. 29 (1999) 861–866.
- [63] G. Falzone, M. Balonis, G. Sant, X-AFm stabilization as a mechanism of bypassing conversion phenomena in calcium aluminate cements, Cem. Concr. Res. 72 (2015) 54–68.
- [64] B.Z. Dilnesa, E. Wieland, B. Lothenbach, R. Dähn, K. Scrivener, Fe-containing phases in hydrated cements, Cem. Concr. Res. 58 (2014) 45–55.
- [65] M. Vespa, E. Wieland, R. Dähn, B. Lothenbach, Identification of the thermodynamically stable Fe-containing phase in aged cement pastes, J. Am. Ceram. Soc. 98 (2015) 2286–2294.
- [66] H.F.W. Taylor, D.E. Newbury, An electron microprobe study of a mature cement paste, Cem. Concr. Res. 14 (1984) 565–573.
- [67] U. Mäder, A. Jenni, C. Lerouge, S. Gaboreau, S. Miyoshi, Y. Kimura, V. Cloet, M. Fukaya, F. Claret, T. Otake, M. Shibata, B. Lothenbach, 5-year chemico-physical evolution of concrete-claystone interfaces, Mont Terri rock laboratory (Switzerland), Swiss J. Geosci. 110 (2017) 307–327.
- [68] S.A. Bernal, R. San Nicos, R.J. Myers, R. Mejia de Gutierrez, F. Puertas, J.S.J. Van Deventer, J.L. Provis, MgO content of slag controls phase evolution and structural changes induced by accelerated carbonation in alkali-activated binders, Cem. Concr. Res. 57 (2014) 33–43.
- [69] I.G. Richardson, A.R. Brough, G.W. Groves, C.M. Dobson, The characterization of hardened alkali-activated blast-furnace slag pastes and the nature of the calcium silicate hydrate (C-S-H) phase, Cem. Concr. Res. 24 (1994) 813–829.
- [70] H. Taylor, Crystal structures of some double hydroxide minerals, Mineral. Mag. 39 (1973) 377–389.
- [71] I. Richardson, Clarification of possible ordered distributions of trivalent cations in layered double hydroxides and an explanation for the observed variation in the lower solid-solution limit, Acta Crystallogr. B 69 (2013) 629–633.
- [72] D.G. Bennett, D. Read, M. Atkins, F.P. Glasser, A thermodynamic model for blended cements. II: cement hydrate phases; thermodynamic values and modelling studies, J. Nucl. Mater. 190 (1992) 315–325.
- [73] W. Gao, Z. Li, Solubility and K_{sp} of $\text{Mg}_4\text{Al}_2(\text{OH})_{14} \cdot 3\text{H}_2\text{O}$ at the various ionic strengths, Hydrometallurgy 117–118 (2012) 36–46.
- [74] R.J. Myers, B. Lothenbach, S. Bernal, J.L. Provis, Thermodynamic modelling of alkali-activated slag-based cements, Appl. Geochem. 61 (2015) 233–247.
- [75] M. Zajac, S.K. Bremseth, M. Whitehead, M. Ben Haha, Effect of $\text{CaMg}(\text{CO}_3)_2$ on hydrate assemblages and mechanical properties of hydrated cement pastes at 40 °C and 60 °C, Cem. Concr. Res. 65 (2014) 21–29.
- [76] B. Lothenbach, A. Nonat, Calcium silicate hydrates: solid and liquid phase composition, Cem. Concr. Res. 78 (2015) 57–70.
- [77] I. Richardson, Tobermorite/jennite- and tobermorite/calcium hydroxide-based models for the structure of CSH: applicability to hardened pastes of tricalcium silicate, β-dicalcium silicate, Portland cement, and blends of Portland cement with blast-furnace slag, metakaolin, or silica fume, Cem. Concr. Res. 34 (2004) 1733–1777.
- [78] A. Muller, K. Scrivener, A. Gajewicz, P. McDonald, Use of bench-top NMR to measure the density, composition and desorption isotherm of C-S-H in cement paste, Microporous Mesoporous Mater. 178 (2013) 99–103.
- [79] A. Muller, K. Scrivener, J. Skibsted, A. Gajewicz, P. McDonald, Influence of silica fume on the microstructure of cement pastes: new insights from ¹H NMR relaxometry, Cem. Concr. Res. 74 (2015) 116–125.
- [80] C.S. Walker, S. Sutou, C. Oda, M. Mihara, A. Honda, Calcium silicate hydrate (C-S-H) gel solubility data and a discrete solid phase model at 25 °C based on two binary non-ideal solid solutions, Cem. Concr. Res. 79 (2016) 1–30.
- [81] S.-Y. Hong, F.P. Glasser, Alkali binding in cement pastes: part I. The C-S-H phase, Cem. Concr. Res. 29 (1999) 1893–1903.
- [82] E. L'Hôpital, B. Lothenbach, D. Kulik, K. Scrivener, Influence of calcium to silica ratio on aluminium uptake in calcium silicate hydrate, Cem. Concr. Res. 85 (2016) 111–121.
- [83] E. L'Hôpital, B. Lothenbach, G. Le Saout, D.A. Kulik, K. Scrivener, Incorporation of aluminium in calcium-silicate hydrate, Cem. Concr. Res. 75 (2015) 91–103.
- [84] E. L'Hôpital, B. Lothenbach, K. Scrivener, D.A. Kulik, Alkali uptake in calcium alumina silicate hydrate (C-A-S-H), Cem. Concr. Res. 85 (2016) 122–136.
- [85] D.A. Kulik, M. Kersten, Aqueous solubility diagrams for cementitious waste stabilization systems: II, end-member stoichiometries of ideal calcium silicates hydrate solid solutions, J. Am. Ceram. Soc. 84 (2001) 3017–3026.
- [86] J. Haas, A. Nonat, From C-S-H to C-A-S-H: experimental study and thermodynamic modelling, Cem. Concr. Res. 68 (2015) 124–138.
- [87] S.V. Churakov, C. Labbez, Thermodynamics and molecular mechanism of Al incorporation in calcium silicate hydrates, J. Phys. Chem. C 121 (2017) 4412–4419.
- [88] D. Kulik, J. Tits, E. Wieland, Aqueous-solid solution model of strontium uptake in C-S-H phases, Geochim. Cosmochim. Acta 71 (2007) A530.
- [89] B. Lothenbach, G. Le Saout, M. Ben Haha, R. Figi, E. Wieland, Hydration of a low-alkali CEM III/B-SiO₂ cement (LAC), Cem. Concr. Res. 42 (2012) 410–423.
- [90] R. Myers, S.A. Bernal, J.L. Provis, A thermodynamic model for C-(N)-A-S-H gel: CNASH_{ss}. Derivation and validation, Cem. Concr. Res. 66 (2014) 27–47.
- [91] D. Kulik, Dual-thermodynamic estimation of stoichiometry and stability of solid solution end members in aqueous-solid solution systems, Chem. Geol. 225 (2006) 189–212.
- [92] J. Tits, E. Wieland, C.J. Müller, C. Landesman, M.H. Bradbury, Strontium binding by calcium silicate hydrates, J. Colloid Interface Sci. 300 (2006) 78–87.
- [93] D.D. Wagman, E.H. Evans, V.B. Parker, R.H. Schumm, I. Halow, S.M. Bailey, K.L. Churney, L. N.R., The NBS tables of chemical thermodynamic properties. Selected values for inorganic and C1 and C2 organic substances in SI units, J. Phys. Chem. Ref. Data 11 (Suppl. 2) (1982) 1–392.
- [94] I.G. Richardson, The calcium silicate hydrates, Cem. Concr. Res. 38 (2008) 137–158.
- [95] J.J. Chen, J.J. Thomas, H.F.W. Taylor, H.M. Jennings, Solubility and structure of calcium silicate hydrate, Cem. Concr. Res. 34 (2004) 1499–1519.
- [96] K. Garbev, M. Bornfeld, G. Beuchle, P. Stemmermann, Cell dimensions and composition of nanocrystalline calcium silicate hydrate solid solutions. part 2: X-Ray and thermogravimetry study, J. Am. Ceram. Soc. 91 (2008) 3015–3023.
- [97] X. Gaona, D.A. Kulik, N. Macé, E. Wieland, Aqueous-solid solution thermodynamic model of U(VI) uptake in C-S-H phases, Appl. Geochem. 27 (2012) 81–95.
- [98] A.J. Allen, J.J. Thomas, H.M. Jennings, Composition and density of nanoscale calcium-silicate-hydrate in cement, Nat. Mater. 6 (2007) 311–316.
- [99] J.J. Thomas, A.J. Allen, H.M. Jennings, Density and water content of nanoscale solid C-S-H formed in alkali-activated slag (AAS) paste and implications for chemical shrinkage, Cem. Concr. Res. 42 (2012) 377–383.
- [100] J.L. Provis, S.A. Bernal, Geopolymers and related alkali-activated materials, Annu. Rev. Mater. Res. 44 (2014) 299–327.
- [101] R.J. Myers, S.A. Bernal, J.L. Provis, Phase diagrams for alkali-activated slag binders, Cem. Concr. Res. 95 (2017) 30–38.
- [102] C.S. Walker, D. Savage, M. Tyrer, K.V. Ragnarsdottir, Non-ideal solid solution aqueous solution modeling of synthetic calcium silicate hydrate, Cem. Concr. Res. 37 (2007) 502–511.
- [103] L. Gomez-Zamorano, M. Balonis, B. Erdemli, N. Neithalath, G. Sant, C-(N)-S-H and N-A-S-H gels: Compositions and solubility data at 25 °C and 50 °C, J. Am. Ceram. Soc. 100 (2017) 2700–2711.
- [104] R.J. Myers, E. L'Hôpital, J.L. Provis, B. Lothenbach, Effect of temperature and aluminium on calcium (aluminosilicate) hydrate chemistry under equilibrium conditions, Cem. Concr. Res. 68 (2015) 83–93.
- [105] R.J. Myers, E. L'Hôpital, J.L. Provis, B. Lothenbach, Composition-solubility-structure relationships in calcium (alkali) aluminosilicate hydrate (C-(N,K)-A-S-H), Dalton Trans. 44 (2015) 13530–13544.
- [106] G.D. Miron, D.A. Kulik, S.V. Dmytrieva, T. Wagner, GEMSFTS: code package for optimization of geochemical model parameters and inverse modeling, Appl. Geochem. 55 (2015) 28–45.
- [107] L. Nicoleau, E. Schreiner, Determination of Ca^{2+} complexation constants by monomeric silicate species at 25 °C with a Ca^{2+} ion selective electrode, Cem. Concr. Res. 98 (2017) 36–43.
- [108] A. Jenni, U. Mäder, C. Lerouge, S. Gaboreau, B. Schwyn, In situ interaction between different concretes and Opalinus clay, Phys. Chem. Earth, 70–71 (2014) 71–83.
- [109] A. Dauzères, G. Achiedo, D. Nied, E. Bernard, S. Alahache, B. Lothenbach, Magnesium perturbation in low-pH concretes placed in clayey environment—solid characterizations and modeling, Cem. Concr. Res. 79 (2016) 137–150.

- [110] D. Bonen, M.D. Cohen, Magnesium sulfate attack on portland cement paste—II. Chemical and mineralogical analyses, *Cem. Concr. Res.* 22 (1992) 707–718.
- [111] M. Santhanam, M.D. Cohen, J. Olek, Mechanism of sulfate attack: a fresh look: part 1: summary of experimental results, *Cem. Concr. Res.* 32 (2002) 915–921.
- [112] U.H. Jakobsen, K. De Weerd, M.R. Geiker, Elemental zonation in marine concrete, *Cem. Concr. Res.* 85 (2016) 12–27.
- [113] C. Roos, S. Grangeon, P. Blanc, V. Montouillout, B. Lothenbach, P. Henocq, E. Giffaut, P. Vieillard, S. Gaboreau, Crystal structure of magnesium silicate hydrates (M-S-H): the relation with 2:1 Mg-Si phyllosilicates, *Cem. Concr. Res.* 73 (2015) 228–237.
- [114] E. Bernard, B. Lothenbach, F. Le Goff, I. Pochard, A. Dauzères, Effect of magnesium on calcium silicate hydrates (C-S-H), *Cem. Concr. Res.* 97 (2017) 61–72.
- [115] D.R.M. Brew, F.P. Glasser, Synthesis and characterisation of magnesium silicate hydrate gels, *Cem. Concr. Res.* 35 (2005) 85–98.
- [116] B. Lothenbach, D. Nied, E. L'Hôpital, G. Achiedo, A. Dauzères, Magnesium and calcium silicate hydrates, *Cem. Concr. Res.* 77 (2015) 60–68.
- [117] W.-S. Chiang, G. Ferraro, E. Fratini, F. Ridi, Y.-Q. Yeh, U. Jeng, S.-H. Chen, P. Baglioni, Multiscale structure of calcium-and magnesium-silicate-hydrate gels, *J. Mater. Chem. A* 2 (2014) 12991–12998.
- [118] E. Bernard, B. Lothenbach, D. Rentsch, I. Pochard, A. Dauzères, Formation of magnesium silicate hydrates (M-S-H), *Phys. Chem. Earth* 99 (2017) 142–157.
- [119] J.A.T. Smellie, Maqarin Natural Analogue Study: Phase III, SKB, SKB Technical Report 98-04, Stockholm, Sweden, 1998.
- [120] S.J. Chipera, J.A. Apps, Geochemical stability of natural zeolites, *Rev. Mineral. Geochem.* 45 (2001) 117–161.
- [121] R. Arthur, H. Sasamoto, C. Walker, M. Yui, Polymer model of zeolite thermochemical stability, *Clays Clay Miner.* 59 (2011) 626–639.
- [122] J.L. Provis, G.C. Lukey, J.S. van Deventer, Do geopolymers actually contain nanocrystalline zeolites? A reexamination of existing results, *Chem. Mater.* 17 (2005) 3075–3085.
- [123] B. Lothenbach, G. Le Saout, E. Gallucci, K. Scrivener, Influence of limestone on the hydration of Portland cements, *Cem. Concr. Res.* 38 (2008) 848–860.
- [124] K. De Weerd, M. Ben Haha, G. Le Saout, K.O. Kjellsen, H. Justnes, B. Lothenbach, Hydration mechanisms of ternary Portland cements containing limestone powder and fly ash, *Cem. Concr. Res.* 41 (2011) 279–291.
- [125] F. Deschner, F. Winnefeld, B. Lothenbach, S. Seufert, P. Schwesig, S. Dittich, F. Goetz-Neunhoffer, J. Neubauer, Hydration of a Portland cement with high replacement by siliceous fly ash, *Cem. Concr. Res.* 42 (2012) 1389–1400.
- [126] T.G. Jappy, F.P. Glasser, Synthesis and stability of silica-substituted hydrogarnet $\text{Ca}_3\text{Al}_2\text{Si}_{3-x}\text{O}_{12-4x}(\text{OH})_{4x}$, *Adv. Cem. Res.* 4 (1991) 1–8.
- [127] A. Vollpracht, B. Lothenbach, R. Snellings, J. Haufe, The pore solution of blended cements: a review, *Mater. Struct.* 49 (2016) 3341–3367.
- [128] W.R. Smith, R.W. Missen, *Chemical Reaction Equilibrium Analysis: Theory and Algorithms*, Wiley-Interscience, New York 1982. Reprinted With Corrections, Krieger, Malabar, FL, (1991).
- [129] T. Matschei, F.P. Glasser, New approaches to quantification of cement hydration, in: J. Stark (Ed.), 16 Internationale Baustofftagung (ibaustil), Weimar, Germany, 2006, pp. 390–400.
- [130] B.J. Merkel, B. Planer-Friederich, *Groundwater Geochemistry. A Practical Guide to Modeling of Natural and Contaminated Aquatic Systems*, Springer Berlin, 2008.
- [131] G.M. Anderson, D.A. Crerar, *Thermodynamics in Geochemistry: The Equilibrium Model*, Oxford University Press, Oxford, 1993.
- [132] D. Kulik, Minimising uncertainty induced by temperature extrapolations of thermodynamic data: a pragmatic view on the integration of thermodynamic databases into geochemical computer codes, *The Use of Thermodynamic Databases in Performance Assessment*, OECD, Barcelona, 2002, pp. 125–137.
- [133] J.W. Johnson, E.H. Oelkers, H.C. Helgeson, SUPCRT92: a software package for calculating the standard molal thermodynamic properties of minerals, gases, aqueous species, and reactions from 1 to 5000 bar and 0 to 1000 °C, *Comput. Geosci.* 18 (1992) 899–947.